Gold Nanoparticles as Drug Delivery Agents. Detoxifying the Chemotherapeutic Drug Cisplatin

(copia xifrada)

Joan Comenge Farre

Maig 2013

Universitat Autònoma de Barcelona
Departament de Bioquímica i Biologia Molecular

Gold Nanoparticles as Drug Delivery Agents. Detoxifying the Chemotherapeutic Drug Cisplatin

Joan Comenge Farré
Inorganic Nanoparticles Group
Institut Català de Nanotecnologia

Maig 2013

Gold Nanoparticles as Drug Delivery Agents. Detoxifying the Chemotherapeutic Drug Cisplatin

Memòria presentada per

Joan Comenge Farré

Per optar al grau de

Doctor per la Universitat Autònoma de Barcelona

Programa de Doctorat en Bioquímica, Biologia Molecular i Biomedicina

Tesi realitzada sota la direcció del Dr. Víctor Franco Puntes,
Inorganic Nanoparticles Group, Institut Català de Nanotecnologia,
i amb la tutoria de la Dra. Ester Boix Borràs,
Departament de Bioquímica i Biologia Molecular, Universitat Autònoma de Barcelona.

Cerdanyola del Vallès, Maig 2013

Contents

Prologue

In this thesis dissertation, the use of gold nanoparticles as agents for delivery of cisplatin is discussed. The book has been organized following a logic sequence that starts by the synthesis of gold nanoparticles, followed by their functionalization, first with surfactants and then with the drug to finally analyze the performance of these drug delivery vehicles in *in vitro* and in *in vivo* experiments. Every chapter has been structured so to allow its individual lecture.

Although aspects applicable to other drug delivery systems such as the colloidal and chemical stability in physiological media, the drug release profile, etc. are discussed here using our system as an example, this work does not pretend to be a general discussion about the state of the art in nanomedicine and/or drug delivery, but a contribution to these growing areas. However, I encourage the lecture of some of the very interesting references provided here to achieve a deeper understanding in specific aspects.

This multidisciplinary work could have not been possible without the contribution and advice of a great number of people. Thus, I feel the obligation to acknowledge all those that directly contribute to this work especially all the members of the Inorganic Nanoparticles Group, led by Prof. Víctor Puntes, for their invaluable help and knowledge, but also Prof. Fernando Domínguez and Carmen Sotelo from school of medicine at Santiago de Compostela, prof. Franciso Romero from Molecular Science Institute at València and Dr. Óscar Gallego and Prof. Agustí Barnadas from the Santa Creu I Sant Pau Hospital at Barcelona for their active contribution and discussions about this work. Last but not least, my gratitude to all the members of the Radiation Biology Group lead by Prof. Kevin Prise in the Centre of Cancer Research and Cell Biology at Belfast for receiving me and teaching me the little I know about this field.

Also, a special mention goes to Nanotargeting S.L. for trusting in this project.

It is impossible to extend here my gratitude to all of those that indirectly contribute to the work so I will let you know one by one personally. Just be patient.

Chapter 1

Introduction

Many of the conventional therapies can be improved through the use of drug delivery systems (DDS). They are designed mainly to modify the pharmacokinetics and biodistribution of small molecular drugs. This is of special importance in the case of anticancer therapies in which a widespread distribution of small molecular chemotherapeutic drugs is often limiting treatments due to severe side effects that make impossible to reach the full benefits of the therapy. In this context, nanotechnology emerges as a disruptive technology to design carriers that improve the delivery of drugs to their target organs.

1.1 Engineering AuNPs as scaffolds for drug delivery

Although a plethora of nanoparticles (NPs) including polymeric NPs, liposomes, dendrimers, metallic NPs, etc. have been used to design nanocarriers for drug delivery,[1, 2] we will focus the discussion on the use of gold nanoparticles (AuNPs). The synthesis of AuNPs have been first described by J. Turkevich at 1954,[3] but it was not until last years that advances on the engineering of these NPs allowed researchers to control the size, shape, and functionalization of these nanocarriers and thus starting using them as scaffolds for drug delivery. Thus, new synthetic protocols make possible to achieve biocompatible spherical AuNPs from 5 to 200 nm with a monodispersity lower than 10 %.[4] The control over the size is a key point in the use of AuNPs in biomedicine since it influences important biological properties such as interaction with proteins, biodistribution and clearance rate. The variety of sizes of AuNPs that can be easily obtained facilitated a better understanding of the role played by this property in

important parameters for cancer treatment with NPs such as accumulation in tumors, blood half-life, or penetration. From a simplistic point of view, one could say that the final fate of the NPs is strongly influenced by their size since smallest AuNPs (<5 nm, core + surfactant) are rapidly cleared up by the kidneys and the the largest ones (>100 nm) are removed easily from the circulation by the immune system.[5] Sizes in between showed the best accumulation and penetration in tumors; at this range of sizes other parameters such as the presence of stealthing agents or different surface charge should be tuned case by case to achieve the desired behavior. In addition, shape of the AuNPs is also important. Spherical NPs are usually the chosen option when they wanted to be used just as carriers due to the simple synthesis and easy functionalization. However, other shapes such as nanorods or nanoboxes have been used too. These advanced AuNPs have special physicochemical properties that make them appealing to be used not only as vehicles but also as effectors by themselves. They present a surface plasmon resonance (SPR) in the near infrared (NIR) region, which make them suitable to be used in photothermal therapy in which NIR light is absorbed by NPs, delivering toxic amounts of heat.[6] In this type of therapy, working with wavelengths that can penetrate deep into tissue such as IR is required and only non-isotropic AuNPs present a SPR at this region.

Regarding functionality, chemistry on gold planar surfaces has been extensively studied to obtain molecular Self-Assembled Monolayers (SAMs).[7] Thus, this technology has been easily adapted to functionalize AuNPs in solution. However, some considerations need to be taken into account for NPs: the curvature radius may play a role in the determination of important properties of the molecules conjugated to small NPs such as apparent pka [8] and the coverage density[9] of the attached ligands amongst others. Also, AuNPs need to be stabilized during the synthesis to avoid aggregation by means of conjugation to a surfactant. Thus synthetic protocols in which the surfactant is weakly bound to the NPs (e.g. sodium citrate), and therefore can be easily exchanged by other ligands, are recommended for further functionalization of these AuNPs.[4] Note that physiological conditions (high ionic strength) are harsh for citrate-capped AuNPs. Conjugation may also result in destabilization of NPs if special care is not taken.[10]

AuNPs show affinity to different chemical groups such as phosphates, carboxylic acids, ammines and specially to thiols. Thus, one can found in the literature AuNPs conjugated to a great variety of molecules including alkanethiols, polymers, proteins, amino acids, and drugs amongst others.[11] Interestingly, the control over the conjugation facilitates engineering multifunctional AuNPs. Hence, it would be possible to create a nanocarrier that contains, for example, a molecule to stealth the DDS from the immune system, a ligand

that promotes uptake by specific cells, and the drug which in its turn can be attached via a responsive link which release the drug only after a specific response such as a pH drop.

Last but not least, the greater monodispersity of AuNPs compared to other metallic or polymeric NPs is another advantage of using this type of NPs

1.2 Nanoparticles for anticancer therapy: Advances and challenges of a new therapy

NPs are perfect candidates to be used in anticancer therapy since they showed passive accumulation in tumors due to the Enhanced Permeation and Retention effect (EPR). This effect first reported by Matsumura and Maeda[12] exploits the ability of NPs to permeate through the leaky tumor vessels (with fenestrations between 100 and 800 nm [13, 14]) and to be accumulated into the tumor due to the lack of a functional lymphatic system (Figure 1.1). Long-time circulating NPs maximize the EPR effect since the changes to permeate through the tumor vessels are greater. Related to this, the size of NPs plays an important role in determine tumor accumulation and distribution: 60nm AuNPs showed a greater accumulation than 20 nm AuNPs likely due to a slower clearance. However, larger AuNPs are accumulated in the perivascular region of the tumor failing to penetrate deeper, whilst 20 nm AuNPs were still found significantly at 50 μm from the blood vessel.[14]

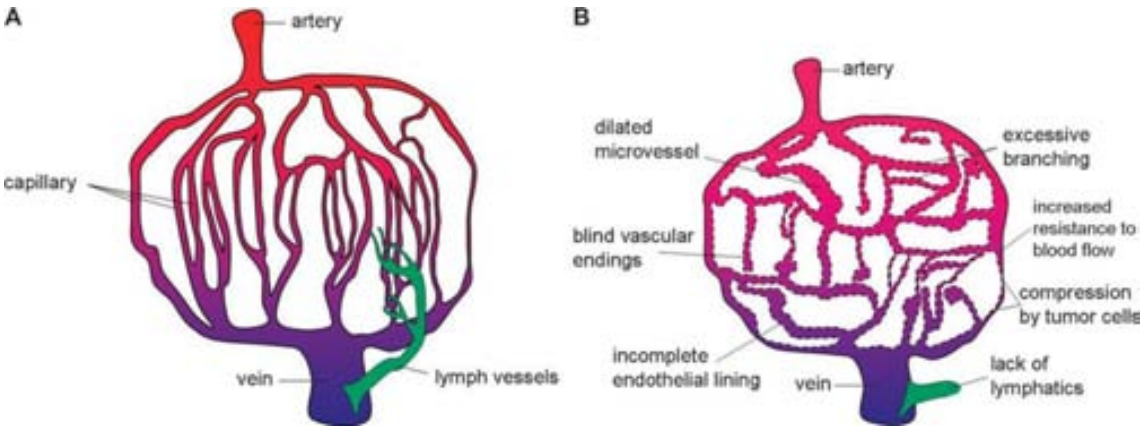

Figure 1.1. Scheme showing the differences of the vascular system of normal tissue (A) and tumor (B). Leaky vessels and non-functional lymphatic system are responsible for the passive accumulation of NPs into tumors. Adapted from reference 15.[15]

The intrinsic property of NPs to be passively accumulated into tumors has been exploited to deliver a great variety of drugs.[1] Some groups proposed to improve further this accumulation by attaching a ligand recognized by receptors overexpressed in tumor cells.

These include epidermal growth factor (EGF)[16], folate[17] and transferrin[18] amongst other. However, there is some controversy regarding the efficiency of this approach.[19] It is not clear that active targeting favors the accumulation in tumor, since physicochemical properties of NPs govern the pharmacokinetics properties of DDS. Thus, size and surface charge and composition (e.g. presence of stealthing agents or not) of NPs seems to play a more important role in determining final distribution of DDS[20] and ligands influence only in interactions directly onto the cell once the cell is reached (e.g. a greater uptake)

Once the NPs are localized in the tumor, different strategies have been used to release the drug. Normally, the strategies are based on the different physicochemical properties found in the cytoplasm compared to the extracellular environment (e.g. blood). For example, NPs are known to be internalized via endocytic pathways, in which a pH drop is produced.[21] Thus, a pH-sensitive link between drug and NPs ensures non-specific release of drug during the circulation through the body.[22] A controlled release can be also achieved by the reduction of an oxidized inactive prodrug in the cytoplasm, releasing the drug in its active form.[23] Also one can take advantage of specific enzymes to cleave the link between NP and drug.[24]

The metallic core of AuNPs conjugates can also act as an effector in thermotherapy as explained above. In addition, AuNPs have been recently proposed as radiosensitizers due to the induction of an Auger cascade after an ionizing event localized in the vicinity of the AuNP surface. These special properties open up the possibility to strategies that use AuNPs as carrier and effector.

Thus the use of AuNPs as carriers for drug delivery might provide several advantages including:

- Increased blood half-life of the small drug
- Accumulation in the tumor via the EPR effect
- Reduced toxicity in normal tissue
- Controlled release of the drug, delivering high payloads directly to the site of action
- Possibility of multiple functionalization which allow combined therapy and/or tuning blood half-life, immune responses toward the vehicle, tumor uptake, etc.
- Increase the solubility of poorly soluble drugs in plasma
- Protection of the drug from immune system and from agents present in the plasma that might deactivate the drug

- Promote a double effect by acting as carriers and as effectors by themselves

However, the use of AuNPs for drug delivery is not without problems and some aspects should be considered:

Classical syntheses of AuNPs render concentrations of AuNPs in the range of 10^{12}-10^{13} NP/mL,[25] thus AuNPs are typically synthesized at the nanomolar scale. Even though high densities of loading have been achieved,[26, 27] concentrations of drugs onto NPs as synthesized will rarely be higher than 10 micromolar. Taking into account that there is a limitation of volume that can be injected into the body (e.g. 10 mL/Kg for intravenous injection in mice), the therapeutic dose might not be reached unless NPs had been previously concentrated. This concentration step is not always straightforward because concentration of AuNPs could lead to aggregation if special care is not taken (e.g. concentration of AuNPs without any surfactant increase the chances of aggregation). Note that colloids are intrinsically out of equilibrium and they tend to minimize surface energy when this is possible either via functionalization or aggregation.

The need of concentration of AuNPs to reach therapeutic doses implies that a single lab-scale synthesis might not be enough to achieve the amount of NPs needed to perform *in vivo* experiments. Thus, not only monodispersity should be guaranteed to control size effects, but also reproducibility batch to batch. In addition, robust synthesis protocols will also facilitate the scale up of the production, which is essential for the transference of the technology to the industry.[28]

The special properties of AuNPs are lost if they aggregate. In too many cases the loss of colloidal stability is behind the lack of (or unexpected) biological behaviors.[20] Therefore, one has to ensure the maintenance of colloidal stability along the process (synthesis – storage – exposure/treatment). It is common to assay the stability of AuNPs in the storage conditions (e.g. in aquose media) even if they are different from the working conditions. However, biological fluids such as cell culture media or blood are complex mixtures of salts, proteins, sugars, etc. that may promote destabilization of AuNPs, and therefore stability should be assayed in this media. The same consideration is valid for the stability of the link with the drug. For example, cisplatin adsorbed on AuNPs is not released in aquose media, whilst it is unspecifically quickly released in cell culture media. On the other hand, cisplatin linked via coordination bond is stable in both media and only released after a pH drop.[26]

The choose of appropriate models to determine the potential therapeutic benefits is also not trivial, specially for new technologies in which the amount of literature is limited. I*n vitro* simple test such as those assessed in monolayer cell cultures do not consider important factors such as tumor vascularity, penetration and other differential properties given by the tumor microenvironment.[15] Consequently, in vitro results do not necessarily reflect the behavior of the assayed DDS in a real case. In this context, 3D cell cultures have been proposed as models to study the behavior of drugs in the particular environment of solid tumors due to the possibility to have an extracellular matrix and different regions of tumor (e.g. hypoxic cells in the intern areas). Since the advantages of using DDS are achieved mainly by modification on the pharmacokinetic properties of the drug, in vivo models are preferred. However, there is a great variety of tumor models including xenografted, orthotopic, and spontaneously and induced autochthonous tumor models.[29] This models show variations between them such as different size of porous in vessels or different immunological responses which may result in different efficiency of the same DDS depending on the model that has been used.

Finally, treatments with AuNPs are still very few and not beyond clinical trials. Thus, there is a lack of knowledge about regulatory aspects. Possible adverse effects of NPs such as acute toxicity and longtime accumulation should not be underestimated and should be studied case by case. There is a controversy regarding the *in vivo* toxicity of NPs and the parameters that play a role in the NPs-induced toxicity.[30] Some works have found no toxic signals after AuNPs administration[31] or small alterations in the biochemical markers due to metabolization of the AuNPs or indicating a temporal inflammation.[32] On the other hand, it is believed that the disfunction of major organs can be related to the presence of NPs at the site of abnormalities. For that reason, there are a lot of studies regarding toxicity in spleen and liver, which are generally accepted to be the organs with the highest accumulation of NPs. The liver toxicity, when found, seems to be associated to an hyperplasia of Kupffer cells that induce an acute inflammation with neutrophils influx.[33] This acute inflammation is a transient response due to the insult of AuNPs, however apoptosis and necrosis of hepatocytes as well as accumulation of AuNPs could be related to toxic effects.[34] Regarding the spleen, macrophages of the periphery seem to be involved in the uptake of NPs by this organ. Thus, leading to a temporal inflammation of the spleen, however in other cases a loss of weight has been observed after intravenous administration.[35] White pulp aberration has been also observed.[36] Any general trend cannot be extracted from the current literature, but it is clear that there are some parameters that have to be taken into account before using AuNPs as a vehicle for medical applications: i. Size of the vehicle, since it will determine the clearance rate and the

biodistribution [36]; ii. Surface composition, it has been seen that by changing the surface composition of AuNPs the toxicological profile might be different[37]; iii. Dose and administration route obviously will play a role in the potential toxicity. Therefore for every AuNP-conjugate, a toxicology study must be done to prove their usability in medical applications.

1.3 Cisplatin as anticancer drug

A paradigmatic case of anticancer drugs are platinum compounds. Cisplatin or cis-diamminedichloroplatinum(II), $[PtCl_2(NH_3)_2]$, was originally synthesized in 1845, but not until 1970 was its antitumor activity established.[38] Today cisplatin is used to treat various types of cancers (i.e., non-small-cell lung cancer, ovarian cancer, germ cell tumors, osteosarcomas, etc), with a cure rate as high as 90% in testicular cancer.[39] After both passive and active cellular uptake, the platinum complex reacts *in vivo* to form adducts with DNA, which ultimately trigger apoptosis.[40] However, chronic cisplatin usage results in resistance by several possible mechanisms including increased interactions with metallothioneins and glutathione, which deactivate the drug, as well as increased DNA repair and/or cisplatin efflux.[41] To counteract resistance and its rapid renal clearance, which lowers the efficiency of cisplatin significantly, very high systemic doses of cisplatin should be administered. Unfortunately, such high dose of cisplatin results in severe systemic toxicity and poor patient wellfare, including nausea/vomiting, renal toxicity, gastrointestinal toxicity, peripheral neuropathy, asthenia, and ototoxicity, thus limiting its clinical use.[41, 42] Of all the toxicities induced by cisplatin, nephrotoxicity is considered to be the dose-limiting factor.[40] Such side effects make it impossible to achieve the full benefit of the treatment in a large number of patients.[43] In humans, the cisplatin treatment generally involves series of intravenous injections administered every 3-4 weeks at a dose of 50-120 mg/m^2 (1.2 – 2.7 mg/Kg). In addition to the undesired side effects, there is also a loss of drug activity in the body associated with poor circulation and poor delivery to the tumor, as well as deactivation mechanisms that irreversibly alter the chemistry of these molecules before reaching the tumor cells.[42] Since its discovery, many attempts to find derivatives has been carried out looking for both reduced side effects and modified body distribution (in order to target different organs), rather than improving cisplatin efficacy.[41, 44] Here, second-generation platinum drugs as carboplatin and oxaliplatin represent an improvement in some cancer treatments, as lung and colorectal respectively, although the limitations observed for cisplatin have not been entirely overcome[40, 41].

1.4 Carrying cisplatin

Hence, recent efforts have been focused on targeting the tumor by using drug delivery systems to avoid the organs to which cisplatin is toxic. As the kidney is responsible for filtration and removal from the blood of molecules smaller than 50 KDa, which corresponds to molecular sizes of around 6 nm in diameter, any larger delivery vehicle will divert the drug away from the kidney.[45] In addition, more than 90 % of the administrated cisplatin is known to bind irreversible to albumin, which deactivates the drug.[46] Thus, a properly designed nanocarrier will not only transport the cisplatin to the tumor, but also protect it against plasma deactivation. In this context, approaches based on the encapsulation and transport of cisplatin have emerged recently. Sterically stabilized polymeric nanoparticles, having excellent stability in plasma, a much longer circulation time, better efficacy, and lower toxicity than free cisplatin have been reported.[47-50] As the case of lipid capsules[51] or polymers, as in Prolindac®, a 22 kDa hydroxypropylmethacrilamide copolymer as a backbone and then a glycine chelator linker which is pH sensitive.[52] Other examples include soluble CNTs,[53] carbon nanohorns,[54] and Fe_3O_4 NPs.[55] Similarly, CytImmune corp. is developing AuNPs as carrier for TNF-a and doxorubicin. In a close related work, Ren *et al.*[56-58] reported the adsorption of commercial cisplatin to gold colloids via ionic interactions. In the case of adsorption via ionic interactions on the surface of the nanomaterials, a non-controlled rapid liberation of the drug is observed as soon as the conjugates are dispersed in highly ionic media as serum.[26]

1.5 References

(1) Davis, M. E.; Chen, Z.; Shin, D. M., Nanoparticle therapeutics: an emerging treatment modality for cancer. *Nat Rev Drug Discov* **2008,** 7, 771-782.
(2) Allen, T. M.; Cullis, P. R., Drug Delivery Systems: Entering the Mainstream. *Science* **2004,** 303, 1818-1822.
(3) Turkevich, J.; Garton, G.; Stevenson, P. C., The Color of Colloidal Gold. *Journal of Colloid Science* **1954,** 9, S26-S35.
(4) Bastús, N. G.; Comenge, J.; Puntes, V. c., Kinetically Controlled Seeded Growth Synthesis of Citrate-Stabilized Gold Nanoparticles of up to 200 nm: Size Focusing versus Ostwald Ripening. *Langmuir* **2011,** 27, 11098-11105.
(5) Sperling, R. A.; Casals, E.; Comenge, J.; Bastus, N. G.; Puntes, V. F., Inorganic Engineered Nanoparticles and Their Impact on the Immune Response. *Current Drug Metabolism* **2009,** 10, 895-904.
(6) Jain, P. K.; El-Sayed, I. H.; El-Sayed, M. A., Au nanoparticles target cancer. *Nano Today* **2007,** 2, 18-29.
(7) Love, J. C.; Estroff, L. A.; Kriebel, J. K.; Nuzzo, R. G.; Whitesides, G. M., Self-Assembled Monolayers of Thiolates on Metals as a Form of Nanotechnology. *Chemical Reviews* **2005,** 105, 1103-1170.

(8) Wang, D.; Nap, R. J.; Lagzi, I. n.; Kowalczyk, B.; Han, S.; Grzybowski, B. A.; Szleifer, I., How and Why Nanoparticleâ€™s Curvature Regulates the Apparent pKa of the Coating Ligands. *J. Am. Chem. Soc.* **2011,** 133, 2192-2197.
(9) Xia, X.; Yang, M.; Wang, Y.; Zheng, Y.; Li, Q.; Chen, J.; Xia, Y., Quantifying the Coverage Density of Poly(ethylene glycol) Chains on the Surface of Gold Nanostructures. *ACS Nano* **2011**.
(10) Ojea-Jimeì⍰nez, I.; Puntes, V., Instability of Cationic Gold Nanoparticle Bioconjugates: The Role of Citrate Ions. *J. Am. Chem. Soc.* **2009,** 131, 13320-13327.
(11) Eugenii, K.; Itamar, W., Integrated Nanoparticle-Biomolecule Hybrid Systems: Synthesis, Properties, and Applications. *Angewandte Chemie International Edition* **2004,** 43, 6042-6108.
(12) Matsumura, Y.; Maeda, H., A New Concept for Macromolecular Therapeutics in Cancer Chemotherapy: Mechanism of Tumoritropic Accumulation of Proteins and the Antitumor Agent Smancs. *Cancer Res* **1986,** 46, 6387-6392.
(13) Vasir, J. K.; Reddy, M. K.; Labhasetwar, V. D., Nanosystems in drug targeting: Opportunities and challenges. *Current Nanoscience* **2005,** 1, 47-64.
(14) Perrault, S. D.; Walkey, C.; Jennings, T.; Fischer, H. C.; Chan, W. C. W., Mediating Tumor Targeting Efficiency of Nanoparticles Through Design. *Nano Letters* **2009,** 9, 1909-1915.
(15) Tredan, O.; Galmarini, C. M.; Patel, K.; Tannock, I. F., Drug Resistance and the Solid Tumor Microenvironment. *J. Natl. Cancer Inst.* **2007,** 99, 1441-1454.
(16) Tseng, C.-L.; Su, W.-Y.; Yen, K.-C.; Yang, K.-C.; Lin, F.-H., The use of biotinylated-EGF-modified gelatin nanoparticle carrier to enhance cisplatin accumulation in cancerous lungs via inhalation. *Biomaterials* **2009,** 30, 3476-3485.
(17) Hilgenbrink, A. R.; Low, P. S., Folate receptor-mediated drug targeting: From therapeutics to diagnostics. *Journal of Pharmaceutical Sciences* **2005,** 94, 2135-2146.
(18) Choi, C. H. J.; Alabi, C. A.; Webster, P.; Davis, M. E., Mechanism of active targeting in solid tumors with transferrin-containing gold nanoparticles. *Proceedings of the National Academy of Sciences* 107, 1235-1240.
(19) Pirollo, K. F.; Chang, E. H., Does a targeting ligand influence nanoparticle tumor localization or uptake? *Trends in Biotechnology* **2008,** 26, 552-558.
(20) Ruenraroengsak, P.; Cook, J. M.; Florence, A. T., Nanosystem drug targeting: Facing up to complex realities. *Journal of Controlled Release* **2010,** 141, 265-276.
(21) Nel, A. E.; Madler, L.; Velegol, D.; Xia, T.; Hoek, E. M. V.; Somasundaran, P.; Klaessig, F.; Castranova, V.; Thompson, M., Understanding biophysicochemical interactions at the nano-bio interface. *Nat Mater* **2009,** 8, 543-557.
(22) Comenge, J.; Sotelo, C.; Romero, F.; Gallego, O.; Barnadas, A.; Parada, T. G.-C.; Domínguez, F.; Puntes, V. F., Detoxifying Antitumoral Drugs via Nanoconjugation: The Case of Gold Nanoparticles and Cisplatin. *PLoS ONE* **2012,** 7, e47562.
(23) Dhar, S.; Gu, F. X.; Langer, R.; Farokhzad, O. C.; Lippard, S. J., Targeted delivery of cisplatin to prostate cancer cells by aptamer functionalized Pt(IV) prodrug-PLGAâ€“PEG nanoparticles. *Proceedings of the National Academy of Sciences* **2008,** 105, 17356-17361.
(24) de la Rica, R.; Aili, D.; Stevens, M. M., Enzyme-responsive nanoparticles for drug release and diagnostics. *Advanced Drug Delivery Reviews* **2012,** 64, 967-978.
(25) Daniel, M. C.; Astruc, D., Gold nanoparticles: Assembly, supramolecular chemistry, quantum-size-related properties, and applications toward biology, catalysis, and nanotechnology. *Chemical Reviews* **2004,** 104, 293-346.
(26) Comenge, J.; Romero, F. M.; Sotelo, C.; Dominguez, F.; Puntes, V., Exploring the binding of Pt drugs to gold nanoparticles for controlled passive release of cisplatin. *Journal of controlled release : official journal of the Controlled Release Society* **2010,** 148, e31-2.
(27) Craig, G. E.; Brown, S. D.; Lamprou, D. A.; Graham, D.; Wheate, N. J., Cisplatin-Tethered Gold Nanoparticles That Exhibit Enhanced Reproducibility, Drug Loading, and Stability: a Step Closer to Pharmaceutical Approval? *Inorganic Chemistry* **2012,** 51, 3490-3497.

(28) Wheate, N. J., Nanoparticles: the future for platinum drugs or a research red herring? *Nanomedicine* **2012,** 7, 1285-1287.
(29) Talmadge, J. E.; Singh, R. K.; Fidler, I. J.; Raz, A., Murine Models to Evaluate Novel and Conventional Therapeutic Strategies for Cancer. *The American Journal of Pathology* **2007,** 170, 793-804.
(30) Khlebtsov, N.; Dykman, L., Biodistribution and toxicity of engineered gold nanoparticles: a review of in vitro and in vivo studies. *Chemical Society Reviews* 40, 1647-1671.
(31) Lasagna-Reeves, C.; Gonzalez-Romero, D.; Barria, M. A.; Olmedo, I.; Clos, A.; Sadagopa Ramanujam, V. M.; Urayama, A.; Vergara, L.; Kogan, M. J.; Soto, C., Bioaccumulation and toxicity of gold nanoparticles after repeated administration in mice. *Biochemical and Biophysical Research Communications* **2010,** 393, 649-655.
(32) Size-dependent in vivo toxicity of PEG-coated gold nanoparticles Journal: International Journal of Nanomedicine Volume: 6 Issue: 1 Pages: 2071-2081 Date: 20 September 2011 Short Title: Size-dependent in vivo toxicity of PEG coated gold nanoparticles.
(33) Cho, W.-S.; Cho, M.; Jeong, J.; Choi, M.; Cho, H.-Y.; Han, B. S.; Kim, S. H.; Kim, H. O.; Lim, Y. T.; Chung, B. H.; Jeong, J., Acute toxicity and pharmacokinetics of 13 nm-sized PEG-coated gold nanoparticles. *Toxicology and Applied Pharmacology* **2009,** 236, 16-24.
(34) Abdelhalim, M.; Jarrar, B., Gold nanoparticles administration induced prominent inflammatory, central vein intima disruption, fatty change and Kupffer cells hyperplasia. *Lipids in Health and Disease* **2011,** 10, 133.
(35) Zhang, X.-D.; Wu, H.-Y.; Wu, D.; Wang, Y.-Y.; Chang, J.-H.; Zhai, Z.-B.; Meng, A.-M.; Liu, P.-X.; Zhang, L.-A.; Fan, F.-Y., Toxicologic effects of gold nanoparticles in vivo by different administration routes. *International Journal of Nanomedicine* **2010,** 5, 771-781.
(36) Chen, Y.-S.; Hung, Y.-C.; Liau, I.; Huang, G., Assessment of the In Vivo Toxicity of Gold Nanoparticles. *Nanoscale Research Letters* **2009,** 4, 858 - 864.
(37) Simpson, C. A.; Huffman, B. J.; Gerdon, A. E.; Cliffel, D. E., Unexpected Toxicity of Monolayer Protected Gold Clusters Eliminated by PEG-Thiol Place Exchange Reactions. *Chemical Research in Toxicology* **2010,** 23, 1608-1616.
(38) Rosenberg, B.; Vancamp, L.; Trosko, J. E.; Mansour, V. H., Platinum Compounds: a New Class of Potent Antitumour Agents. *Nature* **1969,** 222, 385-386.
(39) Wang, D.; Lippard, S. J., Cellular processing of platinum anticancer drugs. *Nat Rev Drug Discov* **2005,** 4, 307-320.
(40) Jung, Y.; Lippard, S. J., Direct Cellular Responses to Platinum-Induced DNA Damage. *Chemical Reviews* **2007,** 107, 1387-1407.
(41) Kelland, L., The resurgence of platinum-based cancer chemotherapy. *Nat Rev Cancer* **2007,** 7, 573-584.
(42) Reedijk, J., New clues for platinum antitumor chemistry: Kinetically controlled metal binding to DNA. *Proceedings of the National Academy of Sciences of the United States of America* **2003,** 100, 3611-3616.
(43) Oliver, T. G.; Mercer, K. L.; Sayles, L. C.; Burke, J. R.; Mendus, D.; Lovejoy, K. S.; Cheng, M.-H.; Subramanian, A.; Mu, D.; Powers, S.; Crowley, D.; Bronson, R. T.; Whittaker, C. A.; Bhutkar, A.; Lippard, S. J.; Golub, T.; Thomale, J.; Jacks, T.; Sweet-Cordero, E. A., Chronic cisplatin treatment promotes enhanced damage repair and tumor progression in a mouse model of lung cancer. *Genes & Development* 24, 837-852.
(44) Graham, M. A.; Lockwood, G. F.; Greenslade, D.; Brienza, S.; Bayssas, M.; Gamelin, E., Clinical Pharmacokinetics of Oxaliplatin: A Critical Review. *Clinical Cancer Research* **2000,** 6, 1205-1218.
(45) Soo Choi, H.; Liu, W.; Misra, P.; Tanaka, E.; Zimmer, J. P.; Itty Ipe, B.; Bawendi, M. G.; Frangioni, J. V., Renal clearance of quantum dots. *Nat Biotech* **2007,** 25, 1165-1170.
(46) DeConti, R. C.; Toftness, B. R.; Lange, R. C.; Creasey, W. A., Clinical and Pharmacological Studies with cis-Diamminedichloroplatinum(II). *Cancer Research* **1973,** 33, 1310-1315.

(47) Dhar, S.; Kolishetti, N.; Lippard, S. J.; Farokhzad, O. C., Targeted delivery of a cisplatin prodrug for safer and more effective prostate cancer therapy in vivo. *Proceedings of the National Academy of Sciences* **2011,** 108, 1850-1855.
(48) Farokhzad, O. C.; Cheng, J.; Teply, B. A.; Sherifi, I.; Jon, S.; Kantoff, P. W.; Richie, J. P.; Langer, R., Targeted nanoparticle-aptamer bioconjugates for cancer chemotherapy in vivo. *Proceedings of the National Academy of Sciences* **2006,** 103, 6315-6320.
(49) Moreno, D.; Zalba, S.; Navarro, I.; Tros de Ilarduya, C.; Garrido, M. J., Pharmacodynamics of cisplatin-loaded PLGA nanoparticles administered to tumor-bearing mice. *European journal of pharmaceutics and biopharmaceutics : official journal of Arbeitsgemeinschaft fur Pharmazeutische Verfahrenstechnik e.V* **2010,** 74, 265-74.
(50) Cheng, L.; Jin, C.; Lv, W.; Ding, Q.; Han, X., Developing a Highly Stable PLGA-mPEG Nanoparticle Loaded with Cisplatin for Chemotherapy of Ovarian Cancer. *PLoS ONE* **2011,** 6, e25433.
(51) Burger, K. N. J.; Staffhorst, R. W. H. M.; de Vijlder, H. C.; Velinova, M. J.; Bomans, P. H.; Frederik, P. M.; de Kruijff, B., Nanocapsules: lipid-coated aggregates of cisplatin with high cytotoxicity. *Nat Med* **2002,** 8, 81-84.
(52) [http://www.accesspharma.com/prolindac-content.shtml. (accessed on 2013-04-25)
(53) Feazell, R. P.; Nakayama-Ratchford, N.; Dai, H.; Lippard, S. J., Soluble Single-Walled Carbon Nanotubes as Longboat Delivery Systems for Platinum(IV) Anticancer Drug Design. *J. Am. Chem. Soc.* **2007,** 129, 8438-8439.
(54) Ajima, K.; Murakami, T.; Mizoguchi, Y.; Tsuchida, K.; Ichihashi, T.; Iijima, S.; Yudasaka, M., Enhancement of In Vivo Anticancer Effects of Cisplatin by Incorporation Inside Single-Wall Carbon Nanohorns. *ACS Nano* **2008,** 2, 2057-2064.
(55) Cheng, K.; Peng, S.; Xu, C.; Sun, S., Porous Hollow Fe3O4 Nanoparticles for Targeted Delivery and Controlled Release of Cisplatin. *J. Am. Chem. Soc.* **2009,** 131, 10637-10644.
(56) Huang, X.-L.; Zhang, B.; Ren, L.; Ye, S.-F.; Sun, L.-P.; Zhang, Q.-Q.; Tan, M.-C.; Chow, G.-M., In vivo toxic studies and biodistribution of near infrared sensitive Au-Au2S nanoparticles as potential drug delivery carriers. *Journal of Materials Science-Materials in Medicine* **2008,** 19, 2581-2588.
(57) Ren, L.; Chow, G. M., Synthesis of nir-sensitive Au-Au2S nanocolloids for drug delivery. *Materials Science and Engineering: C* **2003,** 23, 113-116.
(58) Ren, L.; Huang, X.-L.; Zhang, B.; Sun, L.-P.; Zhang, Q.-Q.; Tan, M.-C.; Chow, G.-M., Cisplatin-loaded Au-Au_2S nanoparticles for potential cancer therapy: Cytotoxicity, *in vitro* carcinogenicity, and cellular uptake. *Journal of Biomedical Materials Research Part A* **2008,** 85A, 787-796.

Chapter 2

Synthesis of Biocompatible Gold Nanoparticles with Control of the Size

2.1 Introduction

When using AuNPs for biological applications, special care has to be taken in the synthesis step since the size and size distribution play an important role in some biological responses such as biodistribution, time of circulation, and immune response among other. Moreover, the nanoparticles surface should be ready for further chemical modifications in order to finally link the drug.

The most common approach in the synthesis of AuNPs was introduced by Turkevich in 1951 and involved citrate reduction of a gold salt to produce 20 nm Au NPs with a relatively narrow size distribution.[1,2] This methodology, as well as subsequent modifications,[3] is based on supersaturation of the monomer in solution which induces homogenous nucleation followed by growth of these nuclei without additional nucleation events.[4] This "burst nucleation" is a necessary condition to obtain highly uniform nanoparticles.[5] Nevertheless, the range of Au NPs sizes available to obtain using these methods is small and goes from 7 nm to 25 nm. Frens proposed to decrease the citrate / $HAuCl_4$ ratio in order to increase the nanoparticle size up to 150 nm.[6] However, it has been recently demonstrated that this approach do not follow the "burst nucleation" mechanism and consequently monodispersity becomes poor, and also the spherical shape of the Au NPs is partially lost.[7] To overcome these limitations, a great number of synthetic protocols to achieve better control over the size and shape of nanoparticles have been developed during the last years.[5] Amongst them, the seeding-mediated strategies based on the temporal separation of nucleation and growth processes are considered very efficient

methods to obtain monodisperse NPs.[8-11] In this strategy, small particles are synthesized first and later used as seeds (nucleation centers) to grow larger NPs. For example, Murphy and coworkers proposed the use of a weak reducing agent (ascorbic acid), which reduces Au^{3+} to Au^{+} and prevented the total reduction to Au^{0} unless seeds are present.[12] By using this methodology additional nucleation that would lead to polidispersity is avoided. However, the use of CTAB as capping agent restricts the possibilities of further functionalization since their replacement by thiols is difficult to achieve.[13] This condition is especially important in nanomedicine, where the ability to render a biological functionality to inorganic nanostructures is one of the cornerstones of this emerging field.[14] In this context, citrate-stabilized AuNPs appear as unique candidates since the loosely bound capping layer provided by the sodium citrate can easily be exchanged by thiolated molecules that pseudo-covalently bind (~45 kcal/mol) to the gold surface.[15] However, the control of the size is complicated since the energy needed to form Au nuclei is not much higher than the needed to grow the NPs and therefore to separate nucleation from growth is not trivial. Obviously, the formation of new nuclei during growing stages would lead to a broadening of the size distribution and should be avoided in any seed growth approach.

In this chapter, a kinetically controlled seeded growth methodology to synthesize monodisperse citrate-stabilized gold nanoparticles from 8 to 200 nm will be discussed. By using this methodology, AuNPs of a desired size can be obtained with excellent control of the size (the relative standard deviation is not higher than 15 %) and secondary populations of particles are avoided.

2.2 Experiminetal

Synthesis of Gold Nanoparticles.

Synthesis of Au seeds. A solution of 2.2 mM sodium citrate in Milli-Q water (150 mL) was heated with a heating mantle in a 250 mL three-necked round-bottomed flask for 15 min under vigorous stirring. A condenser was utilized to prevent the evaporation of the solvent. 5 minutes after boiling had commenced, 1 mL of $HAuCl_4$ (25 mM) was injected. The color of the solution changed from yellow to bluish gray and then to red. The resulting particles (~10 nm, ~3 x 10^{12} NPs/mL) are coated with negatively charged citrate ions and hence are well suspended in H_2O.

Seeded growth of AuNPs of up to 30 nm in diameter. Immediately after the synthesis of the Au seeds and in the same vessel, the reaction was cooled until the temperature of the

solution reached 90 ^{0}C. Then, 1 mL of sodium citrate (60 mM) and 1 mL of a $HAuCl_4$ solution (25 mM) were sequentially injected (time delay ~2 min). After 30 min, aliquots of 2 mL were extracted for further characterization by transmission electron microscopy (TEM) and UV-Vis spectroscopy. By repeating this process (sequential addition of 1 mL of 60 mM sodium citrate and 1 mL of 25 mM HAuCl4), up to 14 generations of gold particles of progressively larger sizes were grown (further details in Scheme 2.1). The concentration of each generation of NPs was approximately the same as the original seed particles (~3 x 10^{12} NPs/mL).

Seeded growth of AuNPs of up to 180 nm in diameter. Immediately after the synthesis of the Au seeds and in the same reaction vessel, the reaction was cooled until the temperature of the solution reached 90 ^{0}C. Then, 1 mL of a HAuCl4 solution (25 mM) was injected. After 30 min, the reaction was finished. This process was repeated twice. After that, the sample was diluted by extracting 55 mL of sample and adding 53 mL of MQwater and 2 mL of 60mM sodium citrate (further details in Scheme 2.2). This solution was then used as a seed solution, and the process was repeated again. By changing the volume extracted in each growth step, it is possible to tune the seed particle concentration.

UV-Vis Spectroscopy. UV-visible spectra were acquired with a Shimadzu UV-2400 spectrophotometer. AuNPs solution (1 mL) was placed in a cell, and spectral analysis was performed in the 300 to 800 nm range at room temperature.

Transmission Electron Microscopy. Gold nanoparticles were visualized using 80 keV TEM (JEOL 1010, Japan). Ten microliter droplets of the sample were drop casted onto a piece of ultrathin Formvar-coated 200-mesh copper grid (Ted-pella, Inc.) and left to dry in air. TEM images of the prepared colloidal Au NPs were used for the size distribution measurements. For each sample, the size of at least 100 particles was measured and the average size and the standard distribution were obtained. ImageJ was used to perform the image analysis. ImageJ is open source free software, and the macro used here was developed by Dr. Ralph Sperling and can be found in Google docs free of charge at: https://docs.google.com/document/edit?id=1zNkzP5Ntan62CeRhABFzc2ZMcH8ZsUsC643M4f_YjDg

2.3 Results and discussion

2.3.1 Step by step seeding growth approach

It is important to understand the mechanism of AuNPs synthesis before introducing any variation of traditional methodologies to develop improved synthetic routes. Although several methods have been proposed for the bottom-up synthesis, the most popular one is the reduction of gold tetrachloroaurate ($HAuCl_4$) by sodium citrate.[1, 3] When reaction conditions are properly adjusted, a narrow size distribution is achieved. In those cases the size of AuNPs is controlled in a way similar to the concept introduced by LaMer of "burst nucleation",[16] in which many nuclei are generated at the same time, concentration of monomer dramatically decreases, and then they start to grow without any additional nucleation.[4] Because all particles nucleate almost simultaneously, their growth histories are nearly the same, resulting in monodisperse nanoparticles. Thus, the mechanism can be divided into two main stages: nucleation and growth of these nuclei. Hence, it can be assumed that to prepare highly uniform nanoparticles it is necessary to induce a single nucleation event and to prevent additional nucleation during subsequent growth steps.

In our first approach, we used previously synthesized AuNPs as nucleation centres for further growth after successive additions of gold salt (see scheme 2.1 and experimental section). The growth of the seeds is thermodynamically favored respect to the formation of new nuclei; additionally in previous results we observed a decrease of the nucleation rate when decreasing the temperature reaction. For those reasons, we expected that by decreasing the temperature 10 ^{0}C, the nucleation rate will be drastically decreased and hence the growth will be even more favored minimizing the possibility of new nucleation events.

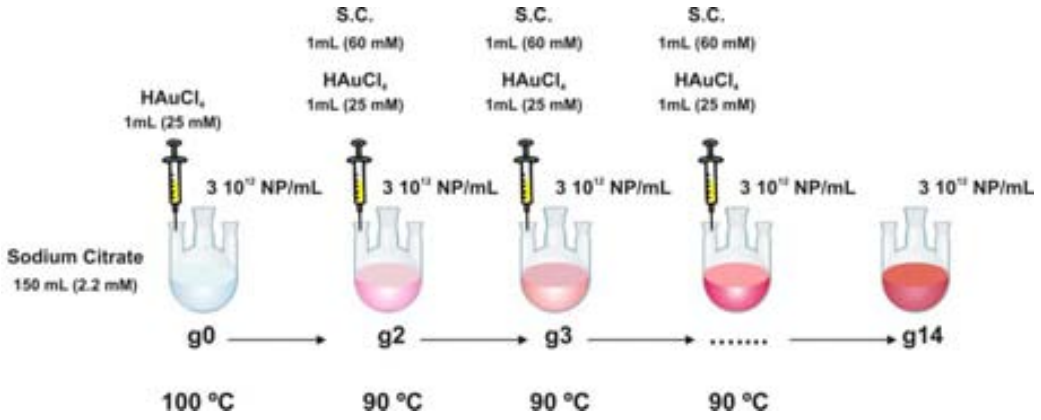

Scheme 2.1: Seeded Growth synthesis of Au NPs by subsequent injections of Au salt.

The success in the growth of the AuNPs by this methodology is observed in the Transmission Electron Microscopy (TEM) images of relevant samples (figure 2.1). The initial seeds were 12.4 ± 1.7 nm, and they were growth up to 30.5 ± 3.9 nm after 13 generations (a generation is the AuNPs resulting from a growth step). No secondary populations are observed in any case, which indicates that no additional nucleation events were occurred. Moreover, a narrow size distribution was maintained all over the subsequent generations.

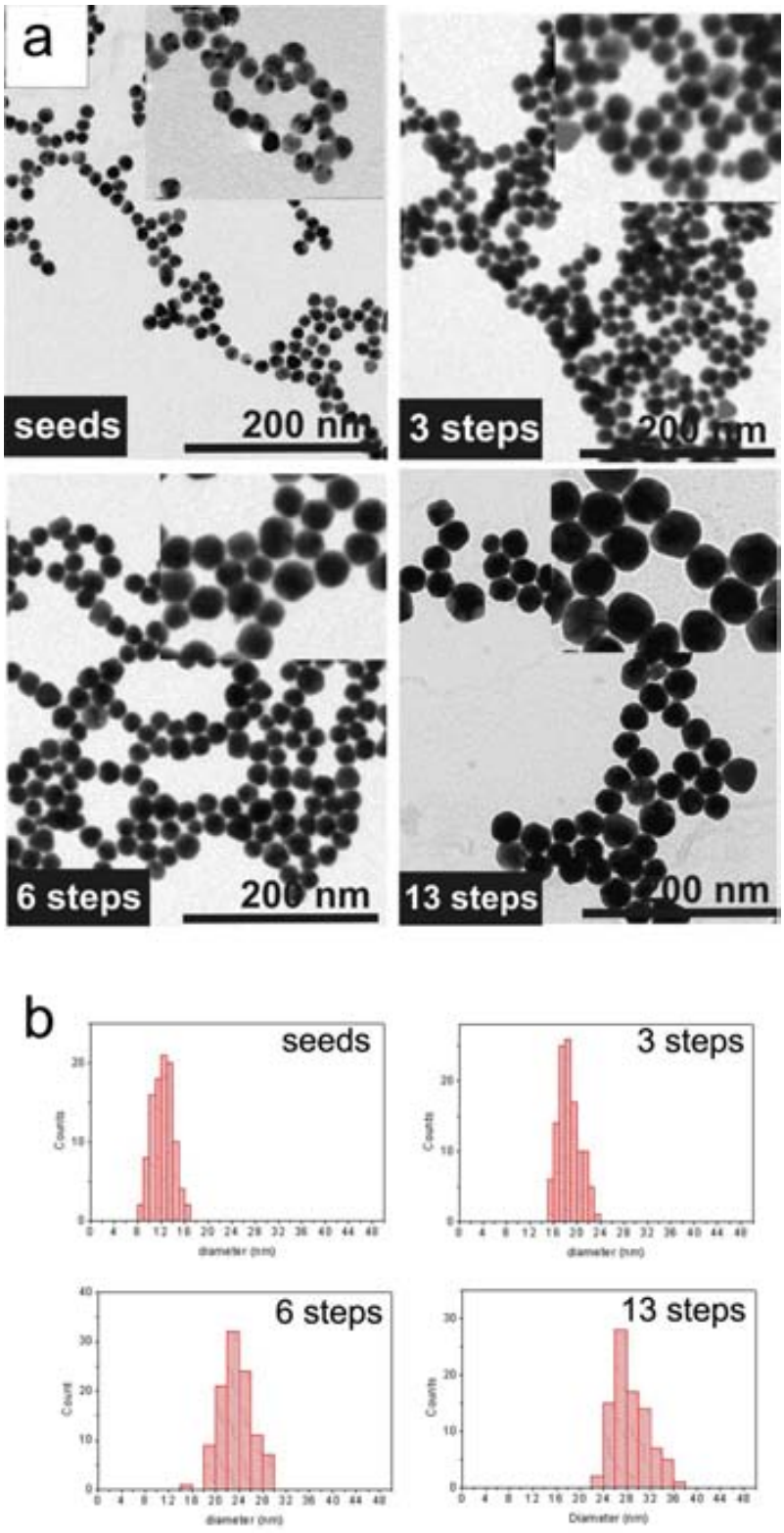

Figure 2.1. TEM characterization of relevant samples. (a) Representative TEM images of seeds, and AuNPs after 3, 6, and 13 growing steps. (b) The histograms showed the size distribution for these AuNPs. Mean sizes values are 12.4 ± 1.7 nm for the seeds, 18.7 ± 1.8 nm for the 3rd generation of AuNPs, 23.5 ± 2.5 nm for the 6th, and finally 30.5 ± 3.9 for the 13th .

Additionally, the growth process was monitored by UV-VIS spectroscopy (Figure 2.2). The 6.3 nm red-shift of the SPR peak as well as the increase in the intensity (from 0.336 to 4.52) is consistent with the Mie theory in which the λ_{max} as well as the intensity of the SPR increase with the volume of the AuNP.[3, 17] This is related to an increase of the extinction coefficient as AuNPs size increases.[18] Note that the first generations are not very sensitive to changes on the λ_{max}. This deviation for smaller NPs has been reported elsewhere[18].

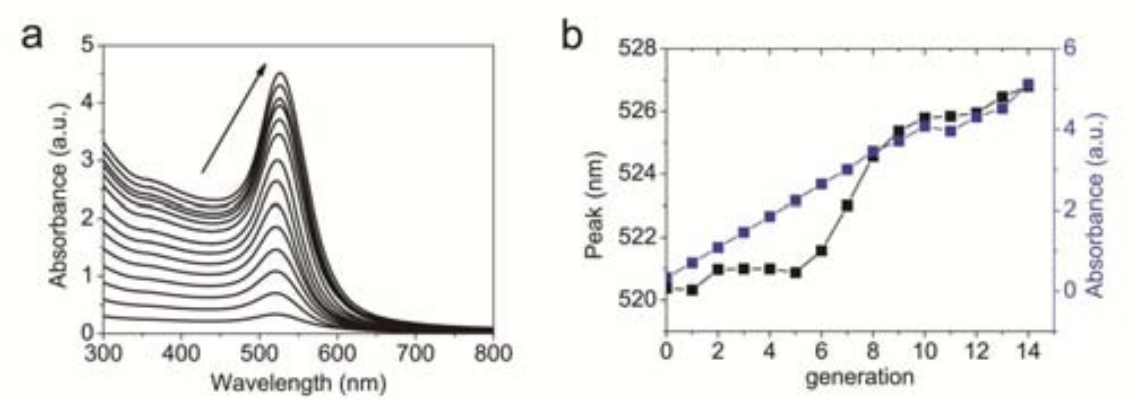

Figure 2.2. UV-VIS monitorization of the growing steps. A red-shift of the SPR peak and a progressive increase of the Absorbance were observed. This is in agreement with the Mie theory in which the extinction coefficient increases with the volume of the metallic NP.

The pH control is an important point here since each growth step involves the reduction of $HAuCl_4$ by citrate.[7] Protons are formed in the first stage of this reaction[19,20]:

$$\begin{cases} C_6H_5O_7^{3-} \rightarrow C_5H_4O_5^{2-} + CO_2 + 2e^- + \mathbf{H^+} \\ AuCl_4^- + 2e^- \rightarrow AuCl_2^- + 2\,Cl^- \end{cases}$$

This step is followed by the disproportionation of aurous species to gold atoms. This later step does not affect the pH values. To compensate the decrease of pH, an extra amount of sodium citrate is needed in every growth step in order to buffer the solution. In fact, a parallel experiment was carried out without the addition of this extra-amount of sodium citrate and the pH after each generation was measured (Figure 2.3). It is observed a constant decrease of 0.3 units of pH after each generation of NPs achieving a value of 3.14 after 14 generations. At this point, the AuNPs precipitated. This can be explained by considering the pKa values of sodium citrate (6.4, 4.8 and 3.2). Since at pH 3.14 all the carboxylic groups from citrate are protonated, the electrostatic interactions cannot maintain particles stable in solution. Thus, the amount of sodium citrate added in each

growth step (1mL, 60mM) was the experimentally determined in order to keep a constant pH ~7 during the whole growth process.

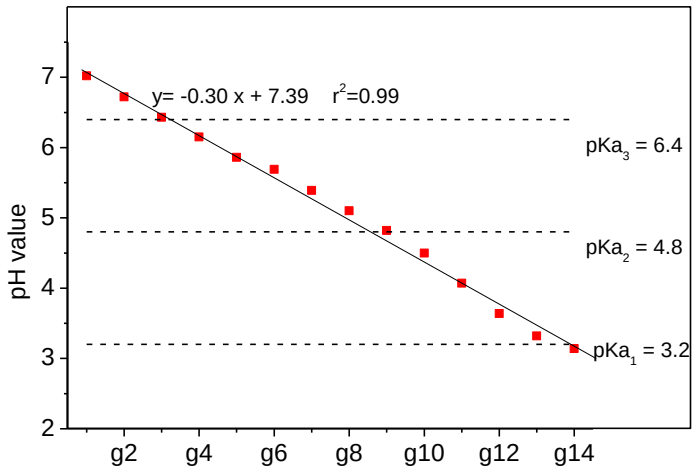

Figure 2.3 pH values after each growing step and pKa values of sodium citrate (6.4, 4.8 and 3.2). When solution pH is lower than pKa_1 value for sodium citrate, all its carboxylic groups are protonated and hence electrostatic interactions cannot keep particles stable in solution, leading to immediate irreversible aggregation.

2.3.2 Growth after dilution of the seeds

Considering that all the gold is consumed by the reaction (confirmed by ICP-MS), that the particles are spherical and finally that no secondary nucleation events take place; it is possible to estimate the final size of the AuNPs by a simple approach based on the known amount of Au added and on the weight of a AuNP.

$$\text{Weight of a NP} = \text{weight of a seed} + \frac{\text{weight Au added}}{n^o\ seeds}$$

$$V_{NP} \cdot \rho_{Au} = (V_{seed} \cdot \rho_{Au}) + \frac{\text{weight Au added}}{n^o\ seeds}$$

$$(4/3\ \pi\ r_{NP}^3) \cdot \rho_{Au} = (4/3\ \pi\ r_{seed}^3) \cdot \rho_{seed} + \frac{\text{weight Au added}}{n^o\ seeds}$$

$$r_{NP}^3 = {}^3/_4 \frac{\text{weight Au added}}{\pi \rho_{Au} \; n^o \, seeds} + r_{seed}^3 \quad \textbf{(equation 2.1)}$$

Where V_{NP} is the volume of a NP, is ρ_{Au} gold density, r_{NP} is the radius of the NP.

According to this theoretical approach, the amount of gold needed to obtain 50 nm AuNPs from 10 nm seeds at 3.2 x 10^{12} NP/mL would be the equivalent of 125 consecutive injections. One could think on the addition of a higher amount of gold in each injection. Unfortunately, this would not be possible because the ratio seeds to gold monomer should be kept between a certain range to avoid secondary nucleation (vide infra). Thus, the previous growth protocol was modified by the addition of a dilution step every three additions of $HAuCl_4$ as shown in scheme 2.2. The advantage of this approach is that one can synthesize large AuNPs in a few steps and without compromising the stability and the monodispersity of the NPs. AuNPs were grown up to 14 growing steps and all the generations analyzed by TEM and UV-VIS. Representative images of every step are shown in figure 2.4. It is observed that the monodispersity is maintained in all the samples as well as the absence of secondary populations. AuNPs were grown from the initial seeds (8.4 ± 1.0 nm) to the 14th generation (180.5 ± 10.7 nm). We decided to stop the synthesis here, but, in principle, there is no reason against keep growing these AuNPs. Although, the NPs are rather faceted and thus not perfectly spherical, the growth is very uniform, avoiding formation of elongated NPs such as the ones obtained by the Frens approach.[6]

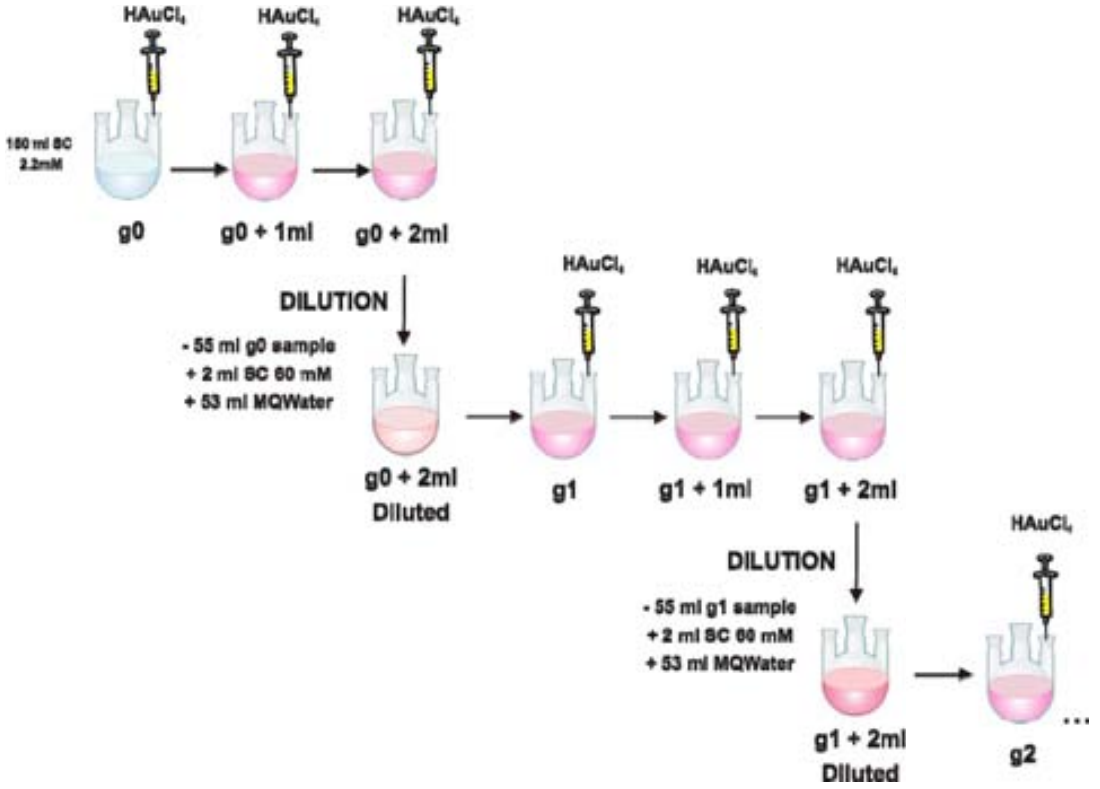

Scheme 2.2 Seeded growth synthesis of AuNPs up to 180 nm. Dilution steps were introduced in this approach to facilitate the growth to larger sizes.

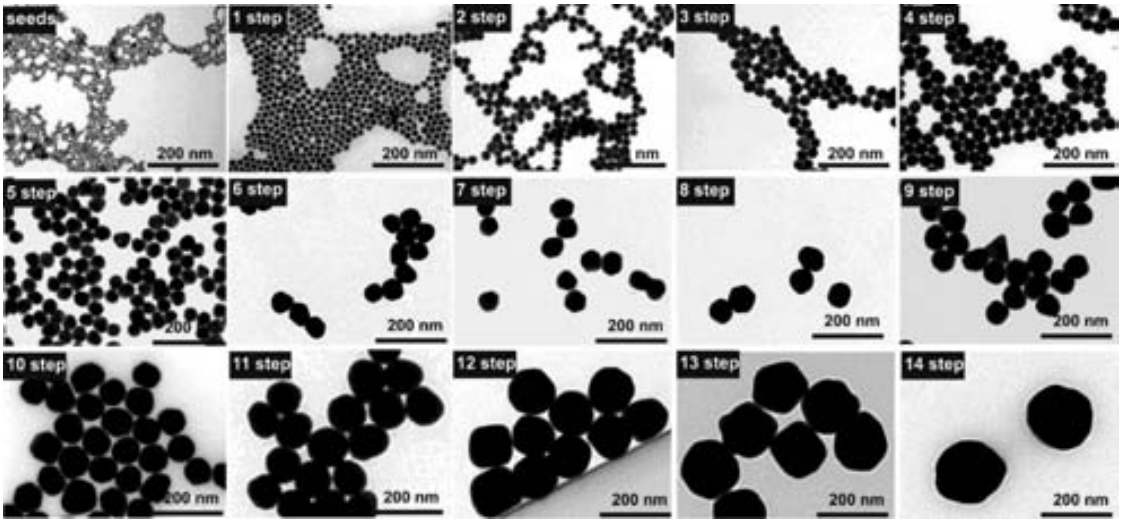

Figure 2.4 Representative TEM images of every growth step. Monodispersity and absence of secondary populations are maintained all over the process. The morphology of the AuNPs is quasi-spherical in all cases avoiding the formation of elongated AuNPs.

A summary of sizes and size distributions, as well as SPR peak position is provided in table 2.1. Obviously, the final concentration of AuNPs depends on the dilution factor applied (95/150 in our case). As expected, a detailed analysis of the SPR position revealed a linear behavior due to the dependence of the peak position on the volume of the NPs.[18] This tendency is however disrupted for AuNPs larger than 100 nm, in which appears a quadrupolar component of the SPR. Note that standard deviation is never higher than 10 % of mean value except for the seeds. Note also that the actual size of the AuNPs is quite similar to the theoretical size calculated as explained above (equation 2.1). Thus the presumptions made to calculate the formula (sphericity, all the added gold is consumed, and no secondary populations) are likely accomplished.

Growth step	Diameter ± sd (nm)	sd (%)	Concentration (NPs/mL)	SPR peak (nm)	Theoretical Diameter
Seeds	8.4 ± 1.0	11.9	3.0×10^{12}	518	
1st	17.6 ± 1.2	6.8	1.9×10^{12}	521.5	18.2
2nd	22.3 ± 2.2	9.8	1.2×10^{12}	523.5	24.5
3rd	31.1 ± 2.8	9.0	7.6×10^{11}	525.5	30.4
4th	36.0 ± 2.4	6.6	4.8×10^{11}	527.5	36.7
5th	42.2 ± 2.3	7.8	3.1×10^{11}	530.5	43.7
6th	54.4 ± 3.3	6.1	1.9×10^{11}	535	51.5
7th	64.8 ± 3.4	5.2	1.2×10^{12}	540	60.5
8th	69.3 ± 4.5	6.5	7.8×10^{10}	542.5	70.7
9th	80.1 ± 5.4	6.7	4.9×10^{10}	546.5	82.6
10th	96.1 ± 5.6	5.8	3.1×10^{10}	555.5	96.4
11th	109.2 ± 7.6	6.9	2.0×10^{10}	574.5	112.4
12th	123.6 ± 10.6	8.6	1.2×10^{10}	606	131.0
13th	150.0 ± 9.9	6.6	7.9×10^{9}	649	152.6
14th	180.5 ± 10.7	5.9	5.0×10^{9}	720	177.8

Table 2.1 Summary of sizes, concentration and SPR peak position of AuNPs after 14 consecutive growing steps. The theoretical size is also shown.

2.3.3 Variation of seed and gold salt concentrations

From the results above, it is observed that the final size of the nanoparticles will depend on the amount of seeds and gold added in solution. Taking into account these two parameters, it seems possible to obtain AuNPs of a desired size. In this section, we explore how these parameters affect the resultant AuNPs.

Firstly, the effect of seed concentration on the size of AuNPs after a growing step was studied using 17.0 ± 1.7 nm seeds at concentrations ranging from 4.18×10^{11} NP/mL to 8.36×10^{10} NP/mL. The final volume (75 mL) and the amount of gold precursor added (0.5 mL, 25 mM $HAuCl_4$) were the same in all cases. Size and size distribution were analyzed by TEM imaging and they are showed in figure 2.5 (black squares). As expected, the higher is the concentration of seeds, the smaller is the growth of the resultant NPs. Hence, 23.3 ± 1.7 nm AuNPs were obtained at the highest concentration (4.18×10^{11} NP/mL), whilst 36.6 ± 4.4 nm AuNPs were obtained when 5 times less seeds were added. It is also observed the fitting of the empirical values with the ones predicted using the equation 2.1. Also note the greater increase in the size for high dilutions of the seeds. Thus, one could think that a high dilution of seeds could lead to large AuNPs. However, it should be taken into account that new nucleation events must be avoided to get a single population of AuNPs with narrow size distribution. This cannot be ensured when very few AuNPs are present in solution. In fact, at the lower concentration assayed here a small percentage of a secondary population of AuNPs appeared. Therefore the addition of subsequent growth steps seems to be the appropriate strategy to get larger AuNPs. Additionally, it is shown here the great control of the process and the ability to get AuNPs of a desired size. Obviously, it is necessary to know previously both the size and the concentration of the seeds to make the required calculations.

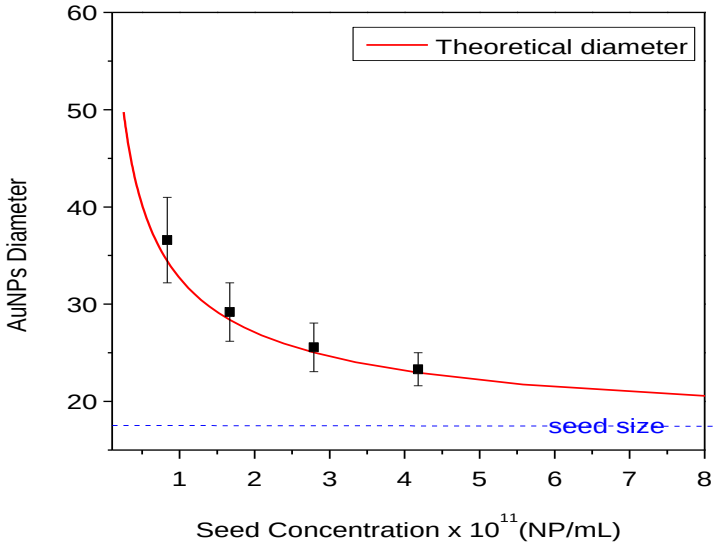

Figure 2.5 Theoretical and empirical AuNPs diameter in function of the concentration of seeds. The final size depends on the concentration of seeds added. It is observed here how the empirical values match satisfactorily the theoretical value.

The other component of this system that can be modified is the amount of $HAuCl_4$ added in a growth step. We followed a similar strategy to analyze the role played by the precursor: The concentration of 17.0 ± 1.7 nm seeds was kept constant (1.71 x 10^{11} NP/mL), whilst the concentration of $HAuCl_4$ was varied from 0.022 mM to 0.334 mM. The size of the resultant AuNPs, as measured by TEM, as well as the predicted value are shown in table 2.2. Obviously, the size of the AuNPs increased as the amount of gold precursor increased. Here, the predicted size calculated from equation 2.1 also matches the empirical value. However, a secondary population of small AuNPs was clearly observed when the highest concentration of $HAuCl_4$ was assayed. Thus, new nucleation of NPs was not avoided in the case of the highest $HAuCl_4$ concentration and consequently the monodispersity of this sample was lost. This can be also observed analyzing the SPR peak shift: The peak shifts to higher values as long as the amount of gold added increases, but at 0.334 mM the peak shifts to a smaller wavelength indicating the deficient growth of the AuNPs. Since part of the Au added was consumed by the formation of new AuNPs, which in addition competed with the initial seeds for the remaining Au, the resultant AuNPs are polydisperse with an unpredictable size. Hence, it is important to add the precursor in successive steps instead of a single one which would increase the concentration of precursor too much causing new nucleation.

$HAuCl_4$ (mM)	Size (nm)	Theoretical size (nm)	SPR peak (nm)
0.022	19.5 ± 2.1	19.3	519.9
0.083	24.7 ± 2.1	23.9	522.1
0.167	28.6 ± 2.7	28.2	524.1
0.334	xxx	34.2	522.2

Table 2.2 Size of AuNPs depending on the amount of gold added.

Summarizing, it has been demonstrated here the possibility to obtain AuNPs of a desired size just by adjusting the amounts of seeds and $HAuCl_4$ according to a simple theoretical approach. The less seeds and the higher amount of gold added, the larger are the resultant AuNPs. However, the variation of both components should be in a certain range to avoid new nucleation events and therefore the formation of a secondary population of AuNPs. Thus, a range of sizes can be obtained in a single step by adjusting these two parameters, but a subsequent synthesis step should be introduced if larger AuNPs are desired. For example, starting with 17 nm seeds it is easy to obtain AuNPs *à la carte* from 18 to 35 nm, but if larger AuNPs are desired, an additional synthesis step (normally implying dilution of the AuNPs) will be required.

2.4 Conclusions

The control of the size and morphology of NPs are key points in the synthesis of inorganic NPs. In the field of biomedicine, and specifically in the use of AuNPs as scaffolds for drug delivery, achieving a great control over the synthesis is recommended since some important properties such as biodistribution are strongly influenced by the size of the scaffold rather than by the composition. In fact, size effects are paramount at the nanoscale.

Here it has been demonstrated that the synthesis of AuNPs is very well controlled in terms of morphology, size and size distribution. Our approach is based on a seeding growth synthesis due to the fact that the growth of AuNPs is to some extend thermodynamically favored respect to the formation of Au nuclei. To even favor more the growth, the temperature was decreased to 90 ^{0}C instead of the 100 ^{0}C required for the synthesis of new AuNPs. AuNPs up to 30 nm can be synthesized by successive growing steps of $HAuCl_4$.

The pH control has been shown to be crucial to maintain colloidal stability, since protons are formed in every growth step. To obtain AuNPs up to 180 nm, dilution steps were introduced to minimize the consumption of Au. In addition, it has been shown the possibility to nicely control the final size of AuNPs by adjusting the amounts of either seeds or gold precursor. The separation of nucleation and growth is the main factor that determines the success of the synthesis and therefore must be always accomplished if monodispersity is wanted.

2.5 References

(1) Turkevich, J.; Garton, G.; Stevenson, P. C., The Color of Colloidal Gold. *Journal of Colloid Science* **1954,** 9, S26-S35.
(2) Daniel, M. C.; Astruc, D., Gold nanoparticles: Assembly, supramolecular chemistry, quantum-size-related properties, and applications toward biology, catalysis, and nanotechnology. *Chemical Reviews* **2004,** 104, 293-346.
(3) Kimling, J.; Maier, M.; Okenve, B.; Kotaidis, V.; Ballot, H.; Plech, A., Turkevich Method for Gold Nanoparticle Synthesis Revisited. *The Journal of Physical Chemistry B* **2006,** 110, 15700-15707.
(4) Polte, J.; Ahner, T. T.; Delissen, F.; Sokolov, S.; Emmerling, F.; Thünemann, A. F.; Kraehnert, R., Mechanism of Gold Nanoparticle Formation in the Classical Citrate Synthesis Method Derived from Coupled In Situ XANES and SAXS Evaluation. *J. Am. Chem. Soc.* **2010,** 132, 1296-1301.
(5) Park, J.; Joo, J.; Kwon, S. G.; Jang, Y.; Hyeon, T., Synthesis of monodisperse spherical nanocrystals. *Angewandte Chemie-International Edition* **2007,** 46, 4630-4660.
(6) Frens, G., Controlled Nucleation for Regulation of Particle-Size in Monodisperse Gold Suspensions. *Nature-Physical Science* **1973,** 241, 20-22.
(7) Ji, X. H.; Song, X. N.; Li, J.; Bai, Y. B.; Yang, W. S.; Peng, X. G., Size control of gold nanocrystals in citrate reduction: The third role of citrate. *J. Am. Chem. Soc.* **2007,** 129, 13939-13948.
(8) Perrault, S. D.; Chan, W. C. W., Synthesis and Surface Modification of Highly Monodispersed, Spherical Gold Nanoparticles of 50â˜200 nm. *Journal of the American Chemical Society* **2009,** 131, 17042-17043.
(9) Bigall, N. C.; Halrtling, T.; Klose, M.; Simon, P.; Eng, L. M.; Eychmuller, A., Monodisperse Platinum Nanospheres with Adjustable Diameters from 10 to 100 nm: Synthesis and Distinct Optical Properties. *Nano Letters* **2008,** 8, 4588-4592.
(10) Jana, N. R.; Gearheart, L.; Murphy, C. J., Evidence for seed-mediated nucleation in the chemical reduction of gold salts to gold nanoparticles. *Chemistry of Materials* **2001,** 13, 2313-2322.
(11) Bastús, N. G.; Comenge, J.; Puntes, V. c., Kinetically Controlled Seeded Growth Synthesis of Citrate-Stabilized Gold Nanoparticles of up to 200 nm: Size Focusing versus Ostwald Ripening. *Langmuir* **2011,** 27, 11098-11105.
(12) Jana, N. R.; Gearheart, L.; Murphy, C. J., Seeding growth for size control of 5-40 nm diameter gold nanoparticles. *Langmuir* **2001,** 17, 6782-6786.
(13) Leonov, A. P.; Zheng, J.; Clogston, J. D.; Stern, S. T.; Patri, A. K.; Wei, A., Detoxification of Gold Nanorods by Treatment with Polystyrenesulfonate. *Acs Nano* **2008,** 2, 2481-2488.
(14) Eugenii, K.; Itamar, W., Integrated Nanoparticle-Biomolecule Hybrid Systems: Synthesis, Properties, and Applications. *Angewandte Chemie International Edition* **2004,** 43, 6042-6108.

(15) Sellers, H.; Ulman, A.; Shnidman, Y.; Eilers, J. E., Structure and binding of alkanethiolates on gold and silver surfaces: implications for self-assembled monolayers. *J. Am. Chem. Soc.* **1993,** 115, 9389-9401.
(16) LaMer, V. K.; Dinegar, R. H., Theory, Production and Mechanism of Formation of Monodispersed Hydrosols. *Journal of the American Chemical Society* **1950,** 72, 4847-4854.
(17) Haiss, W.; Thanh, N. T. K.; Aveyard, J.; Fernig, D. G., Determination of Size and Concentration of Gold Nanoparticles from UV−Vis Spectra. *Analytical Chemistry* **2007,** 79, 4215-4221.
(18) Njoki, P. N.; Lim, I. I. S.; Mott, D.; Park, H.-Y.; Khan, B.; Mishra, S.; Sujakumar, R.; Luo, J.; Zhong, C.-J., Size Correlation of Optical and Spectroscopic Properties for Gold Nanoparticles. *The Journal of Physical Chemistry C* **2007,** 111, 14664-14669.
(19) Kumar, S.; Gandhi, K. S.; Kumar, R., Modeling of Formation of Gold Nanoparticles by Citrate Method&#x2020. *Industrial & Engineering Chemistry Research* **2007,** 46, 3128-3136.
(20) Young, J.; Lewinski, N.; Langsner, R.; Kennedy, L.; Satyanarayan, A.; Nammalvar, V.; Lin, A.; Drezek, R., Size-controlled synthesis of monodispersed gold nanoparticles via carbon monoxide gas reduction. *Nanoscale Research Letters* **2011,** 6, 1-11.

Chapter 3

Conjugation of AuNPs to Achieve Stable and Functional Scaffolds for Drug Delivery

3.1 Introduction

The world of NPs and the world of cells and biomolecules are quite different and often incompatible. Functionalization of NPs surface is our tool to interact at the nano-bio interface.[1] Thus, engineering properly the AuNPs surface is a crucial step to determine the final fate of the AuNPs since it will provide the functionality of interest and it will determine important properties such as surface charge and stability.

A great variety of chemical groups such as thiols, amines, phosphates or carboxylic acids have affinity to the AuNPs surface.[2] This versatility allows the functionalization with different molecules such as organic molecules, proteins, DNA, polymers, etc.[3] Among all the possible links, the SH-Au bond is the most widely exploited due to its pseudo-covalent character (≈45 Kcal/mol)[4], this high bond strength allow the exchange with other ligands which bind Au more weakly such as citrate, amines, or phosphates. In addition, the high strength makes the bond very stable over the time. Thus, the use of thiolated molecules is a common strategy to functionalize AuNPs. Examples of this strategy includes conjugation with alkanethiols,[5] thiolated DNA,[6] proteins or peptides containing a superficial cysteine residue,[7] and polymers with a terminal SH group.[8] Alkanethiolates, such as 11-mercaptoundecanoic acid (MUA), have been largely used to obtain self-assembled monolayers (SAM) onto Au surfaces[9] due to the presence of a thiol and a hydrophobic chain which allow a very compact packing of the layer. In addition, a terminal group gives the desired functionality and/or charge to the AuNPs. This is of special importance since

some of their biological properties such as potential toxicity or cell uptake are dramatically influenced by the surface charge given by this layer.[10] Moreover, the presence of terminal groups allows further conjugation steps. For example, EDC coupling or other click chemistry processes between the monolayer and a molecule of interest have been largely studied.[11] Other strategies of functionalization are based on a non-specific absorption of molecules onto the AuNP surface. These include unspecific absorption of protein as in the case of the well-known protein corona[12, 13], or weak interactions with chemical groups such as phosphates from a DNA strand or OH groups from polymers such as PEG, amongst others.[1] In this case the link with the AuNPs is weaker than it was for thiolated molecules.

Interestingly, by mixing AuNPs and surfactant molecules, AuNPs conjugates with a specific functionality can be properly inserted in the biological machinery. However, it is worth noting here that minute differences on the resulting conjugate, often ignored, might have a dramatic impact in the biological response of the system exposed to some determined AuNPs.[14, 15] Taking into account that nanoparticles for biomedical applications are reaching a high level of complexity, the fine control and understanding of the conjugate composition is required to not halt the development of new products. Thus, factors such as conformational changes of the coating molecules or small variations of classic behavior induced by the nanoscale have to be considered before using the nanoparticle: For example, the curvature radius of the AuNPs modifies the pKa of attached alkanethiolates,[16] thus two AuNPs with the very same composition might be stable or not at a specific pH depending on the size of the AuNPs. Also, a change on the conformation of components of the monolayer (e.g. PEG), rather than in the composition, modifies dramatically the biological properties of the conjugate.[15]

In this chapter, we carefully examine the conjugation of two widely used molecules (MUA and SH-PEG) to the surface of AuNPs and the design of mixed layers whose properties can be tuned depending on the composition of the layer and the conjugate architecture (global conformation of the ligands). We also propose methods and principles to control the conjugation and to characterize (physically, chemically and biologically) the resulting conjugates and their evolution in physiological conditions. Also, a study to determine how the layer composition influences the protein binding is showed. Note that the first step on tuning NP-cell interactions is to control this protein binding. This is of special relevance, since these are the conjugates that will be used as scaffolds for drug delivery in following chapters.

3.2 Experimental

MUA Self-Assembled Monolayer on AuNPs. Different concentrations of MUA from 0 to 60 μM were added to 20 nm AuNPs (21.3 ± 3.3 nm, 5.0 x10^{11} NP/mL) and 40 nm AuNPs (39.3 ± 4.3 nm, 9.0 x10^{10} NP/mL) solution by adding corresponding volumes of 1mM or 5 mM MUA aqueous solution. Differences of volume were compensated by addition of miliQ water. The conjugation was gently stirred for 21 hours (an aliquote was taken and immediately measured at 30 minutes as well). UV-VIS spectra from 300 to 800 nm were taken for every sample at 30 minutes and 21 hours.

SH-PEG Self-Assembled Monolayer on AuNPs: Different concentrations of SH-PEG (3.4 KDa) from 0 to 15 mM were added to 20 nm AuNPs (21.3 ± 3.3 nm, 5.0 x10^{11} NP/mL) by adding corresponding volumes of 1 mM SH-PEG aqueous solution. Differences of volume were compensated by addition of miliQ water. The conjugation was gently stirred overnight. UV-VIS spectra from 300 to 800 nm were taken for every sample.

Mixed layer-AuNPs obtained by co-conjugation. The different SH-PEG / MUA ratios were prepared by mixing the corresponding volumes of 1mM (or 0.3 mM, or 0.1 mM) solution of each component. 500 μL of these mixtures were subsequently added to 4 mL of AuNPs as synthesized (14.6 ± 1.5 nm, 4.2 x 10^{12} NP/mL) and gently stirred overnight. The SPR bands of the resulting conjugates were analyzed by UV-VIS spectroscopy at the range of 300 to 800 nm. The hydrodynamic diameter was analyzed by DLS.

Mixed layer-AuNPs obtained by ligand exchange. An aqueous solution of SH-PEG (125 μL, 0.3 mM) was added to 1 mL citrate-stabilized AuNPs (15.2 ± 2.0 nm, 3.7 x 10^{12} NP/mL). The conjugation was allowed to run for 6 hours. Then, the excess of SH-PEG was removed by 2 centrifugation cycles (18000 rcf, 30 min) and resuspension of AuNPs in fresh water. Finally, different amounts of MUA (0 to 80 μM) were added to the solution and the agitation was maintained overnight. The resulting AuNPs were analyzed by UV-VIS spectroscopy and DLS.

Quantification of the SH-PEG-FITC loaded on the AuNPs by fluorescence. The excess of SH-PEG-FITC and MUA was removed by 3 centrifugation steps (30000 rcf, 30 min). After the last washing step, AuNPs were suspended in the same volume of an aqueous NaCN solution (100 mM) and stirred for 6h at 37 ºC. The total dissolution of AuNPs was proved by the disappearance of the SPR. All the samples were buffered using CAPS (25 mM, pH 10.6). Known concentrations of SH-PEG-FITC under the same conditions were used to do the calibration curve. 100 μL of standards and samples were loaded in a 96-

well plate and the fluorescence spectra (λ_{ex}=494, λ_{em}=521) was taken. The concentration of SH-PEG-FITC in the samples was calculated from the calibration curve.

Quantification of the SH-PEG-FITC by absorbance. AuNPs were removed from the sample by 3 centrifugation steps (30000 g, 30 min). Centrifugation conditions were more aggressive here to ensure that all the NPs were removed. 25 μL of CAPS buffer (200 μM, pH 10.6) were aded to 975 μL of the resulting supernatant. To prepare the standards the same procedure than the explained above to functionalize the AuNPs was followed but using sodium citrate 2.2 mM instead of the AuNPs solution. The absorbance of standards and samples were measured under the same conditions. The amount of SH-PEG-FITC loaded on the AuNPs was calculated substracting the concentration of the sample from the concentration of the standard.

Stability in physiological and acidic media. AuNPs functionalized with MUA and SH-PEG were concentrated to 2.4 x 10^{14} NP/mL by centrifugation (18000 rcf, 14 min.) of 1 mL of AuNPs and resuspension of the pellet in a final volume of 20 μl. Then these 20 μl were added to 180 μl of DMEM supplemented with 10 % FBS and softly mixed during 30 minutes. To assay the stability in acidic media, 1 mL of previously functionalized AuNPs were brought to pH 2.6 by adding 2.5 μL of a 0.2 M glycine/HCl buffer. The stability in both cases was evaluated by analyzing the broadening and the red-shift of the SPR band.

Protein adsorption. 1.3 mM solution of bovine serum albumin was prepared by diluting 182 mg in 2.1 mL of 5 mM Hepes buffer at pH 7.5. Then 7.7 μL of this solution was added to 1 mL of previously functionalized AuNPs and softly mixed overnight. The changes of the hydrodynamic diameter were analyzed by DLS and the shift of the SPR band by UV-VIS.

Gel electrophoresis. AuNPs were functionalized with relevant ratios of SH-PEG / MUA (0, 0.3, 0.6, 0.74, 0.88, 0.96, and 1) as explained above. Then the samples were splitted in two parts. 1 mL was incubated with 7.7 μL of a 1.3 mM BSA solution in 5 mM Hepes buffer (pH 7.5) overnight and the other part was kept without any modification. Samples were loaded into the wells of a 1% agarose gel.The electrophoresis was run under 60 V in a sodium borate buffer (30 mM, pH 8.5).

3.3 Results and discussion

3.3.1 MUA Self-Assembled Monolayers onto AuNPs.

The choice of MUA to study the formation of SAM onto AuNPs is not trivial. The presence of a terminal thiol group, the relatively long (11 C) hydrocarbon chain, and the carboxylic acid at the other side of the molecule make it a model candidate to form highly stable SAMs. In addition, the presence of the carboxylic groups will allow a further step of cisplatin loading via a coordination bond (see chapter 4).

To understand the formation of MUA SAMs onto AuNPs, different amounts of MUA were added to a solution of AuNPs (21.3 ± 3.3 nm, 5.0 $x10^{11}$ NP/mL) and the shift of the SPR analyzed by UV-VIS. The position of the SPR of the AuNPs after MUA addition is determined by changes in the local refractive index around the NP due to changes in the density of the monolayer which is determined by the concentration of ligand on the surface.[17, 18] Thus, the denser is the layer, the higher is the shift. This is observed in figure 3.1 in which the position of the peak is represented in function of the concentration of MUA added. The SPR varies following a sigmoidal curve, typical of processes involving adsorption on a surface at constant temperatures (e.g. Langmuir isotherms).[19] From this curve, the saturation point, or the point at which adding more MUA causes no change in the SPR peak is determined at approximately 15 μM for the analyzed AuNPs. Taking into account the footprint of MUA in gold, which is reported to be 0.21 nm^2,[4] it can be easily calculated that the amount of MUA needed to completely cover these AuNPs would be 7.25 μM. Thus, at least a 2-fold excess of MUA is needed to be added in this case to ensure a saturation of the monolayer. This excess of ligand is low compared to unspecific and weaker bindings such as the proteins absorbed onto AuNPs, in which excess as high as 5 to 10 times the theoretical amount are required to saturate the surface.[20, 21] Interestingly, there is a slight increase of the peak observed after 21h. This fact, which has been also described in SAMs on Au planar surfaces,[22] it is attributed to an internal slow reorganization of the monolayer, to maximize the surface coverage, and consequently minimize the free surface energy. The differences between 30 minutes and 21 hours are greater for higher MUA excess than for low concentrations. At concentrations much lower than saturation, most of the added MUA is rapidly attached to the highly available surface and therefore the final state (or a very close state) is rapidly reached. On the other side, since the surface is densely occupied at high concentrations of MUA at short times, there is a need of reorganization of the layer before more MUA could be attached. This reorganization is a slow process which is not completed after the first 30 minutes, but

hours. From a practical point of view, this suggests that conjugation of MUA on AuNPs should be carried out overnight to ensure a complete formation of the monolayer.

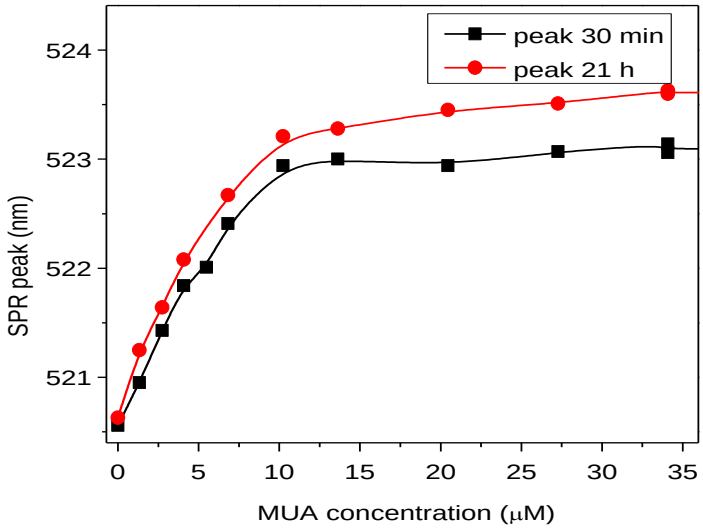

Figure 3.1 Shift of SPR in function of MUA added in solution. The formation of the monolayer was monitored by UV-VIS 30 minutes and 21 hours after MUA addition. The common saturation of a surface behavior is observed. The slight differences between times are due to a slow reorganization of the monolayer.

To evaluate whether the size of AuNPs has an influence on the formation of the MUA SAM, 40 nm AuNPs (39.3 ± 4.3 nm, 9.0 x10^{10} NP/mL) were also functionalized with MUA. The conjugation was run 21 hours under the same conditions than assayed before. In figure 3.2 the variation of peak in function of concentration of MUA added is represented for both 20 nm and 40 nm AuNPs. Note that the concentration is normalized by the surface area of the different AuNPs and the peak shift is normalized from 0 to 1 in order to compare both samples. It is observed that the conjugation of MUA is rather independent of the AuNPs size in this range of sizes, showing an almost identical behavior.

The shift of the SPR as a function of the concentration of added MUA fits quite well the Langmuir isotherm (Figure 3.2 b). This simple approach for adsorption onto surfaces is based on four assumptions:

i. All the surface sites have the same adsorption energy for the adsorbate.

ii. The adsorption at one site does not affect the energy of adsorption of neighboring sites.

iii. All adsorption occurs through the same mechanism.

iv. At the maximum adsorption, only a monolayer is formed.

The experimental points fit quite well this theoretical approach. The constant of Langmuir

(K) can be extracted from this fitting. This corresponds to the constant of adsorption (K_{abs}) assuming that the shift of the SPR is proportional to the coverage of the surface, and that the maximum coverage is 0.21nm^2/molecule.[4] In the case of 20 nm, this is 0.179 μM^{-1}. This constant represents the inverse of the bulk solution concentration required to reach half of the maximum surface coverage. From this constant the free energy of adsorption (ΔG_{ads}) can be also determined.[23]

$AG_{ads} = -RT \ln K/V_m$

where R is the gas constant, T is the temperature (297 K), K is the previously obtained constant (1.79 x 10^5 M^{-1}) and Vm the molar volume of the solution. As concentrations of MUA were low, molar volume of water is used here (18.0 x 10^{-3} M^{-1}). ΔG_{ads} is calculated to be -39.8 kJ mol^{-1}. Despite several approximations have been done to obtain this value, the value is similar to other examples found in the literature in which the loaded molecule was directly measured:-38.7 kJ mol^{-1} for SH-PEG 5 KDa,[24] -35.1 kJ mol^{-1} for SH-DNA[6] or-52.7 kJ mol^{-1} for a short-chain thiolated PEG linked to an antiparkinsonian molecule.[23] Thus, the simple monitorization of the process by UV-Vis spectroscopy gave us information about the thermodynamics and kinetics of the process. Nevertheless, it is worth mentioning here that this simple approach is applicable only in one-component monolayer in which the SPR shift only depends on the number of surfactant molecules per unit of surface (i.e. the density of the layer) and where the Langmuir assumptions are valid. This is not the case of SH-PEG, in which the SPR is also influenced by the conformational changes of the ligand,[18] or proteins where the energy of adsorption at one site is different whether the neighboring sites are occupied or vacant and also depends on the protein orientation.[20]

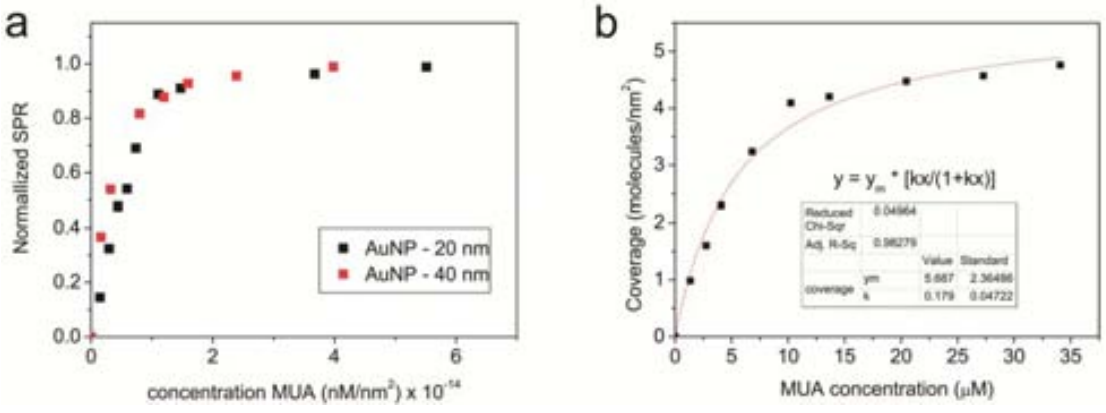

Figure 3.2. MUA monolayer characterization. (a) Shift of the SPR in function of the concentration of MUA and size of AuNPs. Both the shift and the concentration were normalized for comparison. (b) Fitting using the Langmuir approach for 20 nm AuNPs. The value of k can be used to further calculate ΔG_{ads}.

3.3.2 Pegylation of AuNPs.

Polyethylene glycol (PEG) is a linear synthetic polymer, build up by repeating [-CH_2CH_2-O] units. It is uncharged, water soluble, inert and considered as non-toxic and non-immunogenic. It has been extensively used to stealth liposomes and nanostructures from being rapidly cleared by the immune system.[25, 26] To obtain a stable monolayer, SH-PEG-CM (3.4 KDa) was used onto 20 nm AuNPs. Similar as in the case of MUA, the saturation of surface was followed by analyzing the shift of the SPR by UV-VIS spectroscopy 21 hours after the addition of different amounts of SH-PEG (figure 3.3). After normalizing the concentration with the surface area of NPs, it is observed that a saturation point was reached at ca. 2 x 10^{-15} nM/nm^2, which is 10-fold less than in the case of MUA. Thus, the concentration to reach the saturation point is 10 times smaller. This indicates that the density of SH-PEG onto the AuNPs was likely about 10 times smaller, since the bond with Au is also via a SH group and therefore a similar affinity was expected. As the surfactant is stable, what we are looking is at the bonding preference on the NP surface.

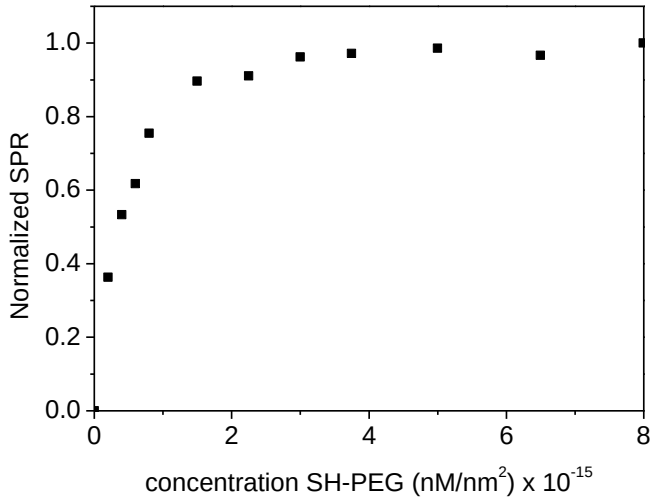

Figure 3.3 SH-PEG monolayer characterization. Shift of the SPR in function of the concentration of SH-PEG added. Both shift and concentration are normalized for comparison.

3.3.3 Mixed layers

Formation of mixed layers on AuNPs via a surfactant layer formed by various components makes possible the achievement of multifunctional AuNPs. The control of this process allows tuning the proportion of every component on the monolayer. This is very important since small variations on the composition or the conformation of the monolayer may

account for great changes in the physicochemical properties of the conjugates. In our case, we were interested on mixed layers formed by MUA to have a highly packed functional layer as chemical substrate to further attach cisplatin, and SH-PEG to confer additional colloidal stability. Mixed layers can be obtained via a co-conjugation of the different components (section 3.3.3.1) or by conjugation of one component and a subsequent exchange of ligands by the other component (section 3.3.3.2). Interestingly, the individual behavior of each compound can help to predict the final population on a mixed layer. Thus, one could use simple analysis of a single component to make a first approach in the design of multicomponent conjugates. However, it is important to determine the impact of the competence for the NPs surface when both components are present in solution and see if the affinities of the individual components for the NP are maintained.

3.3.3.1 Formation of mixed layers by co-conjugation of the components.

14.6 ± 1.5 nm AuNPs were used for these experiments since this is the chosen size for our biological assays (see chapter 5).

Firstly, we analyzed how the addition of different ratios of SH-PEG / MUA affects the loading of these molecules (Figure 3.4). Since both molecules compete for the AuNP surface, it is important to assay whether the proportion of both components in solution is maintained or not after conjugation to AuNPs. The final concentration of the sum of both species was kept constant (30 μM) and only the proportion of both components was modified. SH-PEG of the same molecular weight (3.4 KDa), but modified with a terminal fluorescein (SH-PEG-FITC) was also used to quantify the amount of this molecule on the surface by measuring the absorbance of the supernatants after removing all AuNPs by centrifugation, or by measuring the fluorescence of the attached SH-PEG-FITC after digestion of AuNPs with sodium cyanide of the previously washed AuNPs.[27] In both cases, the amount of SH-PEG on the NPs followed a linear trend reaching a final concentration on the NPs of aproximately 2.3 μM (Figure 3.4).

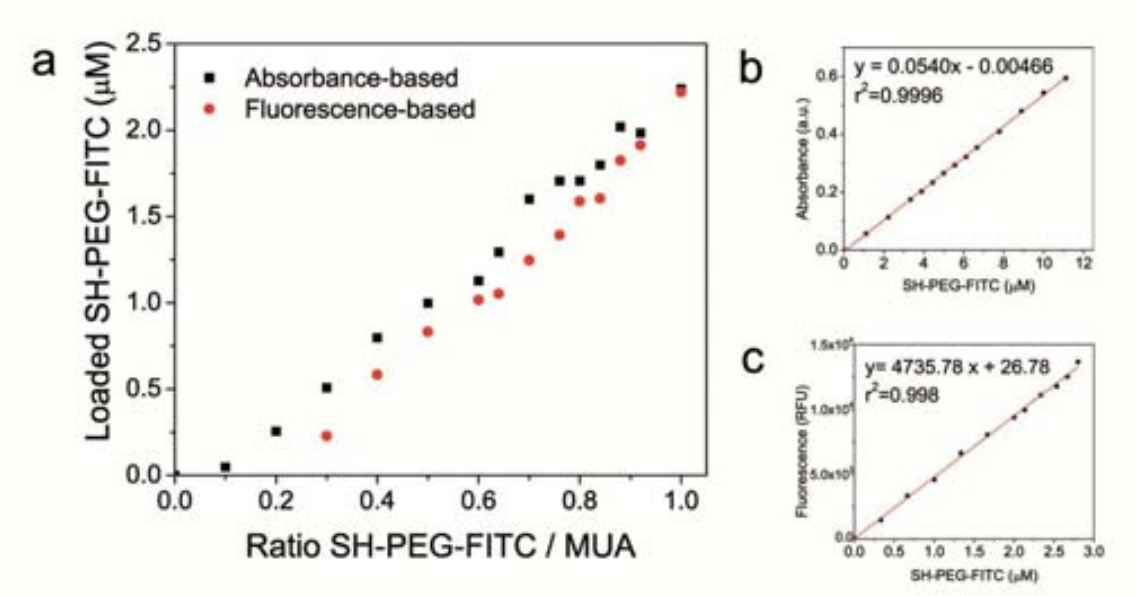

Figure 3.4. Loading of SH-PEG in function of the ratio SH-PEG / MUA added. (a) The loading on the AuNPs was quantified with 2 different methodologies (absorbance and fluorescence after digestion of AuNPs) giving similar results. Note that in the case of the fluorescence-based measures, the lower ratios could not be measured due to the impossibility of digesting completely the AuNPs, likely due to the compactness of the MUA shell. The standard curves are also showed (b and c).

This value corresponds to a final coverage of 334 molecules per NP, representing a footprint of 2.0 nm^2 which is also in agreement with the 10-fold lower saturation point than MUA found for SH-PEG in figure 3.3. Note that in the case of lower ratios (high [MUA]), this could not be easily measured due to the difficulty to totally digest the NPs, likely due to the compactness of the layer when MUA is the highly predominant component of the SAM.[28] Although the amount of MUA has not been directly measured, one could assume that the surface which is not occupied by SH-PEG will be occupied by MUA. The proportion of MUA that is loaded on the NP will be always higher than the added. For example, in the case of the ratio 0.5, the amount of SH-PEG loaded is ca. 0.9 μM, which corresponds to 131 molecules per NP and a 39% of surface coverage. Assuming that the remaining 61% is covered by MUA, and taking into account that the footprint for alkanethiols on gold is reported to be 0.21 nm^2,[4] the number of MUA per NP would be ca. 1945, which is 15 times higher than the amount of SH-PEG. Therefore, even if both attach with a thiol group, the resulting interactions and packing between neighbouring molecules favors MUA with respect to the SH-PEG molecules. This can be explained by the fact that MUA is a smaller molecule than SH-PEG with a hydrophobic chain and a hydrophilic head that favors the formation of dense SAMs on AuNPs[9] readily than SH-PEG does.

The conjugates obtained after adding different ratios SH-PEG / MUA were also analyzed by UV-VIS to monitor the shift of the SPR. In this case, we were not interested in monitoring the formation and saturation of the monolayer in function of the concentration of ligands, but in detecting the changes induced by the different composition of the layer. This is the reason why we worked at a fixed concentration of ligand (30 μM), modifying only the proportion of the components (figure 3.5). Interestingly, a discontinuous behavior was observed: The SPR position was only slightly shifted from ratios SH-PEG / MUA = 0 (all MUA) to ratios ≈ 0.7. From this point, a sharp blueshift from 521.4 nm to 520.5 nm was produced. This discontinuous behavior, also observed for absorbance, cannot be attributed to a differential loading of both components in function of the ratio since the loading of SH-PEG increases constantly as the proportion of SH-PEG added increases (figure 3.4). Therefore this sharp change is not related to great modifications in the layer composition, but to other factors such as conformational changes. In this context, it has been recently reported that the induction of a conformational change of a polymeric ligand onto AuNPs, without affecting the composition of the layer, led to a blueshift of the SPR peak. This is attributed to changes of the local refractive index due to changes in the density of the coating layer close to the AuNP surface.[18] It is also known that a high density of SH-PEG grafted on the NPs surface lead to a change of configuration from folded to stretched or radial, also known as mushroom and brush conformations respectively.[29-31]

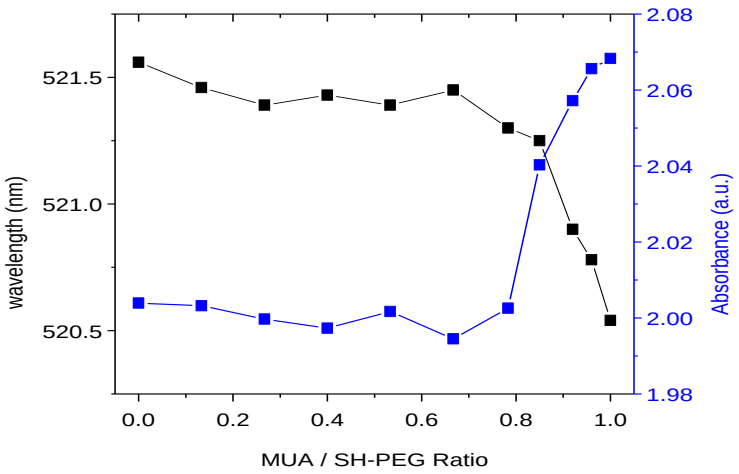

Figure 3.5. Shift and Intensity of the SPR in function of the MUA / SH-PEG ratio added. The discontinuous behavior observed here differs from the continuous loading of SH-PEG. This is explained considering a stretching of SH-PEG chains at high densities.

Thus, the observed blueshift is attributed to a stretching of the SH-PEG chains induced at high grafting densities of SH-PEG. To corroborate this point, the hydrodynamic diameter of the conjugates, measured by Dynamic Light Scattering (DLS), was also monitored in function of the SH-PEG / MUA ratios (Figure 3.6a). DLS gives the measure of the diameter that a sphere with the same translational diffusion speed than the corresponding nanoparticle would have[32] and its value is influenced by the length of the ligands as well as by the compactness of the layer.[20] Interestingly, a similar behavior than the previously shown for UV-VIS was observed here: A slight increase of the hydrodynamic diameter was produced until ratios ≈ 0.7 in which the hydrodynamic diameter raised rapidly from 14.9 nm to 27.6 nm. This is in agreement with the predicted stretching of the SH-PEG chains. This is even more clearly observed when the hydrodynamic diameter is plotted in function of the SH-PEG loaded onto AuNPs measured by fluorescence as explained above (Figure 3.6 b). The initial loading of SH-PEG did not cause a significant change on the hydrodynamic diameter. On the contrary, when the amount of SH-PEG loaded on the AuNPs reached values around 1 μM, the hydrodynamic diameter dramatically increased. Thus, the change on SH-PEG conformation is produced here at loadings around the 45 % of the maximum amount of SH-PEG able to load onto the AuNPs (2.3 μM).

We have demonstrated here the importance of not only analyze the mixed layer in terms of composition, but also taking into account conformational changes of SH-PEG. It is relevant to detect this point, since it will determine the change in the stabilization mechanism as well as the protein adsorption profile of this kind of conjugates (see section 3.3.5).

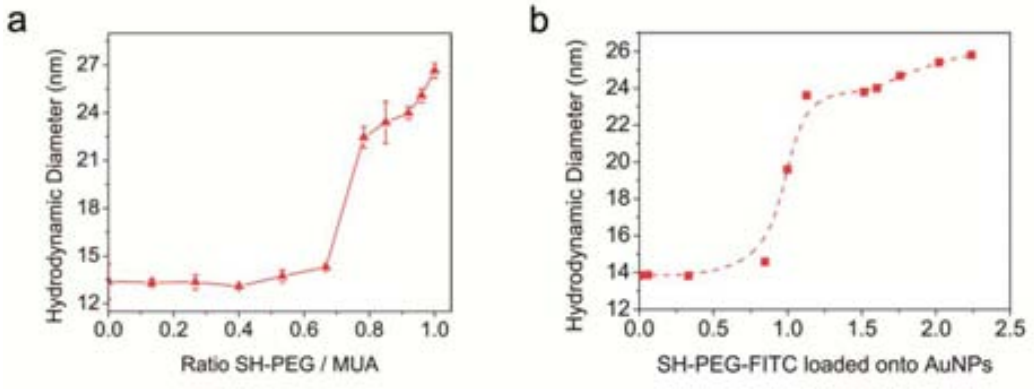

Figure 3.6. Hydrodynamic diameters in function of the composition of the mixed layer. (a) Measure of the hydrodynamic diameter depending on the ratio SH-PEG / MUA added. (b) The diameter is shown in function of the loading of SH-PEG-FITC. Note that b shows the amount of SH-PEG loaded onto NPs whilst a shows the amount of SH-PEG added in solution.

3.3.3.2 Formation of mixed layers by ligand exchange

It has been observed in previous sections that MUA is an excellent SAM-forming agent because thiol group has a great affinity for Au, the hydrophobic chain favors the formation of a compact shell, and the negatively charged carboxylate groups confer electrostatic stability to the AuNPs. Those reasons give more affinity for AuNPs surface to MUA than to SH-PEG and consequently, MUA is supposed to be able to displace the SH-PEG, and to completely wash away SH-PEG from the surface when enough excess is added. Formation of mixed layer by a partial replacement of one of the components of the monolayer has been also reported in the literature.[24, 33] In this section a methodology to replace SH-PEG with MUA to obtain mixed layers will be described. However, we strongly recommend the use of co-conjugation (explained in section 3.3.3.1) to obtain this kind of mixed layers due to its simplicity and greater reproducibility.

First, AuNPs were functionalized with SH-PEG (3.4 KDa) as explained in section 3.3.2. Then, the excess of SH-PEG was removed and different amounts of MUA were added to the AuNPs solutions and softly stirred overnight. The resulting AuNPs were analyzed by UV-VIS spectroscopy and DLS (Figure 3.7). The general trend was that as the concentration of added MUA increased, the hydrodynamic diameter decreased (MUA is shorter than SH-PEG), and SPR-band was red-shifted (the coating layer is more compact when MUA is predominant). However, some deviations from the general trend are also observed and are difficult to explain due to the complexity of the process in which substitution of the components takes place together with conformational changes of the components on the monolayer. Moreover, the substituted ligands (SH-PEG) are ready to compete again for the NP surface with the substituting ligands (MUA). Hence, different stages were observed: In the first points, changes in the hydrodynamic diameter and SPR peak were small, which would indicate that MUA started to exchange with SH-PEG without causing any conformational change in the later. Then, more remarkable changes are observed from 15 to 30 μM of MUA, which could be attributed to a loss of SH-PEG density and therefore to a change of the conformation from brush to mushroom. From that point until 60 μM changes are less evident. This is consequent with a substitution of the SH-PEG in the mushroom conformation by MUA. It is worth remembering that it has been observed in previous section how a progressive loading of SH-PEG resulted in very little variation on UV-VIS and DLS measures as long as SH-PEG conformation had not been changed to brush.

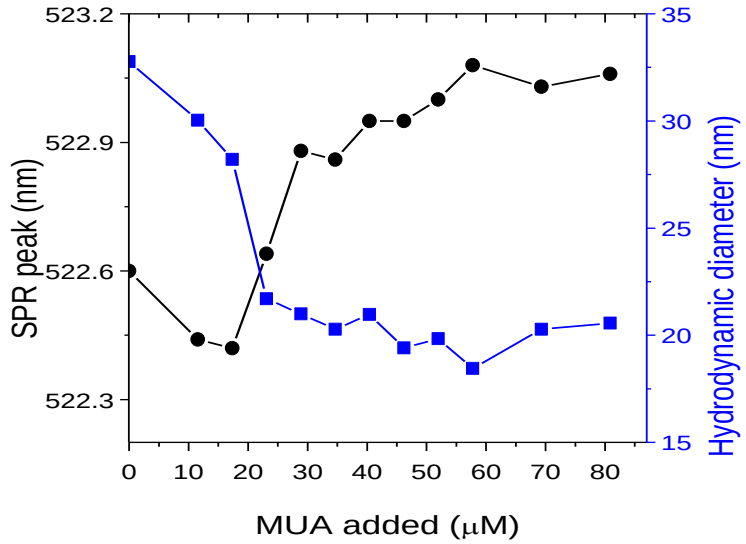

Figure 3.7. Monitorization of SH-PEG substitution by addition of MUA. The changes produced in the hydrodynamic diameter (blue squares), SPR peak (black circles) and Zeta-potential (red triangles) after adding differents amounts of MUA are indicative of the ligand exchange.

3.3.4 Stability in function of the layer composition at physiological conditions

3.3.4.1 MUA-capped AuNPs

As it is stated at the beginning of this chapter, surfactant layer determines several physicochemical properties of the NPs which obviously have an influence on the stability of NPs in different media.[34] For example, the complex mixture of electrolites present in physiological media would induce the compression of the Stem layer leading to aggregation of electrostatically stabilized AuNPs if they had not been previously protected with steric repulsor. This phenomenon is often unnoticed since the protein, present also in physiological media, covers the NP via the well-known protein corona, conferring steric stability to the NP. However, at high concentration of NPs this protein corona might be insufficient to guarantee the colloidal stability of NPs. Unfortunately, high concentrations of AuNPs are often required to reach doses of interest in *in vivo* and *in vitro* studies, in which there is a limitation on the volume of AuNPs solution that can be added to the cell culture or the animal.

To illustrate that aggregation in physiological media depends on the concentration of AuNPs, 10 % v/v of MUA capped AuNPs solution at different concentrations was added to

cell culture media (CCM, DMEM supplemented with 10 % Foetal Bovine Serum) and the peak position of SPR was measured by UV-VIS. Aggregation of AuNPs is known to broaden and shift to longer wavelengths the SPR band as well as to increase the absorption at the 600 – 800 nm range.[35] First, the stabilizing role of the protein corona was confirmed since all the concentrations aggregated when assayed in DMEM not supplemented with Fetal Bovine Serum (FBS). Then, as expected, it was confirmed that the stability of AuNPs in DMEM supplemented with FBS is concentration dependent (figure 3.8). At low concentrations of AuNPs in CCM (≤ 4.75 x 10^{12} NP/mL) are very stable due to the spontaneous formation of the widely described protein corona[36, 37]: Briefly, proteins are adsorbed on the nanoparticles surface, in this case on the MUA layer, conferring stability against aggregation by steric repulsion. In the case of higher concentrations (≥ 9.5 x 10^{12} NP/mL), a red-shift and a broadening of the SPR band were observed even in the presence of 10% FBS. This indicates that proteins in the media were not capable of stabilizing high concentrations of MUA-capped AuNPs. Protein in cell culture media is approximately at 0.1 mM while the highest concentration of AuNPs used here is 2.5 x 10^{13} NP/mL (41.5 nM). Since the protein in the media is not limiting, the aggregation is likely due to a kinetic issue: highly concentrated nanoparticles contact between them before proteins have the chance to be adsorbed conferring stability. It must be pointed out that the methodology followed in all the experiments here was making a dilution of the NPs and then adding 10 % v/v of this solution to the CCM. Previous observations showed that if a low volume - even a small drop- of a very high concentration of NPs is added to a large volume of CCM, AuNPs aggregate rapidly, even though the resultant mixture has a low NP concentration. On the other hand, if one dilutes first the NP solution in water and then uses this solution to reach the same final concentration in CCM, the stability is higher.

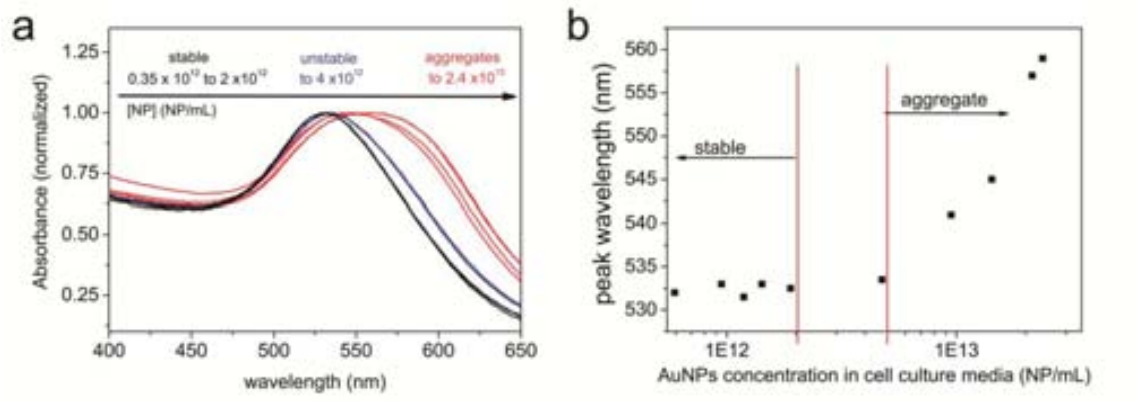

Figure 3.8. Stability of AuNPs in cell culture media in function of the AuNPs concentration. The broadening and great redshift of SPR at high concentration of AuNPs in cell culture media show the aggregation of AuNPs (a). The different behavior in function of the concentration is observed in the plotting of the peaks (b). Low concentrations were stabilized by the rapid formation of a protein corona. However, this mechanism was unable to stabilize high concentrations.

Therefore, the spontaneous formation of the protein corona in CCM is not rapid enough to avoid aggregation of the nanoparticles when high concentrations of AuNPs are assayed. An easy alternative to circumvent this problem is to preincubate AuNPs with BSA in a low ionic strength buffer before the addition of these nanoparticles to CCM. Albumin is the major protein in serum and the most abundantly adsorbed onto hydrophilic surfaces,[38] while in the case of hydrophobic surfaces, fibrinogen and immunoglobulins play an important role and share the surface of the NP with albumin.[13] To evaluate the concentration of BSA needed to stabilize AuNPs, different amounts of BSA in HEPES (pH 7.5, 5mM) were added to a 1.0 x 10^{14} NP/mL solution of MUA-capped Au NPs. The formation of the protein corona can be followed either by Dynamic Light Scattering (DLS) or UV-VIS spectroscopy (Figure 3.9 a). In DLS measurements, it is observed a gradual increase in the hydrodynamic diameter with higher concentrations related to the progressive formation of a more compact BSA shell,[20] reaching an 8 nm increase at the saturation point, which is in agreement with a BSA layer of 4 nm thickness (BSA has an equivalent diameter of 3.6 nm). The same behavior is observed when analyzing the red-shift of the SPR band by UV-VIS spectroscopy confirming the formation of the protein corona[12] (Figure 3.9 b).

Further analysis of the stability of these preparations at the highest concentration assayed in the previous stability test (2.5 x 10^{13} NP/mL) confirmed that preincubation of the AuNPs with concentrations of BSA ≥ 10 nM was enough to stabilize these NPs in CCM since

the SPR band was not shifted after adding the AuNPs in CCM (Figure 3.10). On the contrary, AuNPs which had not been previously incubated with BSA showed a great red shift as well as a broadening of the band indicative of aggregation. Thus, protein corona is able to stabilize the AuNPs at higher concentrations if they have been preincubated with albumin in a low ionic strength media (as 2.2 mM sodium citrate) before adding them to physiological media. Protein corona formation is spontaneous in cell culture media,[12] hence the preincubation with BSA should not show any different biological effect if the conjugation has been performed properly to avoid any loss of NP stability during the process. It should be noted however, that protein corona spontaneously formed is much more complex, with other proteins such as immunoglobulins and fibrinogen forming part of the corona. Note also that protein corona, specially in the early stages, is dynamic. Hence, proteins which have greater affinity to NP surface, even if they are at low concentration, slowly replace abundant proteins.[13, 38] Thus it is likely that this process may still take place even after the preincubation with albumin which does not show a high affinity for NPs surface.

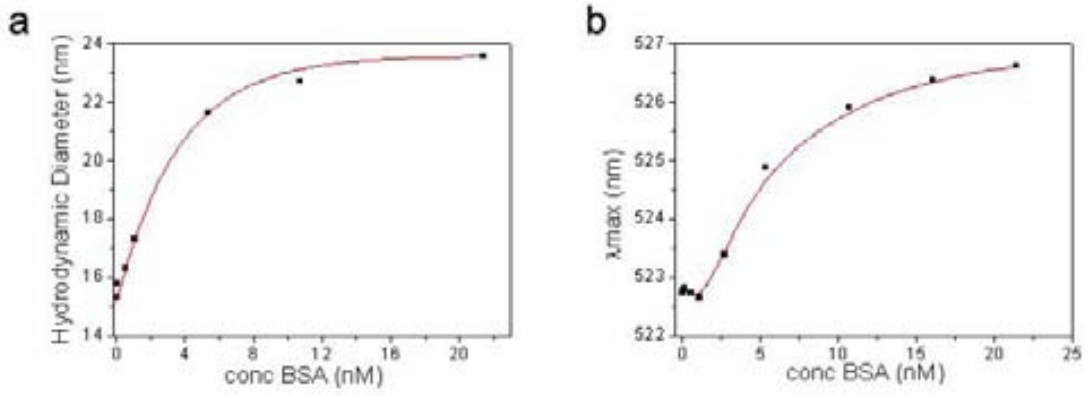

Figure 3.9. Monitoring the protein corona formation. The protein shell increase its density of packing as more protein is added until a full monolayer is achieved which is translated to an increase in the hydrodynamic diameter (a) and to a red shift of the SPR band (b). This is tracked by Dynamic Light Scattering and UV-VIS spectroscopy respectively.

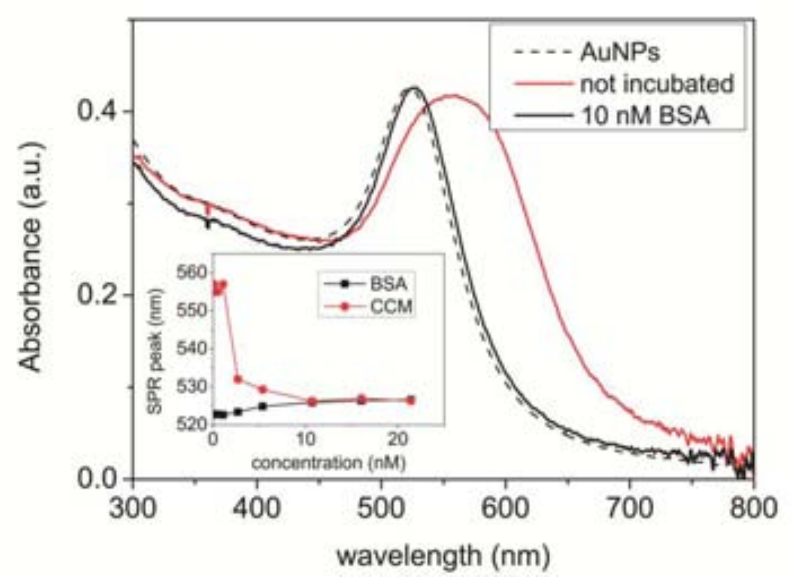

Figure 3.10. Stabilization of AuNPs by protein corona. AuNPs aggregated in cell culture media if they had not been previously stabilized. Aggregation caused a great shift of the SPR peak as well as a broadening of the band. The inset shows the difference of the SPR peaks before and after adding the conjugates to CCM in function of the BSA added. The minimum amount of BSA that shows no difference is 10 nM.

3.3.4.2 Mixed layers. Stability Dependence on the layer composition.

The presence of SH-PEG on the surfactant layer is known to confer stability to the AuNPs.[39] Here, the stability is tested in function of the mixed layer composition. Different AuNPs with varying compositions of the layer were obtained as explained in section 3.3.4. After the removal of the excess of ligand, 20 μL of AuNPs (2.4 x 10^{14} NP/mL) were added to 180 μL of 10 % FBS-supplemented DMEM in all cases. The stability was assayed by measuring the SPR band by UV-VIS spectroscopy after 30 minutes (figure 3.11 a). As expected, AuNPs which have MUA predominance over SH-PEG aggregate in physiologic conditions. On the contrary, AuNPs become stable from ratios SH-PEG / MUA higher than 0.7 which coincides with the point where the rise in the hydrodynamic diameter, associated to a conformational change of the SH-PEG.

The stability at acidic pH was also tested. MUA-capped AuNPs are elecrostatically stabilized due to the negative charge given by the deprotonated carboxylic groups. Therefore, MUA-capped AuNPs become unstable once the pH is decreased below its pKa, and the carboxylic groups subsequently protonated (indeed, an effective surface charge of > |30| mV is needed to keep NPs stable in solution following the DVLO theory[40]). On the other hand, the sterically stabilized NPs should be stable at any pH. To prove the stability

of bifunctionalized AuNPs in a wide range of pH, the pH of the AuNPs solution was brought to 2.6 by using a Glycine / HCl buffer and the SPR band measured by UV-VIS spectroscopy (figure 3.11 b). Similarly as it was observed in the stability at physiologic conditions, the aggregation of nanoparticles was evident for ratios of added SH-PEG / MUA lower than 0.7. Thus, here again the change in the mechanism of stabilization from electrostatic to steric coincides with the change in the conformation of SH-PEG. Otherwise the non-stretched PEG is unable to stabilize sterically the AuNPs.

From these experiments the importance of not only the composition of the layer, but on the conformation is proved. It seems clear, that the additional stability conferred by SH-PEG here is due to a change on the stabilization mechanism. MUA stabilizes the AuNPs via electrostatic repulsions, however when SH-PEG is stretched an additional steric stabilization is gained. From this moment, the steric stabilization is the main mechanism against aggregation since they stabilize the NPs under a wider range of conditions (including high ionic strength and low pH). Thus, the identification of the point at which the conformational change takes place is crucial in terms of stability. Note also that functionality given by MUA or any other alkanethiols is maintained since at ratios 0.7, the occupation of the surface by SH-PEG is just above the 50 %, leaving plenty of space for MUA. In fact, there would be space for ca. 1590 molecules of MUA per NP according to calculations based on the theoretical footprint of MUA on Au (0.21 nm^2). Therefore, by tuning the mixed layer, one can guarantee both functionality given by MUA and stability given by SH-PEG. This extra stability is based on a steric hindrance instead of on an electrostatic repulsion. Thus, the stability is not affected by the composition of the media and/or the concentration of NPs.

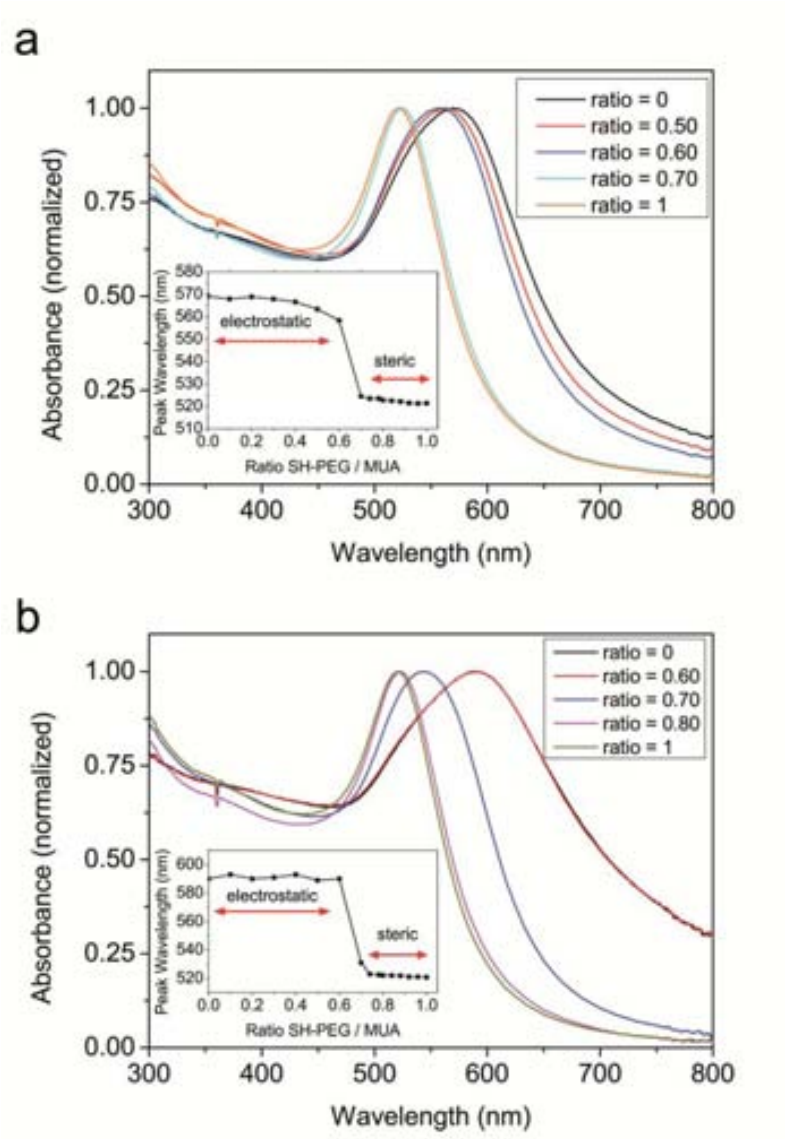

Figure 3.11. Stability in physiologic and acidic media of concentrated AuNPs. (a) The stability of AuNPs functionalized with different SH-PEG / MUA ratios was assayed by adding 10 % of 2.4 x 10^{14} NP/mL solution in DMEM supplemented with FBS. Destabilization is traduced to a broadening and redshift of the SPR band. At ratios higher than 0.7 the stability is recovered due to the steric stabilization given by SH-PEG in the *brush* conformation (b) To assay the stability in acidic media, the pH was decreased to 2.6 using a Gly/HCl buffer. The protonation of the carboxylic groups causes the loss of colloidal stability when the stability of the NPs is governed by MUA. On the other hand, AuNPs remain stable when they are sterically stabilized (PEG in the *brush* conformation).

3.3.5 Influence of the layer composition and conformation on the protein adsorption

We have discussed the importance of the mixed layer composition in terms of stability. However, this is not the only goal pursued when a nanocarrier is pegylated. The role of PEG as stealthing agent from the immune system for drug delivery systems has been widely exploited. Hence, this methodology has been used to modify objects asliposomes, interferon-α and viruses for biomedical applications.[41, 42] Although, the mechanism of stealthing is not totally unveiled, it is accepted that avoiding the adsorption of opsonins plays a central role. Opsonins are proteins of the immune system, such as immunoglobulins and proteins of the complement, which binds an antigen, ultimately triggering an immune response. In addition, the absortion of proteins from the sera has been reported to influence the uptake of AuNPs by cells. Therefore, the inhibition of protein adsorption needs to be studied when designing the mixed layer since it likely affects some biological properties of the carrier. To study the adsorption of proteins onto the different conjugates, they were prepared as explained in section 3.3.4.1, purified from the excess SH-PEG and MUA and then incubated with 10 μM BSA overnight. Albumin was chosen as model protein to simplify the system and because it has been identified as the main, if not the only, serum protein absorbed to these types of NPs.[38] The adsorption of protein was then analyzed by DLS, UV-VIS and gel electrophoresis. In figure 3.11, it is shown that when MUA was the only component of monolayer, there was an increase in the hydrodynamic diameter after adding BSA. The size increase was 8.1 nm and it is explained by the adsorption of a monolayer of BSA on the MUA layer.[2] This size increase became only 5.2 and 3.7 nm at ratios 0.70 and 0.74 respectively. The lower increase of size is attributed to less protein adsorption.[20] When the ratios were higher than 0.78 the size before and after addition of BSA was the same indicating that under this conditions the protein adsorption was completely inhibited as expected. The same tendency was observed in the SPR peak analysis (Figure 3.11b). The increase in the peak wavelength is attributed to the change in the surrounding dielectric environment of the Au surface due to the adsorption of protein.[19] This wavelength shift was up to 4.55 nm for MUA-capped AuNPs incubated with BSA. The difference became smaller from the ratio 0.70 (3.75 nm) here too. This difference decreased to 2.83, 2.17, and 1.34 nm at ratios 0.74, 0.78, and 0.8 respectively. At higher ratios, the difference was not significant. Thus, the point where PEG adopts the stretched conformation is related to a change on the phyisicochemical properties of the conjugate once again. In this case, it is clearly seen how the adsorption of protein is precisely tunned in function of the composition and conformation of the mixed layer. This indicates that steric hindrance allows a better control of NP-protein

interactions than modifications of the surface charge. In fact, differences on total surface charge seem to not influence the degree of protein adsorption as the change on conformation of SH-PEG does. Obviously, changes from negative to positive values would have induced a different behavior.

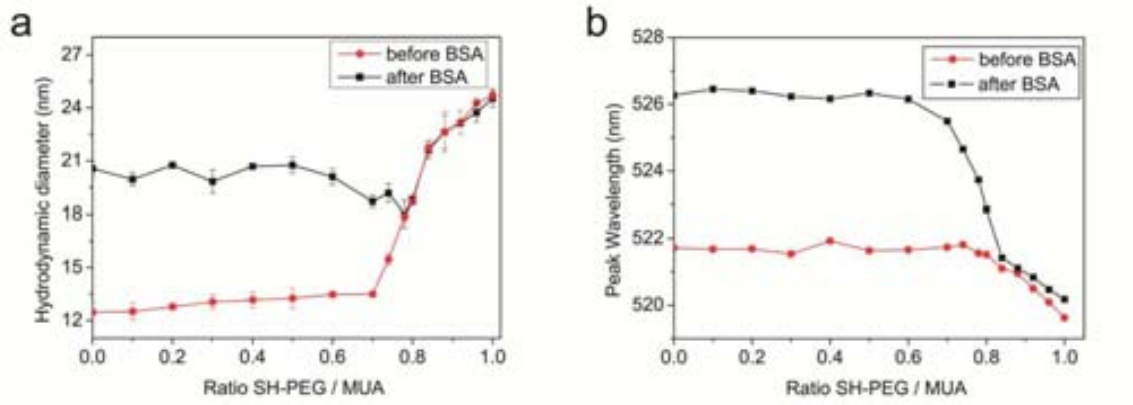

Figure 3.11. Tunning the protein adsorption. (a) Hydrodinamic Diameter before and after incubation with BSA. The formation of a protein corona at lower ratios is clearly related to the increase of the hydrodinamic diameter. The increase of size is from ratio 0.70. From ratios 0.78 to 1 this difference on size is negligible and therefore protein adsorption is totally inhibited. **(b)** SPR peak before and after incubation with albumin. The same behavior was found by analysizing the peak of the SPR band. The differences between before and after addition of albumin are reduced from ratios 0.7 to 0.8. From 0.84 to 1 the diferences are negligible.

Gel electrophoresis was performed to further confirm the different interaction with proteins when changing the composition of the monolayer (figure 3.12). Relevant ratios of SH-PEG / MUA –AuNPs previously incubated overnight with albumin and without incubation were loaded into the wells of a 1 % agarose gel. The electrophoresis was run 1 h at 60 V in a 30 mM sodium borate buffer at pH 8.5. At ratios < 0.7, it was observed a decrease of the electrophoretic mobility mainly due to an increase of the size after albumin adsorption, but also to a decrease of the surface charge. On the other hand, at ratios > 0.8, the mobility was the same after incubation with albumin than without previous incubation indicating that no modification of the size and/or surface charge were induced by albumin incubation. At ratio 0.74, an intermediate behavior was observed, there was a difference between both conditions, but it was minimal. This latter case can be explained because the adsorption of albumin was not fully inhibited, but minimized. It was also observed that when adsorption of protein was not diminished, the electrophoretic mobility after incubation of BSA was the same, independently of the mixed layer

composition. Thus, it is likely that MUA-capped AuNPs and mixed layer-capped AuNPs in which the conformational change have not taken place, would show a similar fate on the organism since the surface would be equally covered by protein corona.

As a side result of this experiment, one can notice the different electrophoretic mobility of the mixed layer-coated AuNPs before incubating with BSA. From ratios 0 to 0.6, the mobility was reduced likely due to a lower negative charge. As expected, the electrophoretic mobility was dramatically reduced due to steric hindrance when the PEG conformational change of SH-PEG was produced, this happens for ratios > 0.74. However, as the proportion of SH-PEG kept increasing, a slight recovery of electrophoretic mobility seems to be produced. This effect is beyond the scope of this work, but one hypothetical explanation could be given by the higher compaction of the stretched SH-PEG shell when the density of this component on the surface is increased. The compaction of the SH-PEG chains may result in a more rigid shell, decreasing the mobility of SH-PEG chains, which would make the conjugate to interact less with agarose and consequently slightly increase its mobility.

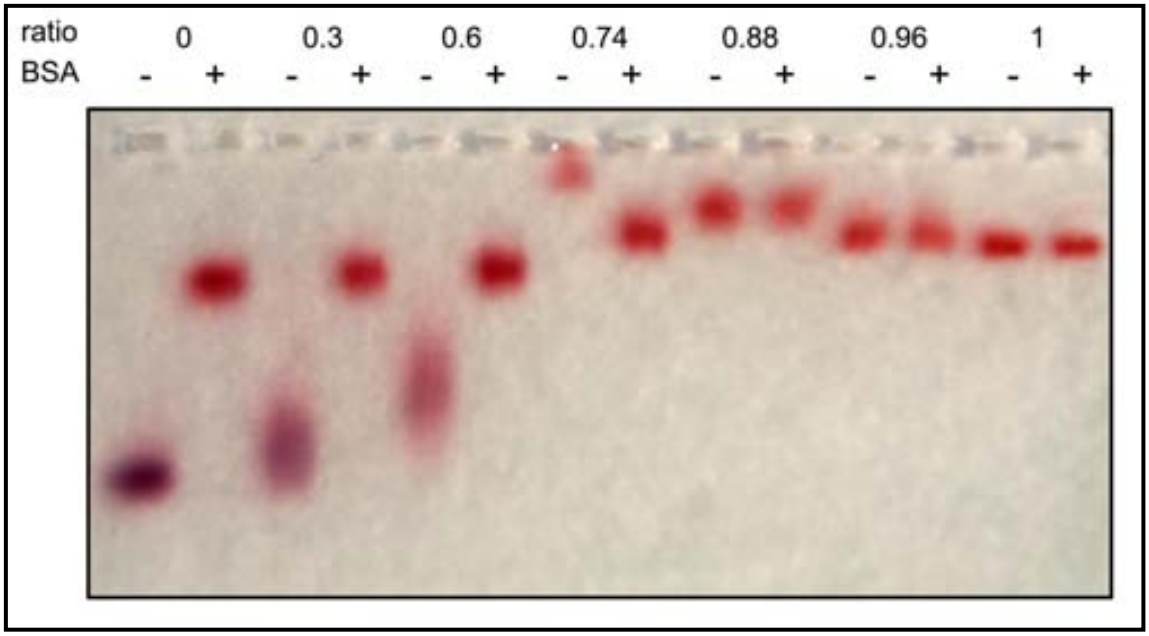

Figure 3.12. Agarose gel electrophoresis of relevant ratios with (+) and without (-) albumin preincubation. The difference between the same AuNPs before and after the addition of albumin indicates the formation of a protein corona. This is inhibited at ratios = 0.88, 0.96 and 1. The purplish color of the ratio = 0 and 0.3 appeared only after drying the gel.

The reduction or total inhibition of protein adsorption has strong consequences in the design of NPs for medicine. For example, a different degree and type of complement activation, which ultimately depends on the recognition of the conjugates by specific proteins, was directly correlated with the conformation of the PEO monolayer on polymeric nanoparticles in a recent work.[15] Briefly, Hamad et al showed that the complement activation was dramatically reduced for the nanospheres which have PEO chains in the *brush* conformation. The changes in the physicochemical properties of the nanoparticles induced by the change of the PEG conformation, especially the different protein adsorption, can account for this different immunological behavior.

From these results, one can distinguish two different regimes:

i. At added ratios SH-PEG /MUA from 0 to 0.7, the SH-PEG has a low influence on the hydrodynamic diameter, since it is in the *mushroom* conformation. Here, the physicochemical properties are governed by MUA and PEG does not show a major influence. Therefore these AuNPs are not stable in physiologic media when working at concentrations higher than 5 x 10^{12} NP/mL, aggregate at acidic pH due to the protonation of carboxylic groups of MUA and the inability of PEG to confer steric stabilization in this *mushroom* conformation

ii. At added ratios from 0.7 to 1, the SH-PEG changes the conformation from *mushroom* to *brush* and new physicochemical properties were aquired subsequently. These AuNPs are stable in physiological media at concentrations as high as 2.4 x 10^{13} NP/mL CCM. Moreover, they are stable at the whole ranges of pH. The protein adsorption is here minimized or even fully inhibited.

3.4 Conclusions

The importance of the surfactant layer for AuNPs that are going to be used as drug delivery agents is demonstrated here since it determines not only the chemical functionality, but also it plays a key role in the stability at physiological conditions. We were interested on two different ligands: MUA to form highly-packed SAM with carboxylic acids to further link cisplatin and SH-PEG to confer additional stability to the vehicle.

MUA showed a high affinity for AuNPs leading to highly compact SAMs onto AuNPs. The formation of MUA SAMs was monitored by the analysis of the SPR shift, which is assumed to be proportional to the density of molecules on the surface. This process fits quite well with the simple Langmuir approach for adsorption onto surfaces, independently of AuNP size in the studied ranges. Therefore, thermodynamic parameters such as free energy of

adsorption were calculated to be quite similar to other examples found on the literature for thiolated molecules.[6, 24] Similarly as in the case of MUA, saturation point was determined for SH-PEG. Although, the link with Au was also via the thiol group, the saturation was reached at 10 times less amount than the amount found for MUA. Thus, the monolayer formed by SH-PEG was not as dense as the one formed by MUA. The lack of hydrophobic chain and the length of the chain accounts for that low density packing. This was corroborated after quantification of SH-PEG on the surface of AuNPs. Footprint of SH-PEG was calculated to be 2.0 nm^2, which is 10-fold higher as the widely reported 0.21 nm^2 for alkanethiols.

Multifunctional NPs were obtained by the formation of mixed layers of MUA and SH-PEG. This can be achieved by ligand exchange or by co-conjugation of both components, being the later, the one that showed a greater reproducibility in our case. The loading of SH-PEG onto the AuNPs was proportional to the amount added. However, the analysis of the SPR shift and the hydrodynamic diameter revealed a discontinuous behavior. This was attributed to conformational changes of SH-PEG: At high densities of SH-PEG (higher than 45 % of coverage) SH-PEG was stretched adopting the brush configuration. It is very important to detect this point since it determines physicochemical changes of the conjugates.

MUA stabilized AuNPs electrostatically; thus MUA-capped (and low SH-PEG density mixed layers-capped) AuNPs were not stable under acidic conditions, in which carboxylic acids are protonated, and when they were exposed to high ionic strength media due to the compression of the Stern layer. On the contrary, SH-PEG in the brush conformation stabilized AuNPs via steric hindrance which turned the NPs to be stable even in acidic and physiological conditions at high concentration. AuNPs can be also stabilized via the formation of a protein corona. At low concentrations, the spontaneously formed corona in CCM was enough to stabilize AuNPs. However, at concentrations above 4×10^{12} NP/mL protein in CCM was not able to stabilize them and an additional preincubation with BSA was required.

The protein adsorption profiles were also dependent on the mixed layer composition and configuration. As seen for the stability, the stretching of SH-PEG resulted in a progressive inhibition of protein adsorption. This have implication on the fate of nanocarriers in the organism since adsorption of protein has been described to influence the immune response and the cell uptake. In fact, it has been recently reported that increasing the

density of a SH-PEG monolayer (and thus stretching the SH-PEG) resulted in a different degree and type of complement activation.[15]

3.5 References

(1) Eugenii, K.; Itamar, W., Integrated Nanoparticle-Biomolecule Hybrid Systems: Synthesis, Properties, and Applications. *Angewandte Chemie International Edition* **2004,** 43, 6042-6108.
(2) BastÃºs, N. G.; Casals, E.; VÃ¡zquez-Campos, S.; Puntes, V., Reactivity of engineered inorganic nanoparticles and carbon nanostructures in biological media. *Nanotoxicology* **2008,** 2, 99 - 112.
(3) Daniel, M. C.; Astruc, D., Gold nanoparticles: Assembly, supramolecular chemistry, quantum-size-related properties, and applications toward biology, catalysis, and nanotechnology. *Chemical Reviews* **2004,** 104, 293-346.
(4) Sellers, H.; Ulman, A.; Shnidman, Y.; Eilers, J. E., Structure and binding of alkanethiolates on gold and silver surfaces: implications for self-assembled monolayers. *J. Am. Chem. Soc.* **1993,** 115, 9389-9401.
(5) Wang, Y.; Zeiri, O.; Neyman, A.; Stellacci, F.; Weinstock, I. A., Nucleation and Island Growth of Alkanethiolate Ligand Domains on Gold Nanoparticles. *ACS Nano* **2011,** 6, 629-640.
(6) Yang, M.; Yau, H. C. M.; Chan, H. L., Adsorption Kinetics and Ligand-Binding Properties of Thiol-Modified Double-Stranded DNA on a Gold Surface. *Langmuir* **1998,** 14, 6121-6129.
(7) Bastús, N. G.; Sánchez-Tilló, E.; Pujals, S.; Farrera, C.; López, C.; Giralt, E.; Celada, A.; Lloberas, J.; Puntes, V., Homogeneous Conjugation of Peptides onto Gold Nanoparticles Enhances Macrophage Response. *ACS Nano* **2009,** 3, 1335-1344.
(8) Xia, X.; Yang, M.; Wang, Y.; Zheng, Y.; Li, Q.; Chen, J.; Xia, Y., Quantifying the Coverage Density of Poly(ethylene glycol) Chains on the Surface of Gold Nanostructures. *ACS Nano* **2011**.
(9) Love, J. C.; Estroff, L. A.; Kriebel, J. K.; Nuzzo, R. G.; Whitesides, G. M., Self-Assembled Monolayers of Thiolates on Metals as a Form of Nanotechnology. *Chemical Reviews* **2005,** 105, 1103-1170.
(10) Nel, A. E.; Madler, L.; Velegol, D.; Xia, T.; Hoek, E. M. V.; Somasundaran, P.; Klaessig, F.; Castranova, V.; Thompson, M., Understanding biophysicochemical interactions at the nano-bio interface. *Nat Mater* **2009,** 8, 543-557.
(11) Bartczak, D.; Kanaras, A. G., Preparation of Peptide-Functionalized Gold Nanoparticles Using One Pot EDC/Sulfo-NHS Coupling. *Langmuir* **2011,** 27, 10119-10123.
(12) Casals, E.; Pfaller, T.; Duschl, A.; Oostingh, G. J.; Puntes, V., Time Evolution of the Nanoparticle Protein Corona. *ACS Nano* **2010,** 4, 3623-3632.
(13) Lundqvist, M.; Stigler, J.; Elia, G.; Lynch, I.; Cedervall, T.; Dawson, K. A., Nanoparticle size and surface properties determine the protein corona with possible implications for biological impacts. *Proceedings of the National Academy of Sciences* **2008,** 105, 14265-14270.
(14) Walkey, C. D.; Olsen, J. B.; Guo, H.; Emili, A.; Chan, W. C. W., Nanoparticle Size and Surface Chemistry Determine Serum Protein Adsorption and Macrophage Uptake. *J. Am. Chem. Soc.* **2011,** 134, 2139-2147.
(15) Hamad, I.; Al-Hanbali, O.; Hunter, A. C.; Rutt, K. J.; Andresen, T. L.; Moghimi, S. M., Distinct Polymer Architecture Mediates Switching of Complement Activation Pathways at the Nanosphere−Serum Interface: Implications for Stealth Nanoparticle Engineering. *ACS Nano* **2010,** 4, 6629-6638.

(16) Wang, D.; Nap, R. J.; Lagzi, I. n.; Kowalczyk, B.; Han, S.; Grzybowski, B. A.; Szleifer, I., How and Why Nanoparticles Curvature Regulates the Apparent pKa of the Coating Ligands. *J. Am. Chem. Soc.* **2011,** 133, 2192-2197.
(17) Ghosh, S. K.; Nath, S.; Kundu, S.; Esumi, K.; Pal, T., Solvent and Ligand Effects on the Localized Surface Plasmon Resonance (LSPR) of Gold Colloids. *The Journal of Physical Chemistry B* **2004,** 108, 13963-13971.
(18) Tagliazucchi, M.; Blaber, M. G.; Schatz, G. C.; Weiss, E. A.; Szleifer, I., Optical Properties of Responsive Hybrid Au@Polymer Nanoparticles. *ACS Nano* **2012,** 6, 8397-8406.
(19) Eck, D.; Helm, C. A.; Wagner, N. J.; Vaynberg, K. A., Plasmon Resonance Measurements of the Adsorption and Adsorption Kinetics of a Biopolymer onto Gold Nanocolloids. *Langmuir* **2001,** 17, 957-960.
(20) Ardao, I.; Comenge, J.; Benaiges, M. D.; Álvaro, G.; Puntes, V. F., Rational Nanoconjugation Improves Biocatalytic Performance of Enzymes: Aldol Addition Catalyzed by Immobilized Rhamnulose-1-Phosphate Aldolase. *Langmuir* **2012,** 28, 6461-6467.
(21) Tsai, D. H.; Zangmeister, R. A.; Pease Iii, L. F.; Tarlov, M. J.; Zachariah, M. R., Gas-Phase Ion-Mobility Characterization of SAM-Functionalized Au Nanoparticles. *Langmuir* **2008,** 24, 8483-8490.
(22) Bain, C. D.; Troughton, E. B.; Tao, Y. T.; Evall, J.; Whitesides, G. M.; Nuzzo, R. G., Formation of monolayer films by the spontaneous assembly of organic thiols from solution onto gold. *J. Am. Chem. Soc.* **1989,** 111, 321-335.
(23) Amigo, J. M.; Bastús, N. G.; Hoen, R.; Vázquez-Campos, S.; Varón, M.; Royo, M.; Puntes, V., Analysis of time-dependent conjugation of gold nanoparticles with an antiparkinsonian molecule by using curve resolution methods. *Analytica Chimica Acta* **2011,** 683, 170-177.
(24) Tsai, D.-H.; DelRio, F. W.; MacCuspie, R. I.; Cho, T. J.; Zachariah, M. R.; Hackley, V. A., Competitive Adsorption of Thiolated Polyethylene Glycol and Mercaptopropionic Acid on Gold Nanoparticles Measured by Physical Characterization Methods. *Langmuir* 26, 10325-10333.
(25) Owens Iii, D. E.; Peppas, N. A., Opsonization, biodistribution, and pharmacokinetics of polymeric nanoparticles. *International Journal of Pharmaceutics* **2006,** 307, 93-102.
(26) Vonarbourg, A.; Passirani, C.; Saulnier, P.; Benoit, J.-P., Parameters influencing the stealthiness of colloidal drug delivery systems. *Biomaterials* **2006,** 27, 4356-4373.
(27) Xia, X.; Yang, M.; Wang, Y.; Zheng, Y.; Li, Q.; Chen, J.; Xia, Y., Quantifying the Coverage Density of Poly(ethylene glycol) Chains on the Surface of Gold Nanostructures. *ACS Nano* **2011,** 6, 512-522.
(28) Mei, B. C.; Oh, E.; Susumu, K.; Farrell, D.; Mountziaris, T. J.; Mattoussi, H., Effects of Ligand Coordination Number and Surface Curvature on the Stability of Gold Nanoparticles in Aqueous Solutions. *Langmuir* **2009,** 25, 10604-10611.
(29) Simpson, C. A.; Agrawal, A. C.; Balinski, A.; Harkness, K. M.; Cliffel, D. E., Short-Chain PEG Mixed Monolayer Protected Gold Clusters Increase Clearance and Red Blood Cell Counts. *ACS Nano* **2011,** 5, 3577-3584.
(30) Tsai, D.-H.; DelRio, F. W.; MacCuspie, R. I.; Cho, T. J.; Zachariah, M. R.; Hackley, V. A., Competitive Adsorption of Thiolated Polyethylene Glycol and Mercaptopropionic Acid on Gold Nanoparticles Measured by Physical Characterization Methods. *Langmuir* **2010,** 26, 10325-10333.
(31) Louguet, S.; Kumar, A. C.; Guidolin, N.; Sigaud, G.; Duguet, E.; Lecommandoux, S.; Schatz, C., Control of the PEO Chain Conformation on Nanoparticles by Adsorption of PEO-block-Poly(l-lysine) Copolymers and Its Significance on Colloidal Stability and Protein Repellency. *Langmuir* **2011,** 27, 12891-12901.
(32) Ipe, B. I.; Shukla, A.; Lu, H.; Zou, B.; Rehage, H.; Niemeyer, C. M., Dynamic Light-Scattering Analysis of the Electrostatic Interaction of Hexahistidine-Tagged Cytochrome P450 Enzyme with Semiconductor Quantum Dots. *ChemPhysChem* **2006,** 7, 1112-1118.

(33) Hong, R.; Han, G.; FernÃ¡ndez, J. M.; Kim, B.-j.; Forbes, N. S.; Rotello, V. M., Glutathione-Mediated Delivery and Release Using Monolayer Protected Nanoparticle Carriers. *J. Am. Chem. Soc.* **2006,** 128, 1078-1079.
(34) Ojea-Jimelènez, I.; Puntes, V., Instability of Cationic Gold Nanoparticle Bioconjugates: The Role of Citrate Ions. *J. Am. Chem. Soc.* **2009,** 131, 13320-13327.
(35) Saha, K.; Agasti, S. S.; Kim, C.; Li, X.; Rotello, V. M., Gold Nanoparticles in Chemical and Biological Sensing. *Chemical Reviews* **2012,** 112, 2739-2779.
(36) Cedervall, T.; Lynch, I.; Lindman, S.; BerggÃ¥rd, T.; Thulin, E.; Nilsson, H.; Dawson, K. A.; Linse, S., Understanding the nanoparticleâ€“protein corona using methods to quantify exchange rates and affinities of proteins for nanoparticles. *Proceedings of the National Academy of Sciences* **2007,** 104, 2050-2055.
(37) Casals, E.; Pfaller, T.; Duschl, A.; Oostingh, G. J.; Puntes, V., Time Evolution of the Nanoparticle Protein Corona. *ACS Nano* 4, 3623-3632.
(38) Casals, E.; Pfaller, T.; Duschl, A.; Oostingh, G. J.; Puntes, V. F., Hardening of the Nanoparticle–Protein Corona in Metal (Au, Ag) and Oxide (Fe3O4, CoO, and CeO2) Nanoparticles. *Small* **2011,** 7, 3479-3486.
(39) Lipka, J.; Semmler-Behnke, M.; Sperling, R. A.; Wenk, A.; Takenaka, S.; Schleh, C.; Kissel, T.; Parak, W. J.; Kreyling, W. G., Biodistribution of PEG-modified gold nanoparticles following intratracheal instillation and intravenous injection. *Biomaterials* **2010,** 31, 6574-81.
(40) Sonavane, G.; Tomoda, K.; Makino, K., Biodistribution of colloidal gold nanoparticles after intravenous administration: Effect of particle size. *Colloids and Surfaces B: Biointerfaces* **2008,** 66, 274-280.
(41) Kreppel, F.; Kochanek, S., Modification of Adenovirus Gene Transfer Vectors With Synthetic Polymers: A Scientific Review and Technical Guide. *Mol Ther* **2007,** 16, 16-29.
(42) Immordino, M. L.; Dosio, F.; Cattel, L., Stealth liposomes: review of the basic science, rationale, and clinical applications, existing and potential. *International Journal of Nanomedicine* **2006,** 1, 297-315.

Chapter 4:

Functionalization of AuNPs with Cisplatin

4.1 Introduction

Cisplatin or cis-diamminedichloroplatinum (II), [$PtCl_2(NH_3)_2$], was originally synthesized in 1845, but not until 1970 was its antitumor activity established.[1] FDA approved its use for testicular and ovarian cancer in 1978. Just 5 years later, cisplatin was already the leading anticancer drug in USA. Today cisplatin is used worldwide to treat various types of cancers (i.e., non-small-cell lung cancer, ovarian cancer, germ cell tumors, osteosarcomas, etc), with a cure rate as high as 90% in testicular cancer.[2] However, its use is limited by severe side effects which result in systemic toxicity and poor patient compliance including renal toxicity, nausea, gastrointestinal toxicity, periphereal neuropathy, asthenia, and ototoxicity.[3, 4] This high toxicity profile, specially nephrotoxicity, make it impossible to achieve the full benefit of the treatment in a large number of patients.[5] In addition, acquired resistance and deactivation of the drug by plasma proteins are also limiting factors. Although second-generation platinum drugs (oxaliplatin and carboplatin) represent an improvement in some cancer treatments, the limitations due to toxicity have not been entirely overcome (Figure 4.1).[3, 6]

Recent efforts have been focused on targeting the tumor by using drug delivery systems to avoid organs where cisplatin is toxic. Nanoparticles are good candidates as carriers of cisplatin due to its ability to be accumulated in tumors and to protect cisplatin from plasma deactivation. However, the use of NPs to deliver drugs to the target is not without problems and some considerations should be taken into account before using NPs for drug delivery purposes. Skipping the biological issues, which will be discussed on subsequent

chapters, the typical synthesis of NPs give low concentration of NPs which results in low doses of drug, which might be insufficient to reach therapeutic effects. The attempt to concentrate NPs could lead to a lack of stability if special care is not taken. Not only colloidal stability, but stability of the link should also be guaranteed. Otherwise, unspecific release of the drug would lead to an impairment of the targeting strategy. In this context, responsive links, such as pH- or redox-sensitive links are attracting efforts.[7, 8] Moreover, this strategy ensures that the drug will be protected against being deactivated by plasma proteins which represent as much as the 90 % of the initial dose in classic clinical treatments.

In addition, cisplatin reactivity should be considered to determine a proper functionalization strategy. It is known that cisplatin derivatives have to distinct sides (Figure 4.1): The active one (e.g. the chlorides in cisplatin or water in aq. cisplatin) and the inert one (e.g. the ammonia groups in cisplatin). In the active part, there are the reactive groups (the leaving groups), whilst the inert part influence the biodistribution and tunes the reactivity of the metal center. At low chloride concentration, cisplatin undergoes exchange of chlorides by water ligands (in a process known as aquation). These aqua complexes are much more labile than their chloride counterparts. In fact, this substitution occurs naturally in cytoplasms, where chloride concentration is much lower than in the extracellular environment, and the resulting specie is the active specie that ultimately binds DNA.[9] Also, it is know that aqua species can undergo hydroxylation at high pH, which obviously implies a decrease of reactivity.[10]

The methodology to bind a cisplatin derivative via a pH-sensitive bond to MUA-capped AuNPs is presented here. The conjugation of cisplatin should be strictly controlled to avoid loss of colloidal stability: Concentration of cisplatin, time of reaction and pH influence both stability and loading. A fine control of these 3 parameters, allowed the loading of a great density of drug onto the surface of highly concentrated AuNPs (≈3 x 10^{14} NP/mL) which make possible to reach therapeutic doses. Stability issues in physiological media are also discussed here. Finally this study is extended to other sizes of AuNPs and to mixed layer-capped AuNPs.

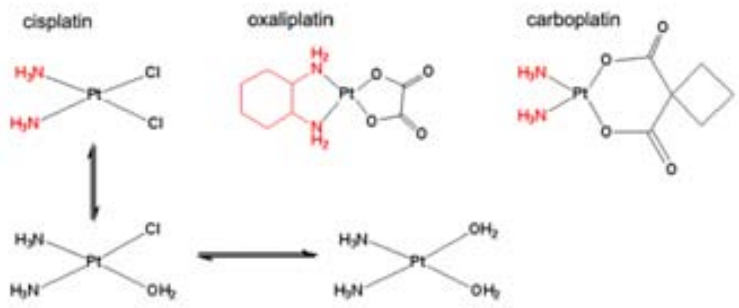

Figure 4.1. Different platinum anticancer drugs approved by the FDA. The active part is drawn in black**,** in all the cases is characterized by the presence of good leaving groups that will allow the Pt atom to bind the target. On the other side, the amines play a role in the modulation of the activity and in the distribution of the drug. In the case of cisplatin, the equilibrium that spontaneously occurs inside the cell (where the chloride concentration drops from 100 mM to 4 mM) is also shown.

4.2 Experimental

Aquation of cisplatin. A solution of $AgNO_3$ (169 mg, 1 mmol) in H_2O (2.5 ml) was added dropwise to a suspension of cisplatin (150 mg, 0.5 mmol) in H_2O (2.5 ml). A white solid (AgCl) precipitated and the yellow color of the initial mixture vanishes after completing the addition. The resulting suspension was heated to 50 ºC for 1 h and AgCl was then separated by centrifugation. The supernatant solution was evaporated to dryness and the residue recrystallized from an ethanol/water mixture.

Synthesis of MUA-capped AuNPs. AuNPs (13 nm) were synthesized following a seeding growth mechanism based on the standard method of gold salt reduction by citrate[11-13]. Specifically, Au seeds (7.5 nm, 5.5 x 10^{12} NP ml^{-1}) were synthesized by adding an aqueous solution of $HAuCl_4$ (1ml, 25 mM) to a boiling sodium citrate solution (150 ml, 2.2 mM). When the reaction was completed, the temperature was decreased to 90 ºC and $HAuCl_4$ (1ml, 25 mM) was added to the previously synthesized AuNPs. This step is repeated 2 more times in order to get the final AuNPs (13.3 nm, 5.5 x 10^{12} NP ml^{-1}). The conjugation of MUA was carried out by adding 2.2 ml of a 10 mM MUA basic solution to 50 ml of 13 nm AuNPs solution and stirred softly overnight.

AuNPs of different sizes (from 9 nm to 60 nm) were obtained after a seeding growth synthesis as explained in chapter 2. The 4 nm AuNPs were obtained by reduction of gold salt by $NaBH_4$. Briefly, a 0.25 mM solution of HAuCl4 was prepared in a 0.25 mM solution

of sodium citrate (150 mL). Then, 1.5 mL of an ice cold solution of $NaBH_4$ (0.1 M) was rapidly added under vigorous stirring. The solution turned to orange-red immediately.

Concentration of MUA-capped AuNPs. The conjugates were concentrated up to 2.75 x 10^{14} NP ml^{-1} by a destabilization-resuspension step. 2.5 ml of glycine / HCl buffer (200 mM, pH=2.6) was added to 50 mL of MUA capped AuNPs to destabilize them due to the protonation of MUA SAM. The solution was then centrifuged (2 min, 2500 rcf) and the supernatant removed. The pellet was resuspended in 1 ml tricine buffer (50 mM, pH=8). The excess of MUA was removed by a dialysis step (x1000, overnight). Surface Plasmon Resonance of AuNPs was determined at wavelengths from 300 to 800 nm.

Conjugation of $[Pt(H_2O)_2(NH_3)_2]^{2+}$ to MUA capped AuNPs. 5 µL of $[Pt(H_2O)_2(NH_3)_2](NO_3)_2$ aqueous solution (16.9 mg ml^{-1}) were added to 1 ml of MUA capped AuNPs (13 nm, 2,75 x 10^{14} NP ml^{-1}) at pH 8.3. The solution was softly mixed during 25 minutes and the reaction was stopped by removing the excess of cisplatin derivative by dialysis (x1000, overnight). Concentrations of aq. cisplatin and reaction times were modified in the concentration and time monitoring experiments. Actual conditions are indicated in the results section. Also, the concentrations used in the other sized AuNPs are indicated in the corresponding table.

Colloidal stability in blood. 17 µL of AuNP-cisplatin (2.75 x 10^{14} NP ml^{-1}) were added to 500 µL of human blood and gently mixed over 24 h. Colloidal stability was assayed by using DLS and UV-Vis spectroscopy.

pH-dependent release. The release of cisplatin in physiological conditions was performed in solutions consisting of 50 mM buffer species, 120 mM NaCl, and 20 % Foetal Bovine Serum (FBS). Buffer species were HEPES for pH 7.6, MES for pH 6.2 and 4.4, Glycine/HCl for pH 4.4 and 3.8 and Acetate for pH 4.4. 100 µL of AuNP-cisplatin were added to 900 µL of the corresponding buffered solution and mixed over differing lengths of time (2, 8, 24, and 144 hours). AuNPs were removed by means of two centrifugation steps (30 minutes, 35000 rcf). The amount of Pt in the supernatant was analyzed by using ICP-MS.

Stability of the link in physiologic conditions. 10 % of AuNPs-cisplatin (aquated and non-aquated) were added to cell culture media (DMEM with 4500 mg glucose/L, sodium bicarbonate and pyridoxine hydrochloride without L-Glutamine and phenol red) and incubated for 50 hours. AuNPs were removed by two centrifugation steps (30 minutes, 35000 rcf) and the amount of Pt in the subsequent supernatants analyzed by ICP-MS.

pH-dependent release in mixed layer-capped AuNPs. 50 μL of $[Pt(H_2O)_2(NH_3)_2](NO_3)_2$ (0.34 mg/mL) were added to 1 mL of mixed-layer AuNPs. The conjugates were gently stirred for 30 minutes and dialyzed overnight against a 1000-fold excess of deionized water.The buffers were prepared by adding 30 mM buffering specie (Hepes for pH 7.5, MES for pH 5.4, Glycine for pH 3.8), 120 mM NaCl, and 10 % FBS. 10 % (v/v) cisplatin conjugates were incubated with corresponding buffers during 148 hours. Then, AuNPs were removed by 2 centrifugation steps (35000 rcf, 30 min) and the amount of Pt in the supernatant analyzed by Inductively Plasma Coupled Mass Spectroscopy (ICP-MS). The loading of cisplatin on the AuNPs is also determined in every ratio assayed here.

4.3 Results and discussion

4.3.1 Modification (aquation) of cisplatin to promote coordination bond.

Cisplatin undergoes the substitution of Cl by H_2O in media which have low concentration of Cl^- (Figure 4.1). This occurs naturally inside the cell where the concentration of Cl^- drops from ≈100 mM to ≈4 mM. The aqua ligands in the resulting $[PtCl(H_2O)(NH_3)_2]^+$ and $[Pt(H_2O)_2(NH_3)_2]^{2+}$ are more labile than Cl^-, activating the drug and allowing the platinum atom to bind to bases on DNA.[14] We were interested in this specie instead of commercial cisplatin since H_2O is a better leaving group than Cl^-, allowing the formation of coordination bonds between the Pt molecule and the deprotonated MUA carboxylic groups on the NP. Otherwise, the commercial cisplatin molecule would be electrostatically attached to MUA.[15] The $[Pt(H_2O)_2(NH_3)_2]^{2+}$ solution was obtained by adding a solution of $AgNO_3$ to commercial cisplatin $[Pt(Cl)_2(NH_3)_2]$ to promote the exchange of Cl^- by H_2O ligands. After purification by recrystallization-washing steps, the solid $[Pt(H_2O)_2(NH_3)_2](NO_3)_2$ was obtained and dissolved in water before use. Final yield was 89 %. The substitution of ligands was proved by mass spectroscopy (ES-MS) with the appearance of aquated cisplatin (aq. cisplatin) peaks at m/z = 263, 264, 265 and 267 corresponding to the 4 Pt isotopes (^{194}Pt, ^{195}Pt, ^{196}Pt and ^{198}Pt) (Figure 4.2). No peaks at m/z=300 were observed, proving that no commercial cisplatin was present.

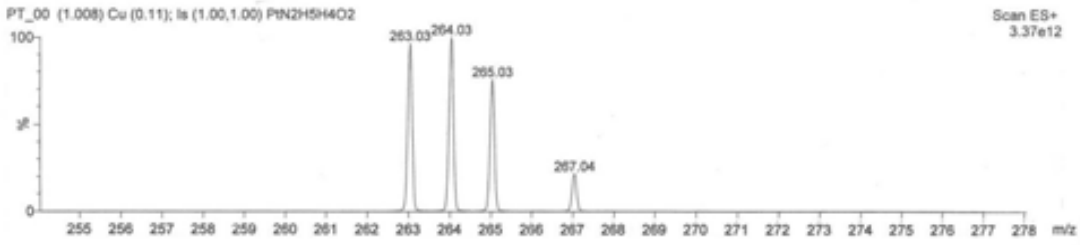

Figure 4.2 ES-MS spectrum of aquated cisplatin. Peaks corresponding to $[Pt(H_2O)_2(NH_3)_2 - H^+]^+$ were observed. The region m/z=100 to 500 was analyzed and no peaks at 300 were observed (not shown).

4.3.2 Conjugation of aquated cisplatin to MUA-capped AuNPs

We propose to attach aq. cisplatin via a coordination bond between carboxylic acids of MUA-capped AuNPs (13.3 nm, 2.8 x 10^{14} NP/mL) and the Pt atom of aq. cisplatin. This bond is known to be pH-sensitive and it is broken at acidic pH.[16] Thus, the stability of the link will be ensured during the circulation of the vehicle through the organism and the release will be only promoted after cell internalization via endocytic pathway, where the pH drops to acidic values.[17] Note that the mild acidic tumor environment is not enough to break the bond.

Several considerations regarding the reactivity of aq. cisplatin might be taken into account before conjugation to AuNPs: At high pH, aqua ligands can undergo deprotonation to give hydroxo complexes ($pK_{a1} \approx 5.5$, $pK_{a2} \approx 7.3$).[10] This reaction should be avoided since hydroxo-species are less reactive and thus coordination bond would not be formed. Unfortunately, we cannot work at low pH since AuNPs are electrostatically stabilized by MUA, which should be deprotonated to maintain the negative charge. The pK_a value of carboxylic acids in a MUA SAM is reported to be between 6–8,[18] therefore the working pH must be above this value to ensure colloidal stability. It is also known that hydroxylation is very slow at pH < 9.[10] Therefore, working at pH 8.3 ensures both colloidal stability and formation of the conjugate via a coordination bond.

Additionally, the negative charge given by MUA can be also quenched by the loading of aq. cisplatin. Thus, it is important to avoid an excessive quenching of charges to ensure colloidal stability. To choose appropriate conditions for the conjugation of aq. cisplatin, different amounts of aq. cisplatin were assayed and also the time evolution of the reaction was monitored. It is observed in figure 4.3a that low concentrations of aq. cisplatin did not induce the aggregation of AuNPs after 20 minutes. On the contrary, AuNPs became

unstable for concentrations of aq. cisplatin ≥ 0.386 mM. Regarding the time evolution, it is shown in figure 4.3b the spectra of AuNPs took before and every 5 minutes after addition of aq. cisplatin (0.480 mM). AuNPs were progressively losing their stability, as it is observed by the broadening of the peak; finally leading to aggregation and precipitation, as observed by the decrease in the absorbance.

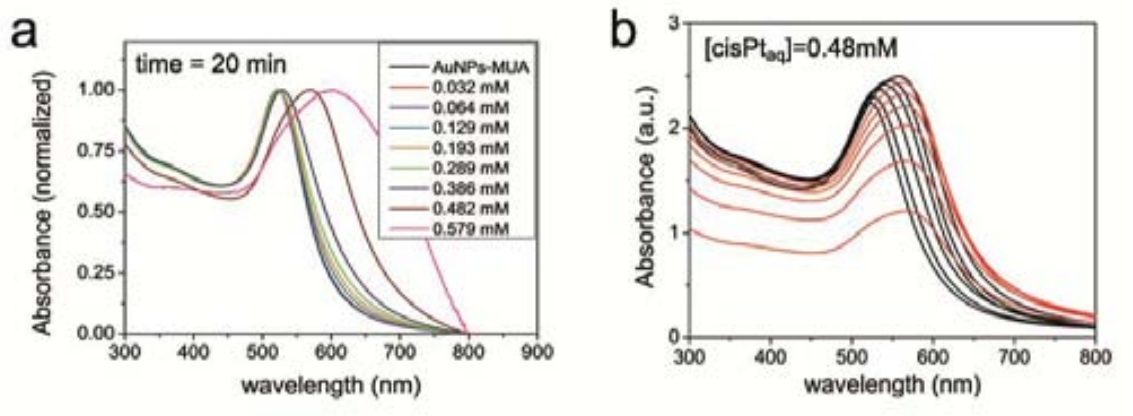

Figure 4.3 Stability of conjugates depending on concentration of aq cisplatin and time of reaction. (a) The SPR band was just slightly shifted for [aq. cisPt] < 0.386 which indicate the stability of these AuNPs. On the other side, concentrations higher than 0.386 mM led to aggregation of AuNPs. (b) The time evolution spectra showed a progressive aggregation of AuNPs at higher concentrations.

To achieve the maximum loading of aq. cisplatin without compromising colloidal stability, aq. cisplatin was added in a slight excess (0.165 mM) to highly concentrated AuNPs after adjusting the pH at 8.3. The reaction was monitored by zeta potential to avoid an excessive quenching of charge (Figure 4.4). The reaction was stopped by removing the excess of aq. cisplatin after 25 minutes by dialysis, when surface charge was -30.8 mV. It is commonly accepted that values above +/- 30 are needed to achieve colloidal stability.[19] This fact is in agreement with our observations that ζ-potential values that are less negative than -25 mV led to destabilization of the AuNPs and precipitation due to excessive quenching of the negatively charged carboxylic acid groups by aq. cisplatin.

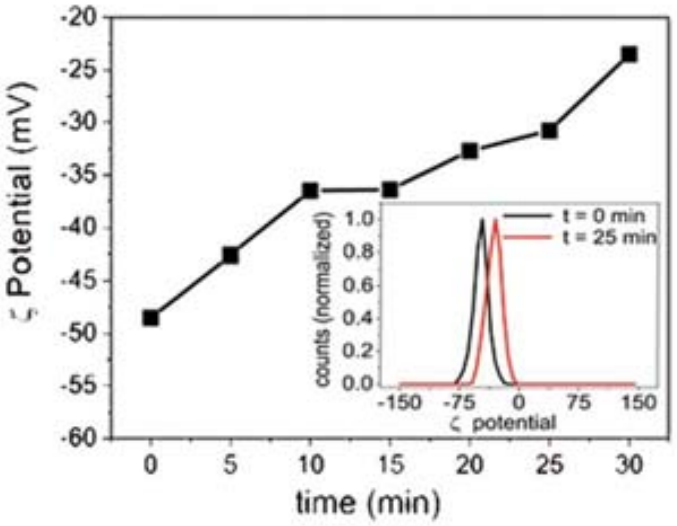

Figure 4.4 Time evolution of zeta-potential after addition of $[Pt(H_2O)_2(NH_3)_2]^{2+}$. It is shown the quenching of negative charge on the MUA due to the formation of a coordination bond between the carboxylic acid group and aq. cisplatin. Conjugates remained stable at ζ-potential values more negative than –25 mV.

At the end of the process, the loading of aq. cisplatin on the NP as measured by inductively coupled plasma mass spectrometry (ICP-MS) was 42.3 ± 0.8 mg Pt L^{-1}, which represents an approximate loading of 470 cisplatin molecules per NP. Taking into account the footprint of MUA on Au, which has been reported to be 0.21 nm^2, the number of MUA molecules per AuNP is calculated to be 2646. Assuming that every cisplatin binds to two carboxylic groups of MUA, 940 ligands out of 2646 will be occupied. Thus, only 35 % of MUA is quenched by cisplatin according to these theoretical calculations, leaving the other 65 % free to confer electrostatic stability to the NP. This correlates quite well with the loss of charge from -48.5 mV to -30.8 mV (36.5 % of charge is lost). Despite this need of leaving unoccupied MUA groups, the loading density of cisplatin per surface unit is the highest reported ever as far as our knowledge is concerned.

It is important to remark here that high concentration of AuNPs is required to reach significant doses of cisplatin even with this high loading density. The most used syntheses of AuNPs in aquose media give concentrations on the order of 10^{12} NP/mL,[11, 12, 20] which, considering the grafting density of aq. cisplatin, would yield concentration below 1 mg Pt L^{-1}. This extremely low concentration would make very difficult to reach therapeutic benefits since there is a limitation of volume that can be added to animals. For example, not more than 10 mL/kg should be injected to mice in a single bolus injection (i.e. 200 μL for 20 g mouse).[21] In order to overcome the dose limitation, we concentrated our AuNPs

50 times respect to the as synthesized samples. Firstly, we functionalized the AuNPs with MUA as explained in chapter 3. Then, we destabilized the MUA-capped AuNPs by addition of 2.5 ml of glycine / HCl buffer (200 mM, pH=2.6) to 50 mL of NPs. This caused the protonation of carboxylic groups from MUA and consequently the destabilization of the AuNPs. These AuNPs were easily concentrated by centrifugation (2 min, 2500 rcf) and removal of the supernatant. Finally, the pellet was resuspended in 1 mL tricine buffer (50 mM, pH 8.3) in which MUA is deprotonated again. Obviously, the excess of MUA as well as the buffer are removed by dialysis. For a typical in vivo experiment, AuNPs coming from several syntheses are required. Thus, not only narrow size distribution is required but also batch to batch reproducibility.

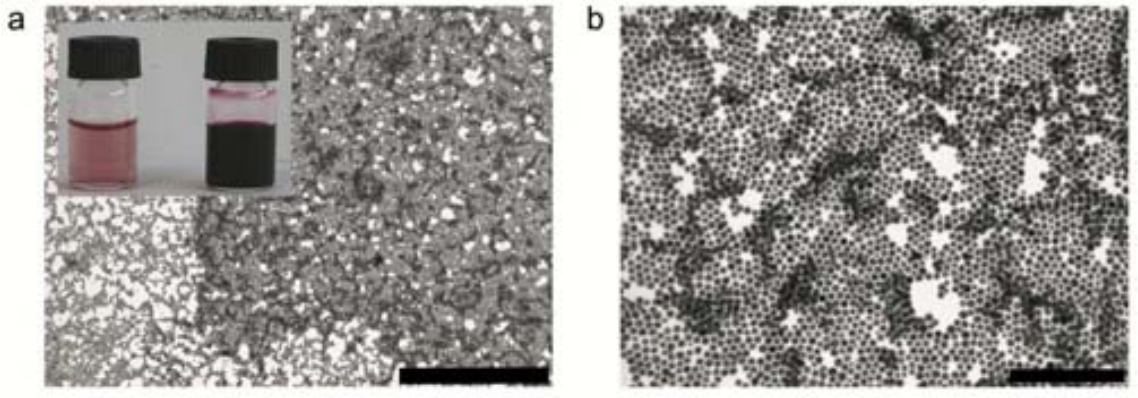

Figure 4.5. Synthesis and concentration of MUA-capped AuNPs. Representative TEM images of MUA-capped AuNPs from 3 different syntheses. Size distribution is 13.3 ± 1.9 nm as calculated measuring the size of > 2000 NPs by ImageJ software. In the inset, it is observed the appearance of AuNPs before and after concentration. Scale bars are 1 μm (a) and 200 nm (b).

4.3.3 Stability in physiological conditions

4.3.3.1 Colloidal Stability

Aggregation of AuNPs would modify the special properties achieved at the nanoscale and would result in a rapid clearance of the carriers by the immune system.[22] In addition, it could lead to misinterpret the in vitro results due to a non-homogenous distribution of NPs on the cell culture.[23] Thus, colloidal stability should be ensured not only during the synthesis step but also in working conditions for success of the in vivo targeting.[24] Since physiologic fluids have high ionic strength, aggregation of AuNPs could occur due to

compression of the Stern layer. Our system was stabilized by the formation of a protein corona by incubation with BSA as described in chapter 3. Briefly, 60 μL of 1.3 mM BSA solution was added to 1 mL of concentrated AuNPs-cisplatin and incubated for 30 minutes. The stability in human blood was then assayed by DLS and UV-VIS spectroscopy (figure 4.6). In DLS measurements, no peaks indicating the presence of aggregates in blood were observed (the 12-nm shift of the AuNPs-cisplatin peak is due to the formation of a transient soft protein corona).[25] Moreover, the aggregation of AuNPs is known to induce a broadening and shift of the SPR band. [26, 27] The spectrum of the AuNPs-cisplatin in blood is the same than the sum of blood and AuNPs-cisplatin spectra. Hence, no modification of the SPR was induced by blood. Therefore it is concluded that there were no aggregation of AuNPs in blood. Similar results were obtained when assayed in cell culture media (90 % DMEM w/o phenol red + 10 % FBS).

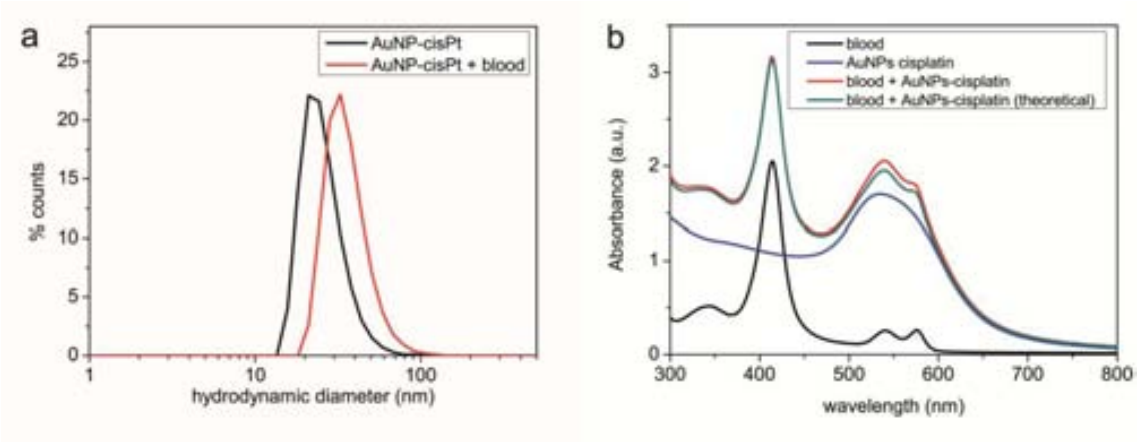

Figure 4.6 AuNPs-cisplatin stability in blood after 24 hours. (a) DLS measure of AuNPs-cisplatin. The 12 nm increase of the hydrodynamic diameter is due to the formation of a protein corona with serum proteins. (b) UV-VIS spectra of AuNPs-cisplatin, blood, and the mixture of both. The superposition of the spectrum obtained empirically and the one that resulted from summing the individual spectra indicates that AuNPs did not change their SPR band.

4.3.3.2 Stability of the link. The importance of coordination bond

The different reactivity of aq. cisplatin and cisplatin (see section 4.3.1) is translated to a different type of link. Briefly, while coordination bond with MUA is formed in the aqueous case, cisplatin is unable to form the coordination bond and it is therefore absorbed more weakly onto the MUA layer. This has implications in the stability of the link between the drug and the NPs. Thus, we tested the release profile of both conjugates in physiological

conditions. 10 % v/v of conjugate were added to cell culture media (DMEM + 10 % FBS) and the amount of Pt after removing AuNPs by centrifugation analyzed by ICP-MS. Both conjugates were stable in the conjugation vial (they are suspended in water). However, when assayed in cell culture media, the release after 55 hours was only 15 % in the coordination bond case whilst it was up to 60 %, with a burst release higher than 40 %, for cisplatin electrostatically linked (Figure 4.7). Cell culture media (as well as body fluids) has high ionic strength and consequently weak absorption is not efficient there. This experiment shows the importance of assaying the stability in working conditions since physiological media are complex media with a mixture of proteins and specially ions that can affect the properties of the conjugates.

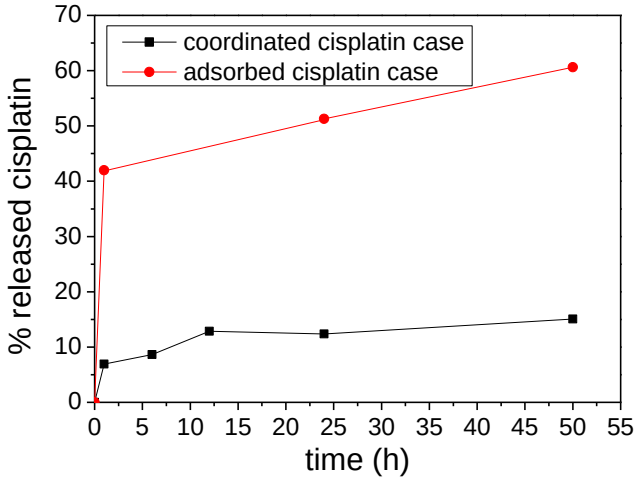

Figure 4.7. Release of cisplatin in cell culture media. Analysis of the amount of Pt in the supernatant after removal of AuNPs was performed by ICP-MS. Cisplatin weakly adsorbed was released in a higher degree than the linked via a coordination bond.

4.3.4 pH dependent release of cisplatin

The strength of the coordination bond has been proved above. Therefore, the release of cisplatin should be triggered in the site of action to have biological effect since cisplatin attached to the AuNP is not active. It is known that NPs are internalized by the endocytic pathway, in which the pH is progressively decreased. Fortunately, the coordination bond between Pt and carboxylic acid is broken under acidic conditions releasing the drug in its active form.[16] To prove the pH sensitivity of our link, AuNPs-cisplatin were incubated at different pH in physiologic conditions (50 mM buffer specie, 120 mM NaCl, 20% FBS) during different times. The amount of Pt was measured by ICP-MS after removing AuNPs

by 2 centrifugation steps. Note that the high affinity of cisplatin for proteins make impossible to assess the pH dependent release by performing a simple dialysis experiment. Only 5 % of the Pt was released from the AuNPs at pH 7.6 after 144 h, while values as high as 40 % of the Pt were reached at pH 4.4, and 67 % at pH 3.8 (Figure 4.8). One could expect that the presence of different nucleophilic species, as the presence of proteins, would alter the AuNP-MUA-CisPt ↔ AuNP-MUA + CisPt equilibrium. However, release seems to be independent of the buffering species, as demonstrated by observation of similar behaviors in three different pH 4.4 buffers. Note that the release at neutral pH here is lower than the release produced in CCM (figure 4.8). This might be attributed to a more complex composition of DMEM compared to the buffering species or to a higher unspecific release for the AuNPs-cisplatin used for the link stability experiment since the release at 1 h is as high as 7 %.

It is shown here that AuNPs-cisplatin linked via a coordination bond will likely travel through the body with no significant release of drug. On the contrary, once the pH is decreased in the endosomes, cisplatin will be released from the NPs. Then, it can exit the endosome by diffusion and enter the nucleus where it finally binds the DNA.

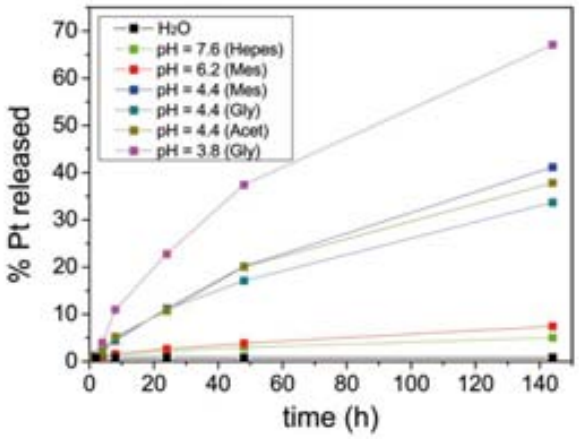

Figure 4.8 Cisplatin release **vs. pH in physiological conditions (high-ionic-strength media with 20% BSA).** At neutral pH the release was almost negligible but it increased at acidic pH values. The different buffering species used are indicated in the legend.

4.3.6 Conjugation of aq. cisplatin to different sizes of AuNPs

The chemistry and the stability issues discussed in the previous sections are very robust and they can be applied to different sizes of AuNPs. The only consideration that needs to be taken into account is the different surface area and consequently the different

availability of carboxylic groups. Thus the amounts of aq. cisplatin added should be adjusted for every size to avoid an excessive quenching of charge that would lead to aggregation of AuNPs.

MUA and subsequently aq. cisplatin were conjugated to different sizes of AuNPs ranging from 4 nm to 59 nm as explained above for 13 nm AuNPs (table 4.1). The amounts of MUA and obviously aq. cisplatin were proportional to the calculated surface area for every size. For example, surface area is 5.6 $x10^{16}$ nm^2/mL for 9.1 nm AuNPs and it is 3.8 x 10^{16} nm^2/mL for 16.8 nm AuNPs. Therefore the amounts of MUA and cisplatin added were 1.5 times greater in the case of 9.1 nm AuNPs than for 16.8 nm. The same protocol was applied for the other sizes.

The SPR of the different species and the loading of cisplatin were analyzed for every size. The analysis of the SPR revealed that no aggregation was produced in any case (Table 1). The expected red-shift after MUA conjugation was produced and it was followed by a slight red-shift due to cisplatin loading. Note also that these shifts are somehow size dependent since greater shifts were observed for smaller sizes. More important, peak analysis revealed that colloidal stability was maintained for every size and therefore that the amounts of aq. cisplatin added were never above the limit of tolerable charge quenching.

Size (nm)	Conc. (NP/mL)	SPR peak AuNPs (nm)	SPR peak AuNPs-MUA (nm)	SPR peak AuNPs-cisPt (nm)
3.8 ± 0.7	4.09E+15	505.88	519.25	522.50
9.1 ± 1.4	2.13E+14	514.68	521.69	525.85
16.8 ± 1.9	4.25E+13	518.79	522.6	524.84
26.5 ± 3.8	8.50E+12	521.75	524.07	525.04
39.6 ± 4.2	2.85E+12	526.73	528.58	528.68
58.6 ± 7.2	9.45E+11	534.91	536.64	536.49

Table 4.1. Analysis of the SPR shift after MUA and aq. cisplatin conjugation in different sizes of AuNPs. No broadening and large shift was observed. Therefore no aggregation occurred in any case.

The loading of cisplatin was quantified by ICP-MS. Results are summarized in table 4.2. As expected, the total loading (mg/L) is dependent on the total available surface. However, the footprint of cisplatin on the different sizes is quite similar (except for the 39.6 nm

AuNPs). Note that optimization of the loading of cisplatin onto 13 nm AuNPs had led to a density of cisplatin ca. 0.8 molecules/nm^2 which is the highest loading density achieved in similar NPs as far as we know. A simple translation of the protocol for different sizes and concentrations without any optimization led to comparable densities for most of the sizes assayed here. Thus, the strategy optimized for 13 nm AuNPs is straightforwardly translated to other sizes just by taking into account the total surface area of the AuNPs of interest. It is worth to mention, however, that different sizes have different fates inside the body.

Size (nm)	Conc. (NP/mL)	Total Surface Ratio	cisPt added (μL) (conc, mg/mL)	cisPt loading (mg Pt/L)	nº cisPt per NP	density (molec/nm^2)
3.8 ± 0.7	4.09E+15	1	7.5 (16.9)	46	34.8	0.76
9.1 ± 1.4	2.13E+14	0.30	22.6 (1.69)	10.9	158.3	0.60
16.8 ± 1.9	4.25E+13	0.20	15.2 (1.69)	6.3	457.5	0.52
26.5 ± 3.8	8.50E+12	0.10	7.5 (1.69)	3.9	1416.2	0.64
39.6 ± 4.2	2.85E+12	0.07	5.6 (1.69)	1.7	1841.1	0.37
58.6 ± 7.2	9.45E+11	0.05	4.1 (1.69)	2.1	6859.2	0.64

Table 4.2. Loadings of cisplatin to different sizes of AuNPs. The amounts of cisplatin added are proportional to the total surface (i.e. the surface of a NP multiplied by the number of NPs). The ratio of the total surface divided by the surface of the 3.8 nm case is provided for comparison. Total loadings were measured by ICP-MS and from this data were obtained the loading per NP and the footprint of cisplatin.

4.3.7 Conjugation of aq.cisplatin to mixed layer (MUA + SH-PEG) AuNPs

Mixed layers allow tuning the properties conferred by monolayers to the AuNPs. In the case of monolayers composed of MUA and SH-PEG, functionality and stability are tuned. The highly packed MUA layer provides plenty of carboxylic acids to further attach cisplatin, whilst SH-PEG is known to confer steric stabilization to the system. Details on the characterization and behavior of these conjugates can be found in section 3.3.3 of the present work. Here the functionalization of these conjugates with cisplatin and their different behaviors are discussed.

The strategy followed to conjugate cisplatin to mixed layer AuNPs was similar to the functionalization of MUA-capped AuNPs. 50 μL of aq. cisplatin (0.34 mg/mL) was added to 1 mL of mixed layer-capped AuNPs. Excess of aq. cisplatin was removed by dyalisis. The

loading of cisplatin in the different conjugates was analyzed by ICP-MS. In these conditions, Pt atom forms a coordination bond with carboxylic acid whilst its affinity with

ether groups from SH-PEG is lower.[10] Consequently, a different drug release behavior is expected depending on the composition of the layer. The release at different pHs at physiological conditions (10 % FBS+ buffer + 120 mM NaCl) after 148 hours is assayed here (Figure 4.9). Note that concentrations of cisplatin were always low to avoid total quenching of carboxylic groups from MUA; this would have led to a loss of colloidal stability. Thus, it is not surprising that at lower ratios, in which there is much more MUA loaded than SH-PEG, the behavior of the conjugates was quite similar since all cisplatin was expected to be linked to MUA. It is shown how cisplatin was only released significantly at acidic pH for ratios < 0.6. On the other hand, at higher ratios, in which the amount of SH-PEG loaded onto the NPs was greater, the unspecific release increased even at neutral pH. Thus, part of the specificity of the link for MUA is lost here. This is explained by the fact that MUA was not in such a great excess and some cisplatin was linked to SH-PEG. Cisplatin bond with SH-PEG is not a coordination, pH-sensitive, bond and therefore the release profile is different. Surprisingly, there is a decrease of the release when SH-PEG is the predominant component of the system (ratios > 0.88). This behavior is repeated in all the conditions and reproduced in different experiments. One possible explanation would be that a highly compact SH-PEG layer could bind cisplatin stronger, due to the crosslinking of a Pt atom by two stretched PEG chains. This strongly bond cisplatin was not significantly released even at low pH. Whichever the reason, it is clear that the pH-sensitivity, which controls the endosomal release of cisplatin in cell but not in blood, is lost in the SH-PEG layer, showing the importance of having mixed layers to tune the responses, in this case, stability (PEG) and functionality (MUA).

Ratio SH-PEG/ MUA	cisPt loading (mg Pt/L)
0	1.013
0.3	1.186
0.6	1.053
0.74	0.971
0.8	0.832
0.84	0.921
0.88	0.680
0.96	0.802
1	1.058

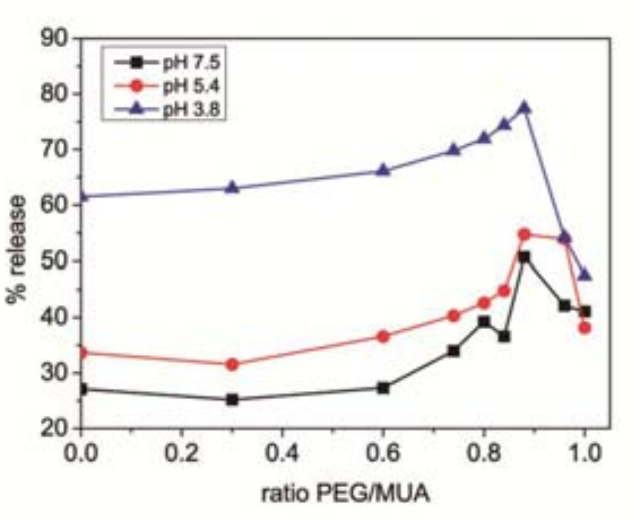

Figure 4.9 Cisplatin loading and pH-dependent release of cisplatin at different ratios of SH-PEG/MUA. The loading of cisplatin depending on the ratio SH-PEG / MUA is shown in the table. The release profile of cisplatin at 3 different pHs was analyzed for the different conjugates. Unspecific release increased as the amount of SH-PEG increased in the mixed layer.

4.3.7 Conjugation of other Pt derivative based on oxaliplatin

The strength of the coordination bond makes the link between AuNPs and aq.cisplatin very stable which is desired to avoid unspecific release of AuNPs. Aq. cisplatin is released at acidic pH. However, this release is slow with consequent low release at short times. Thus, one could think in increasing the efficiency of the triggering by making the link between Pt and AuNP more liable. To make the coordination bond between Pt and carboxylic acids weaker, we tested an aquated derivative of oxaliplatin (figure 4.10) in which the oxalate group was exchanged to water groups to facilitate the formation of the coordination bond. Interestingly, the ammines in the remaining ciclohexane-1,2-diamine group are greater electron donors than ammonia and therefore satisfy better the need of electroneutrality at the metal, polarizing the metal centre. The trans Pt-NHx and Pt-COOR bond of cisplatin share a metal orbital, consequently the polarization induced by the ammine, which is greater than the one induced by ammonia, makes the bond Pt-COOR more labile. This phenomenon is known as the trans effect and it is widely exploited in coordination chemistry, for example to control the specificity in the substitution of ligands.

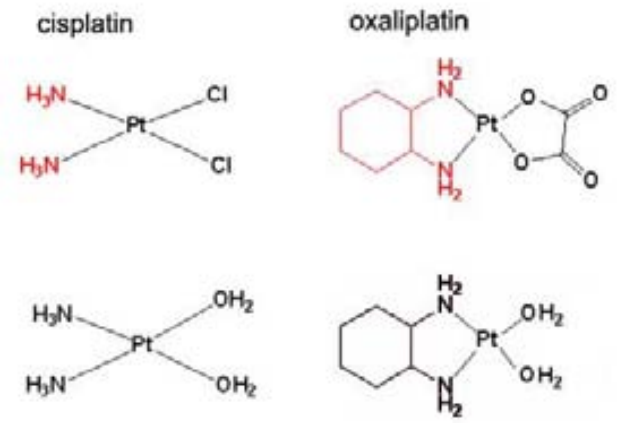

Figure 4.10. Chemical structure of cisplatin, oxaliplatin and their corresponding aquated derivatives.

We tested the conjugation of [Pt(cyclohexane-1,2-diamine)(H_2O)$_2$] (from now on referred as aq. oxaliplatin despite oxalate group is not present) onto 13 nm MUA-capped AuNPs. The conjugation was performed in a similar way that the one optimized for aq. cisplatin. Briefly, 20 μL of aq. oxaliplatin (4.22 mg/mL) was added to 1 mL of AuNPs (2.8 x10^{14} NP/mL). After 25 minutes, the reaction was stopped by removing the excess of aq. oxaliplatin by dialysis against water. The loading of Pt onto the NPs was 39.2 mg/L as assayed by ICP-MS. This corresponds to a loading of 432 molecules/NP, very similar to the loading of aq. cisplatin (470 molec./NP). UV-VIS spectra showed a red-shift after conjugation of MUA and aq. oxaliplatin, but no broadening of the band (Figure 4.10). Thus, no aggregation was produced in this functionalization as well.

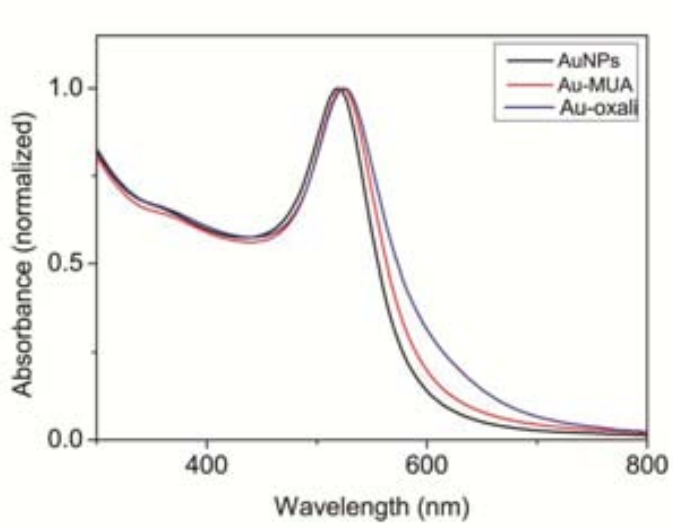

Figure 4.10 UV-VIS spectra of AuNPs after MUA and aq. oxaliplatin conjugation. The slight shifts of the SPR are consequent with conjugation and absence of aggregation.

The release of drug was studied also at pH 7.7 and 5.5 after 144 hours. Interestingly, the release at acidic pH was higher than the one previously observed for aq. cisplatin. Hence, the release of aq. oxaliplatin after 144 hours at pH 5.5 was as high as 72 %, far beyond from the 37 % found in the case of aq. cisplatin at even more acidic pH (4.4). Unfortunately, the unspecific release also increased: 29 % of aq. oxaliplatin at pH 7.7 was released after 144 h, whilst only 5 % was released in the case of aq. cisplatin.

Thus, it is clear that the link between Pt and MUA from AuNPs is more labile in the case of aq. oxaliplatin. However, this causes a drop in the strength of the link and consequently unspecific release at neutral pH is increased.

4.4 Conclusions

Here it has been presented the use of AuNPs as drug delivery scaffolds for cisplatin from the chemical point of view but bearing in mind the biological application. Thus, special attention was paid in some points which cannot be underestimated, namely the concentration of NPs to reach therapeutic doses, the maintenance of both colloidal and link stability in physiological conditions and the triggering of the release by a pH drop.

To achieve a strong bond, aquated cisplatin ($[Pt(H_2O)_2(NH_3)_2]^{2+}$) was used instead of cisplatin ($[Pt(Cl)_2(NH_3)_2]$). The aqua complexes are much more reactive than cisplatin and therefore the formation of a coordination bond with MUA was ensured. This confers high stability to the link in physiological conditions, which guaranteed the avoidance of unspecific release of drug. In addition, this link is pH-sensitive and therefore a pH-drop, typically produced in the endosomes after AuNPs internalization,[17] triggers the controlled release of cisplatin.

Also colloidal stability was assessed during the conjugation and in physiological environments. This is not trivial since the formation of the coordination bond quenches the negative charge given by carboxylic groups which is responsible of maintaining colloidal stability. Thus, concentration of aq. cisplatin and time of reaction should be strictly controlled during the functionalization to avoid excessive quenching. Also the pH working window is narrow and needs to be controlled since cisplatin would be hydroxylated at basic pH, whilst MUA would be protonated leading to a loss of colloidal stability at acidic pH. In biological fluids, in which the ionic strength is high, the stability is also compromised. However, AuNPs-cisplatin can be stabilized by the formation of a protective protein corona.

The loading density of cisplatin onto AuNPs is 1.2 nm^2/molecule, which is the highest reported for similar NPs as far as we know. Despite this high loading density, concentration of AuNPs up to 3 $x10^{14}$ NP/mL are required to achieve therapeutic doses (e.g. 2 mg cisplatin/Kg mouse) due to the limitation of the injectable volume to animals (i.e. 10 mL/Kg). This is approximately 50 times the concentration achieved in classical syntheses in aquose media.

This functionalization methodology was also assessed in other systems. AuNPs of different sizes from 4 to 60 nm were functionalized with aq. cisplatin leading to similar loading densities just by a straightforward adjustment of some parameters. Also mixed layer (MUA/SH-PEG) -capped AuNPs were successfully functionalized. In these AuNPs the importance of controlling the composition of the mixed layer was emphasized since a certain amount of SH-PEG is required to achieve the special properties given by this ligand (i.e. steric stabilization and protein adsorption inhibition), but excessive loading of SH-PEG led to an unspecific release of cisplatin.

Finally, the functionalization with another platinum derivative ([Pt(cyclohexane-1,2-diamine)$(H_2O)_2$]) was carried out. By using this compound, the link between AuNPs and the drug is more labile due to the higher trans effect of ammines compared to ammonia. This resulted in a higher release of drug at acidic pH, but at the expense of increasing the unspecific release.

4.5 References

(1) Rosenberg, B.; Vancamp, L.; Trosko, J. E.; Mansour, V. H., Platinum Compounds: a New Class of Potent Antitumour Agents. *Nature* **1969,** 222, 385-386.
(2) Wang, D.; Lippard, S. J., Cellular processing of platinum anticancer drugs. *Nat Rev Drug Discov* **2005,** 4, 307-320.
(3) Kelland, L., The resurgence of platinum-based cancer chemotherapy. *Nat Rev Cancer* **2007,** 7, 573-584.
(4) Reedijk, J., New clues for platinum antitumor chemistry: Kinetically controlled metal binding to DNA. *Proceedings of the National Academy of Sciences of the United States of America* **2003,** 100, 3611-3616.
(5) Oliver, T. G.; Mercer, K. L.; Sayles, L. C.; Burke, J. R.; Mendus, D.; Lovejoy, K. S.; Cheng, M.-H.; Subramanian, A.; Mu, D.; Powers, S.; Crowley, D.; Bronson, R. T.; Whittaker, C. A.; Bhutkar, A.; Lippard, S. J.; Golub, T.; Thomale, J.; Jacks, T.; Sweet-Cordero, E. A., Chronic cisplatin treatment promotes enhanced damage repair and tumor progression in a mouse model of lung cancer. *Genes & Development* 24, 837-852.
(6) Mani, S.; Graham, M. A.; Bregman, D. B.; Ivy, P.; Chaney, S. G., Oxaliplatin: A Review of Evolving Concepts. *Cancer Investigation* **2002,** 20, 246-263.

(7) Dhar, S.; Gu, F. X.; Langer, R.; Farokhzad, O. C.; Lippard, S. J., Targeted delivery of cisplatin to prostate cancer cells by aptamer functionalized Pt(IV) prodrug-PLGAâ€“PEG nanoparticles. *Proceedings of the National Academy of Sciences* **2008,** 105, 17356-17361.
(8) Comenge, J.; Sotelo, C.; Romero, F.; Gallego, O.; Barnadas, A.; Parada, T. G.-C.; Domínguez, F.; Puntes, V. F., Detoxifying Antitumoral Drugs via Nanoconjugation: The Case of Gold Nanoparticles and Cisplatin. *PLoS ONE* **2012,** 7, e47562.
(9) Klein, A. V.; Hambley, T. W., Platinum Drug Distribution in Cancer Cells and Tumors. *Chemical Reviews* **2009,** 109, 4911-4920.
(10) Kelland, L. R.; Farrell, N., *Platinum-Based Drugs in Cancer Therapy*. Humana Press Inc.: 2000.
(11) Bastús, N. G.; Comenge, J.; Puntes, V. c., Kinetically Controlled Seeded Growth Synthesis of Citrate-Stabilized Gold Nanoparticles of up to 200 nm: Size Focusing versus Ostwald Ripening. *Langmuir* **2011,** 27, 11098-11105.
(12) Kimling, J.; Maier, M.; Okenve, B.; Kotaidis, V.; Ballot, H.; Plech, A., Turkevich Method for Gold Nanoparticle Synthesis Revisited. *The Journal of Physical Chemistry B* **2006,** 110, 15700-15707.
(13) Park, C.; Kim, H.; Kim, S.; Kim, C., Enzyme Responsive Nanocontainers with Cyclodextrin Gatekeepers and Synergistic Effects in Release of Guests. *J. Am. Chem. Soc.* **2009,** 131, 16614-16615.
(14) Jung, Y.; Lippard, S. J., Direct Cellular Responses to Platinum-Induced DNA Damage. *Chemical Reviews* **2007,** 107, 1387-1407.
(15) Comenge, J.; Romero, F. M.; Sotelo, C.; Dominguez, F.; Puntes, V., Exploring the binding of Pt drugs to gold nanoparticles for controlled passive release of cisplatin. *Journal of controlled release : official journal of the Controlled Release Society* **2010,** 148, e31-2.
(16) Tseng, C.-L.; Su, W.-Y.; Yen, K.-C.; Yang, K.-C.; Lin, F.-H., The use of biotinylated-EGF-modified gelatin nanoparticle carrier to enhance cisplatin accumulation in cancerous lungs via inhalation. *Biomaterials* **2009,** 30, 3476-3485.
(17) Nel, A. E.; Madler, L.; Velegol, D.; Xia, T.; Hoek, E. M. V.; Somasundaran, P.; Klaessig, F.; Castranova, V.; Thompson, M., Understanding biophysicochemical interactions at the nano-bio interface. *Nat Mater* **2009,** 8, 543-557.
(18) Bishop, K. J. M.; Grzybowski, B. A., "Nanoions": Fundamental Properties and Analytical Applications of Charged Nanoparticles. *ChemPhysChem* **2007,** 8, 2171-2176.
(19) Sonavane, G.; Tomoda, K.; Makino, K., Biodistribution of colloidal gold nanoparticles after intravenous administration: Effect of particle size. *Colloids and Surfaces B: Biointerfaces* **2008,** 66, 274-280.
(20) Park, J.; Joo, J.; Kwon, S. G.; Jang, Y.; Hyeon, T., Synthesis of monodisperse spherical nanocrystals. *Angewandte Chemie-International Edition* **2007,** 46, 4630-4660.
(21) Diehl, K.-H.; Hull, R.; Morton, D.; Pfister, R.; Rabemampianina, Y.; Smith, D.; Vidal, J.-M.; Vorstenbosch, C. V. D., A good practice guide to the administration of substances and removal of blood, including routes and volumes. *Journal of Applied Toxicology* **2001,** 21, 15-23.
(22) Sperling, R. A.; Casals, E.; Comenge, J.; Bastus, N. G.; Puntes, V. F., Inorganic Engineered Nanoparticles and Their Impact on the Immune Response. *Current Drug Metabolism* **2009,** 10, 895-904.
(23) Cho, E. C.; Zhang, Q.; Xia, Y., The effect of sedimentation and diffusion on cellular uptake of gold nanoparticles. *Nat Nano* **2011,** 6, 385-391.
(24) Ruenraroengsak, P.; Cook, J. M.; Florence, A. T., Nanosystem drug targeting: Facing up to complex realities. *Journal of Controlled Release* 141, 265-276.
(25) Casals, E.; Pfaller, T.; Duschl, A.; Oostingh, G. J.; Puntes, V., Time Evolution of the Nanoparticle Protein Corona. *ACS Nano* 4, 3623-3632.
(26) Grabar, K. C.; Smith, P. C.; Musick, M. D.; Davis, J. A.; Walter, D. G.; Jackson, M. A.; Guthrie, A. P.; Natan, M. J., Kinetic control of interparticle spacing in Au colloid-based surfaces: Rational nanometer-scale architecture. *J. Am. Chem. Soc.* **1996,** 118, 1148-1153.

(27) Kelly, K. L.; Coronado, E.; Zhao, L. L.; Schatz, G. C., The Optical Properties of Metal Nanoparticles: The Influence of Size, Shape, and Dielectric Environment. *The Journal of Physical Chemistry B* **2002,** 107, 668-677.

Chapter 5:

AuNPs-Cisplatin as Drug Delivery Systems: *In Vitro and In Vivo* Experiments

5.1 Introduction

Cisplatin –as other molecular drugs- is small enough to travel along with ions and small nutrients through the body due to the selective permeability of continuous capillaries for ions and small molecules.[1, 2] This results in high index of permeability and distribution through the whole body what is intended to allow the active principle to reach its target.[3, 4] Unfortunately, this widespread distribution of the drug is at the origin of unwanted side effects, causing low drug selectivity and efficiency.[5] In fact, the severe nephrotoxicity induced by cisplatin is a dose limiting factor and in many cases, the treatment must be stopped before therapeutic benefits are reached. In addition, this is a reason to prevent its use in patients with renal insufficiency.

On the contrary, nanoscale objects travel following particular paths through the body.[2, 6] This results in the passive accumulation of nanocarriers in:

i. Organs of the mononuclear phagocyte system[7] (liver, spleen and bone marrow), where blood vessels are fenestrated with gaps ranging between 100 and 1000 nm.

ii. Inflamed tissue, where an increased permeability is achieved through temporal induced gaps to recruit immune cells[1].

iii. Solid tumors,[8] in which its rapid growth results in leaky vessels. These fenestrated vessels allow macromolecules and NPs to permeate through the tumor. In addition, the nanoparticles are retained due to the lack of a functional lymphatic system. This effect

(Enhanced Permeability and Retention effect, EPR) is widely reported in the literature[6, 9] and has been exploited to passively accumulate nanocarriers in tumors.[10]

It is important to choose appropriate NPs since the pharmacokinetics and biodistribution of the conjugates will be governed by the physicochemical properties of the carrier rather than by the ones of the drug.[11] In addition, EPR effect is known to be size dependent. For example, it has been reported that 20 nm PEG-coated AuNPs showed the best behaviour for tumor treatment since they present a high accumulation rate because of their long half-life in blood and an acceptable penetration in the tumor. On the other hand, larger NPs (>40 nm) failed to penetrate deep into the tumour and they were only accumulated at the vicinity of the vessels.[12] Smaller NPs, which would have penetrated deeply, do not have the opportunity to be significantly accumulated in the tumor due to renal clearance. Obviously, these properties would have been modified if colloidal stability had been compromised, showing again the importance of maintaining NPs stable along the process.

Once in its site of action, cisplatin enters the cells mainly by passive diffusion through the membrane, but also it is actively transported by metal transporters.[13] In the cytoplasm, where chloride concentration drops from 100 mM to 4 mM, cisplatin undergoes exchange of chlorides for water ligands. This aquated derivative is much more reactive than the chlorinated one; and it is the active specie. DNA is its primary target: Different types of adducts between the Pt atom and DNA strands are formed, being intrastrand cross-links the most numerous.[14] These adducts interfere with proteins involved in the mechanisms of replication and repairing of DNA, which ultimately lead to apoptosis.[15] This mechanism of cell death is very effective. Thus, there is no need to improve the efficacy of the drug, but to improve its efficiency, mainly by reducing the side effects of cisplatin by means of a better delivery and avoiding organs where cisplatin is known to be highly toxic.

Although a better targeting will likely imply an improvement in the therapy, the potential risks of using nanocarriers should be deeply analyzed. NPs are known to be accumulated not only in the tumor, but also in organs of the mononuclear phagocyte system since the vessels in those organs present also fenestrations. Thus, evaluation of possible adverse effects needs to be considered. Moreover, a usual mistake is to consider NPs as inert systems that do not evolve with time. However, they aggregate if special care is not taken, or release ions under certain conditions. Both processes could lead to adverse effects and/or to a misinterpretation of biological results. For example, aggregation might induce cell death in *in vitro* experiments[16] or to a rapid clearance in *in vivo* assays,[17] which might

lead to an overestimation and underestimation respectively of the capability of the system to cause therapeutic benefit.

In this chapter, AuNPs-cisplatin were tested in *in vitro* assays to evaluate the cell and DNA accumulation as well as cell viability. More importantly, *in vivo* assays using tumor-bearing mice were also performed. This includes evaluation of the therapeutic efficacy and evaluation of the toxicity induced by cisplatin and by AuNPs-cisplatin. Interestingly, nephrotoxicity, which is dose limiting in the clinics, was avoided only in the case of animals treated with AuNPs-cisplatin. In addition, systemic toxicity, as evaluated by body weight loss and analyzing relevant biomarkers, was also improved. Organs in which NPs are known to be accumulated (liver and spleen) were carefully examined showing no adverse long-time effects. Thus, the toxicological profile of cisplatin is clearly reduced without affecting its antitumor activity. The lack of toxicity is correlated to the modification of the pharmacokinetic properties and biodistribution of the drug by conjugation to AuNPs.

5.2 Experimental

Cell culture. The human lung carcinoma derived cell line A549 was obtained from American Tissue Culture Collection (ATCC) and cultured in a 1:1 mixture of Dulbecco´s Modified Eagle´s Medium (DMEM, Sigma-Aldrich) and Ham´s F-12 Medium (Sigma-Aldrich), supplemented of 10 % (v/v) foetal bovine serum (FBS, GIBCO-Invitrogen) and 1 % (v/v) of L-glutamine, penicillin and streptomycin solution (GPS, Sigma-Aldrich).

Cell internalization and DNA accumulation. To quantify Pt and Au cell internalization, 5 x 10^5 cells were plated in 60 mm diameter plates (Falcon) and 24 hour later, medium was changed for treatments diluted in culture medium: free cisplatin or cisplatin conjugated to AuNPs (2 μg cisplatin/ml in both cases). After 0.5, 1, 3, 6, or 24 hours with the treatment, cells were trypsinized and centrifuged, supernatant was removed and cells were resuspended in 0.5 ml 65% HNO_3 (Merck). The amount of Pt and Au was determined by ICP-MS (Bruker 820-MS). To quantify cisplatin bound to DNA, 10^6 cells were treated as above and DNA extraction was performed by phenol/chloroform/isoamylalcohol (50:49:1) extraction.[18] DNA was finally resuspended in 200 μl. This solution was used to determine both the amount of DNA, and Pt and Au by UV-Vis spectroscopy and ICP-MS respectively.

TEM cells imaging. A549 cells were centrifuged for 15 min at 3000 rpm, fixed by immersion for 45 min in 2.5% glutaraldehyde in sodium cacodylate buffer (0.15 M, pH = 7.3), postfixed with 2% osmium tetroxide in the same buffer, dehydrated, embedded in LRWhite resin, Medium Grade, and sectioned. Sections were stained with uranyl acetate and lead citrate and examined in a Zeiss 902 electron microscope (Carl Zeiss, F.R.G.) at 80 kV accelerating voltage.

Cell viability assay. 1000 cells/well were seeded in a 96-well plate and incubated at 37 ^{0}C with 100 μL of DMEM. After 24 hours, the different treatments resuspended in 100 μL of fresh DMEM were added to the corresponding wells. Cells were treated for 48 hours. Finally, cells were washed with 200 μL of PBS, and then 180 μL of fresh media was added. Finally, 20 μL of tetrazolium were added to every well and cells were incubated 1.5 hours. The absorbance was measured at 450 and 620 nm. The amount of formazan is proportional to A_{620}- A_{540} and 100 % of cell viability is assigned to cells that received no treatment.

Therapeutic efficiency of AuNPs-cisplatin in in vivo models. Mice with severe combined immunodeficiency (SCID) between 8 and 14-weeks-old were used to grow xenotransplant flank tumors, one by mouse, by subcutaneous injection of 20 x 10^6 A549 tumor cells. For monitoring, tumors were measured three times weekly and the tumor volume was determined by the formula $V = (A \times B^2) / 2$, where A is the largest diameter and B is the shortest diameter measured by caliper. After 4-5 weeks, once the tumor volumes were ≥ 100 mm^3 and mean tumor size had reached 300 mm^3, mice were divided into four groups of eight mice for treatments, minimizing weight and tumor size differences. Tumor-bearing mice were treated by injection of 3 mg free cisplatin Kg^{-1}, 1.25 mg conjugated cisplatin Kg^{-1}, and controls were maintained without treatment. Treatments were administered in mice anesthetized by ip injection of 2,2,2-tribromoethanol-2-methyl-2-butanol (Avertine®, Sigma Aldrich) two times (day 0 and 3). Mice were monitored for a maximum of 10 days after first dose to avoid excessive tumor load, and mice weight and body weight loss were also monitored according with good laboratory practices to check excessive toxicity of treatments. Complete tumors of all animals were extracted and weighted at endpoint of efficacy studies.

Another round of mice was studied for a longer treatment period. Mice were injected subcutaneously with A549-luc-C8 cells (Caliper) (0,5 x 10^6 cells). Tumours were grown during 9 days before starting the treatment. Tumor growth was monitored every 3 days by in vivo imaging system (IVIS® Spectrum, Caliper), 150 mg D-Luciferine / kg mice was

applied ip 5 minutes before scanning. Mice were placed under the CCD camera and kept under isoflurane anaesthesia (1.5 – 2 %) during the measures. 5 mice received 3 ip injections of 1.5 mg cisplatin Kg^{-1}, 5 mice received the same amount of cisplatin conjugated to AuNPs and 5 mice, controls, were maintained without treatment.

Biodistribution in mice. In vivo biodistribution was performed by treating 2 groups of 12 female tumor-bearing SCID mice (3 mice per point). All mice received a single intraperitoneal (ip) dose of 4 mg cisplatin Kg^{-1} mice. At 0.5, 3, 6 and 24 h after the treatment, blood, heart, lungs, kidney, brain, liver, spleen, ovaries and tumor were collected and weighted. To each organ, previously weighed, were added 3 mL of 65% HNO_3 and kept 3 h at room temperature in closed tubes and then 24 h at 60 º C. Afterwards 2 ml H_2O_2 were added to the sample and heated to 60 ºC. Finally H_2O was added up to a final volume of 10 ml and filtered with 0.22 μm filters. Blood serum was diluted 1:20 and measured by ICP-MS. Blood cells were resuspended in 6 ml of 65% HNO_3 and 2 ml of H_2O_2 and heated in a microwave oven (Milestone Ethos 1) as follows: 2 minutes at 85 ºC, 3.5 minutes at 135 ºC, and 15 minutes at 230 ºC. After cooling down, H_2O was added up to 10 ml final volume. The resulting solutions of the above procedures were directly measured in ICP-MS for the determination of Pt and Au.

Kidney and spleen histology. Proximal tubular degeneration was induced in mice by 3 consecutive ip injections (days 0, 3, 6) of 5 mg cisplatin Kg^{-1} mice. The same dosage was applied in the case of AuNP-cisplatin while control mice received no treatment. Animals were sacrificed 3 days after the last injection. Mouse kidneys and spleen were immersion-fixed in 10% neutral buffered formalin for 24 h and embedded in paraffin routinely. Sections (4 μm thick) were mounted on microslides and stained with hematoxylin-eosin. The specimens were examined and photographed using an Olympus PROVIS AX70 microscope (Olympus, Tokyo, Japan) equipped with an Olympus DP70 camera without prior knowledge of the applied experimental protocol.

5.3 Results and discussion

5.3.1 Cell internalization & DNA accumulation

Low cellular uptake of the drug may limit the efficacy of a chemotherapeutic treatment,[19] therefore cisplatin cellular uptake as DNA binding are employed as sign of therapeutic activity. Adenocarcinomic human alveolar basal epithelial cells (A549) were treated with

both free cisplatin and cisplatin conjugated to AuNPs (AuNP–cisplatin) at the same Pt concentration (6.7 μM, equivalent to 2 μg cisplatin / mL). As can be observed in transmission electron microscopy (TEM) images (Figure 5.1), AuNPs mainly reside inside vesicles that evolve to form late endosomes and endolysosomes (vesicle size and number of particles per vesicle increase with time). These vesicles provide an acidic environment that promotes the release of cisplatin from the AuNPs, and its further escape from the endosomes to continue its journey towards the DNA. Interestingly, the mechanism of drug entry into the cell is modified by the conjugation: free cisplatin enters mainly via passive diffusion through the membrane and by some transporter-mediated routes (e.g., copper transporters)[14], whereas cisplatin attached to AuNPs entered via an endocytic pathway.

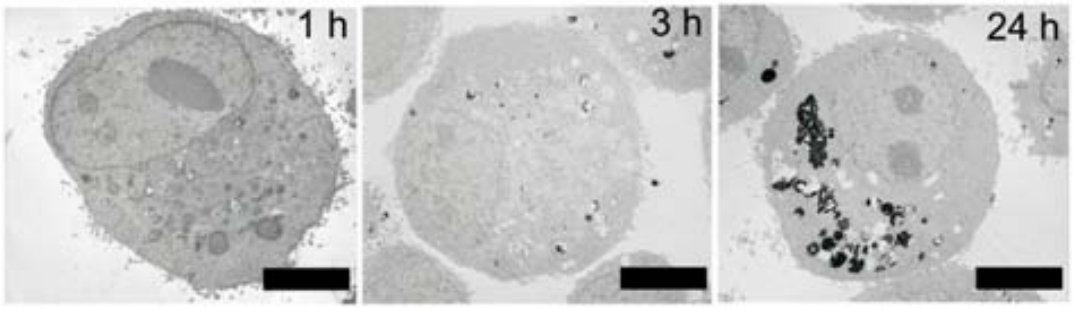

Figure 5.1 Cell internalization. Representative TEM images showing the internalization of particles at 1, 3, and 24 h. It is clearly shown that AuNPs were entrapped in vesicles that progressively fuse. The cell nucleus remained free of AuNPs. Scale bars, 4 μm.

The accumulation of cisplatin in cells was also quantified for both treatments (Figure 5.2). It was observed that cell accumulation of platinum was increased in cells treated with AuNPs-cisplatin compared to cells treated with the same amount of free cisplatin (6.7 μM). Pt levels were slightly increased at short times, whilst a 4-fold increase was observed after 24 hours. As expected, the accumulation kinetics of Au and Pt were linked in the treatment with AuNPs-cisplatin. This greater accumulation in cells was not translated to so great accumulation on the DNA (Figure 5.2b). This is not surprising since only cisplatin that is released from AuNPs, and escapes from the endosomes has the chance to find its target. A decrease of Pt levels in DNA over time was observed in both cases and it can be explained by two mechanisms: The death of cells that had high levels of cisplatin on the DNA and repairing of DNA in which cisplatin has been linked mainly via the nucleotide excision repair (NER) mechanism.[14] It is worth mentioning here that no significant amount of Au was found in the nucleus at any time and therefore the observed Pt came from Pt that had been released from the NPs.

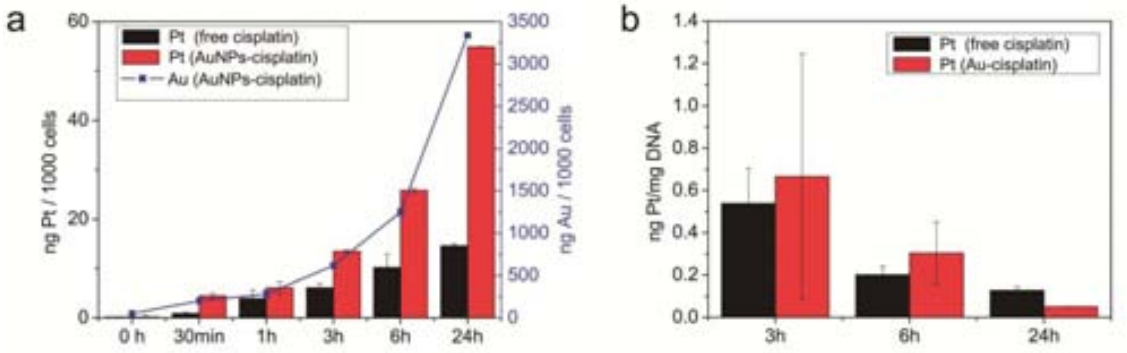

Figure 5.2 Cell and DNA accumulation of cisplatin over time. (a) Amounts of Pt in cell for both treatments and amount of Au for AuNPs-cisplatin treatment. (b) Amount of Pt found in the DNA. No significant amount of Au was found in the DNA.

5.3.2 Cell viability

Cell viability was assessed by EZ4U cell proliferation assay. This assay is based on the reduction of a water-solube tetrazolium salt by the mitochondria of living cells yielding formazan, which has a strong absorption at 450 nm. The absorption is proportional to the amount of tetrazolium reduced. Therefore mitochondrial activity is correlated with cell viability in this assay.

Adenocarcinoma human epithelial cells (A549) were chosen as a model cell for the in vitro tests. Here, 2000 A549 cells/well were seeded in a 96 well plate. 24 hours later cells were treated with concentrations up to 3 x 10^{13} AuNP-cisplatin/mL (32.5 μM of cisplatin) and incubated 48 hours before performing the assay. Then EZ4U assay was performed as indicated by the manufacturer, but adding a previous washing step with PBS to remove the AuNPs in the media to avoid optical interferences with the absorption of formazan. Briefly, cells were washed with 200 μL of PBS, and then 180 μL of fresh media was added. Finally, 20 μL of tetrazolium were added to every well and cells were incubated 1.5 hours.

In this EZ4U 24h assay, no significant decrease of cell viability in A549 cells treated with AuNPs-cisplatin for any of the assayed concentrations was observed. This has not to be necessarily a problem since our system has been designed to show the benefits in *in vivo* experiments. Note that in the organism, free cisplatin is rapidly cleared by the kidneys having a blood half-life of less than 30 minutes and most of the remaining drug is deactivated by plasma proteins before reaching the target.[20] These losses, which have been calculated to be as high as 98 % of the dose used in clinics, do not happen in closed

systems such as cell cultures, where the efficacy of free cisplatin is extremely high. Additionally, in the case of AuNPs-cisplatin, the vehicle protects the drug both from renal clearance and plasma deactivation because the strength of the link avoids unspecific release of cisplatin. However, the release of cisplatin from the NPs is sustained over time after the triggering. For example, the release at pH 4.4 was 10 % after 24 hours (as showed in chapter 4, figure 4.8). Thus, when same doses of free cisplatin and AuNPs-cisplatin are used in *in vitro* experiments, in which there are no loses of drug in any case, it is likely that in the AuNPs-cisplatin treatment, the low release of cisplatin from the AuNPs make the effective dose much lower than when treated with free drug. This is corroborated by the lower accumulation on the DNA after 24 hours. Fortunately, this is largely compensated in *in vivo* experiments, in which 98% of free cisplatin is rapidly lost either by renal clearance or by albumin deactivation, whilst the clearance of AuNPs-cisplatin is much more slow. Note also, that higher doses of AuNPs-cisplatin could not be used due to the impossibility to concentrate more the NPs and the restriction of the volume of treatment that can be added to cells, which is never higher than 10 % of total volume. This lack of efficacy in *in vitro* assays has been reported in other cases which showed later efficacy in *in vivo* experiments.

To prove that the carriers are not toxic by themselves and to show the potential efficacy of our DDS, AuNPs and AuNPs conjugated to aq. oxaliplatin (see section 4.3.7) were also tested. This link is more labile thanks to the ciclohexane-1,2-diamine group and therefore the release of drug is maximized here to show effects even in *in vitro* assays. EZ4U assay was performed as indicated above. It is shown in figure 5.3 that AuNPs conjugated to oxaliplatin retained part of the toxicity observed for free oxaliplatin whilst AuNPs by themselves showed no toxic effect. The same comments than the ones made previously for cisplatin account for the greater efficacy of the free drug here. An additional experiment to discard a large contribution of the oxaliplatin that could have been unspecifically released was also performed. AuNPs-oxaliplatin were incubated in cell culture media for 96 hours and then AuNPs were removed by centrifugation and cells treated with the resultant supernatant. At the highest concentration of AuNPs-oxaliplatin tested here cell viability was 44.7 %, whilst it was 82.2 % with the corresponding supernatant. Even though unspecific release of oxaliplatin seems to contribute to the observed decrease in cell viability of AuNPs-oxaliplatin, its effect is not dramatic.

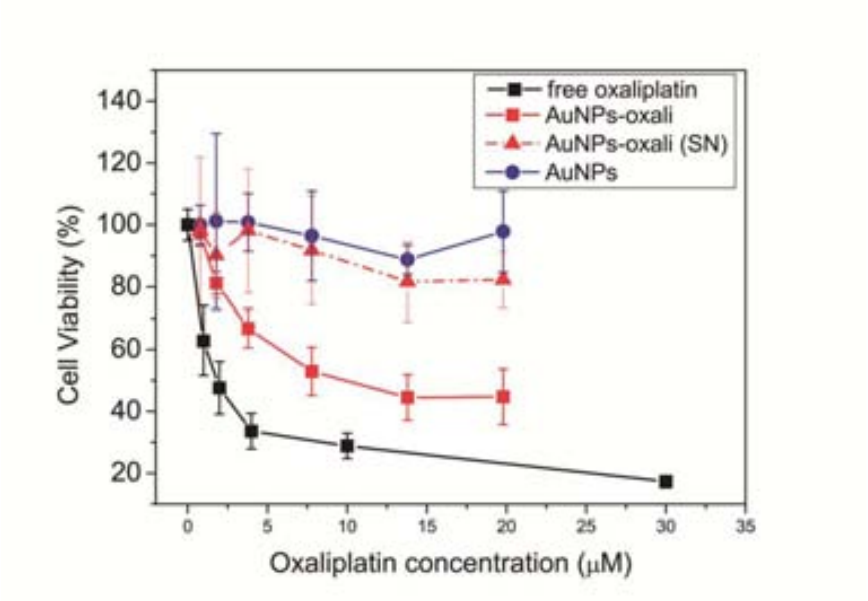

Figure 5.3 Cell viability of A549 cells after treaments with free oxaliplatin and AuNPs-oxaliplatin. In this case oxaliplatin conjugated to AuNPs retains part of its toxic activity in vitro due to the weaker link with the NPs than in the case of cisplatin. The contribution of unspecific release is not dramatic as assessed by analyzing the viability of the supernatant coming from AuNPs-oxaliplatin incubated in cell culture media.

5.3.3 Therapeutic Efficiency of AuNPs-cisplatin in *in vivo* models.

In this section the reduction of the tumor will be analyzed using the same animal model but two different approaches that differ on the treatment length, the methodology to measure tumor volume and the initial size of the tumor. These approaches will be discussed in detail in the following subsections. Animal model used for both treatments were Severely Compromised ImmunoDeficient (SCID) mice bearing A549 xenografted tumors implanted subcutaneously.

If tumor progression has to be measured by size (e.g. using a caliper), initial tumors must be large enough to be measurable, in which case they are normally poorly irrigated and even may contain necrotic areas (section 5.3.3.1). Newer bioluminescent techniques (e.g. IVIS ®), which depend on enzymatic activity, are a good alternative to caliper measurements because they are more sensitive and therefore work properly with smaller tumors. This technique has been used to follow tumorigenesis and response of tumors to treatment in animal models, since the expression of a bioluminescent marker specific of the implanted tumor cells is supposed to be proportional to the number of living cells[21] (section 5.3.3.2). However, environmental factors and therapeutic interferences may cause

some discrepancies between tumor burden and bioluminescence intensity in relation to changes in proliferative activity; this must be taken into account along with the differing individual response to the tumor and the treatments.

5.3.3.1 Short treatment and tumor volume measured by caliper

Tumor-bearing mice were treated by 2 consecutive intraperitoneal injections (day 0 and day 3) of 3 mg free cisplatin/Kg vs 1.25 mg conjugated cisplatin/Kg, and controls were maintained without treatment (5 mice per group) (Figure 5.4). It is observed that the antitumor effect of cisplatin was maintained for the cisplatin conjugated to AuNPs, even though doses of cisplatin conjugated to AuNPs were lower than free cisplatin. This was because greater doses were not achieved due to the limitation of volume that can be injected to mice. Interestingly, even using lower concentration the anticancer effect of cisplatin was not impaired whilst the toxicity induced by cisplatin was clearly reduced as indicated by the absence of body weight loss only in mice treated with AuNPs-cisplatin and by the death of 3 mice in the case of free cisplatin treatment. The toxicity aspects of both treatments will be largely discussed in section 5.3.5.

The recovery of the tumor volume once the treatment was stopped, commonly known as catch up effect, is not strange in the clinics and it was also observed here. It seems clear that to observe greater effects several cycles of treatment should have been performed. However, the mean tumor volume at the beginning of the experiment (300 mm^3) does not allow a long treatment since treatment should be stopped before tumor volume reaches 1600 mm^3.

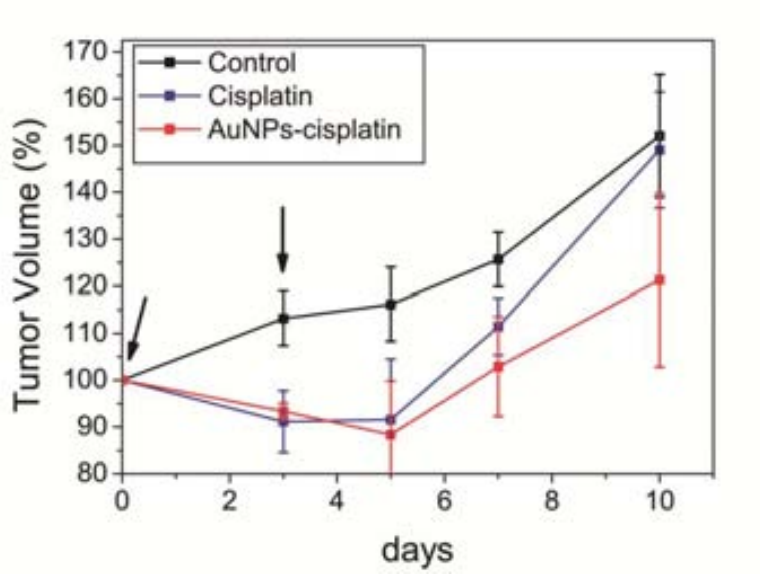

Figure 5.4 Therapeutic efficiency of cisplatin. a, Differences in tumour volumes measured by calliper after two consecutive injections (day 0 and 3) of 3 and 1.5 mg cisplatin (Kg mouse)$^{-1}$ each of free cisplatin and AuNP–cisplatin, respectively. Arrows indicate injection days. Errors are standard error of the mean (n=5, except in the case of free cisplatin where n=5, 4, 3, 2, 2 due to mice death).

5.3.3.2 Long treatment and tumor volume measured by bioluminiscence

To overcome the limitations observed in the previous section, another round of experiments was carried out using smaller tumors. In this case, tumors were grown for only 9 days instead of 3-4 weeks. This small volume makes impossible the measure by caliper and therefore biochemical techniques were used here. In Vivo Imaging System (IVIS®) is based on the detection of bioluminescence produced by cells. Roughly, cells that are implanted to create the tumor are genetically modified to express luciferase. This make tumor cells the only cells of the organism that are able to metabolize luciferin (which is injected 5 minutes before measuring). Metabolization of luciferin results in bioluminescence that is detected by a CCD camera. The intensity of the light is therefore proportional to the volume of the tumor.

In this experiment, 5 mice received 3 ip injections of 1.5 mg cisplatin Kg^{-1}, 5 mice received the same amount of cisplatin conjugated to AuNPs and 5 mice, controls, were maintained without treatment. Here again, the anticancer effect of cisplatin is maintained (Figure 5.5). It is important to remember that our goal was not improving the efficacy of the drug, but its efficiency by reducing side effects, which is the main limitation of cisplatin in the clinics.

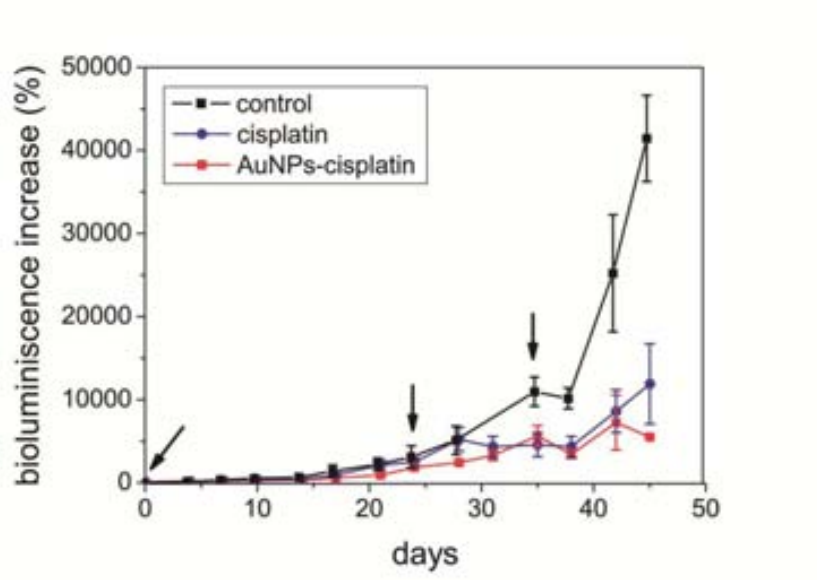

Figure 5.5 Therapeutic efficiency of cisplatin. Increase in bioluminescence measured by IVIS which is proportional to the number of living cells in the tumour. 1.5 mg cisplatin (kg mouse)$^{-1}$ injections were used in both treatments (day 0, 19, and 34). Arrows indicate injection days. Errors are standard error of the mean (n=5).

5.3.4 Biodistribution in mice

It is important to bear in mind that the majority of drugs are normally transported through the small pores (6 – 8 nm) found in the continuous capillaries which are the most widely distributed throughout the organism[2], which causes a widespread distribution of the drug and in many cases unwanted side effects. For effective therapy, it is necessary to deliver therapeutic agents selectively to their target sites, avoiding non-target organs. Such selectivity is key for antitumoral drugs because of their extreme cytotoxicity. By vehiculating the drug using a nanocarrier, the distribution of the drug is controlled by the physicochemical properties of the nanoparticle[10, 22, 23] rather than those of the drug. Therefore biodistribution analysis is one of the most useful tools to anticipate the behavior of the DDS (and similar candidates).

In our experiments, groups of 15 SCID human-tumor-bearing mice were used to assay the biodistribution of both the vehicle and the drug. The same dose of free or AuNP-bound cisplatin was administrated to the mice (4 mg Pt (kg mice)$^{-1}$) via ip injection. This route facilitates the traffic of particles from the peritoneal cavity to the lymphatic system before the particles enter systemic circulation[24], from where they are distributed to the different organs. The amounts of both Pt and Au were measured by ICP-MS at 30 min, and 3, 6, and 24 hours after the injection (Figure 5.6). It is worth noting that from the crude readings it is impossible to determine if the observed Pt is still active, inactive bound to proteins, or

attached to the NPs waiting to be activated. Free cisplatin is known to be removed from the circulation in two steps: an initial rapid renal clearance (less than 1 h) followed by a slow loss from the circulation of the cisplatin bound to plasma proteins (hours to days)[20], with less than about 2 % of total cisplatin reaching the tumor cells. Since the long-circulating cisplatin is mainly bound to protein (90 to 97%) and consequently deactivated[20], neither significant toxicity nor therapeutic benefits are expected from it.[25] This rapid clearance of free cisplatin, which is also observed from all organs in our work, differs considerably from what is observed in the case of the cisplatin bound to AuNPs. First observation is that the amount of Pt in blood sera released from the AuNP-cisplatin conjugates (AuNPs were removed by centrifugation before measuring) was initially negligible (52.12 ± 1.9 μg L^{-1}). However, once the conjugates were processed, mainly by phagocytic organs (vide infra), there was a progressive delayed release of Pt to blood that reached 932.25 ± 343.4 μg L^{-1} at 24 h. In the rest of the organs it is common to see an initial decrease in Pt concentration, from 30 min to 3 hours and then an increase at 6 h and 24 h, likely of the non-conjugated form as the changes of the Au/Pt ratios in organs with time seem to indicate (Figure 5.7); this shows how the Au and cisplatin split and follow different pathways after being processed by cells. The higher the ratio, the less free cisplatin is present. Although the signal from conjugated and non-conjugated cisplatin is difficult to deconvolute, two different behaviors are clearly observed: organs where the ratio progressively decreases (those indicated by dashed lines) and organs where the ratio increases (those indicated by continuous lines). Note that the organs where this ratio increased are phagocytic organs where NPs accumulate. From these results we believe that some information regarding how nanocarriers are processed can be extracted: The stability of the link in blood is proved since the amount of free drug is initially negligible (in agreement with previous *stability t*ests showed in chapter 4). Then AuNPs-cisplatin start to accumulate preferentially in the phagocytic organs and are processed. From there the drug is released again to the systemic circulation in a process that we call secondary release, as the primary release is the release of cisplatin in the tumor cells. However, there is a lack of cisplatin-induced toxicity due to this secondary release, which can be explained because cisplatin levels in blood are much lower than the achieved after free drug administration. Moreover the active form of cisplatin released from the NPs is rapidly deactivated by plasma proteins, even faster than conventional cisplatin, since it is more reactive. Consequently the drug coming from the secondary release is not expected to have significant therapeutic or toxic effects in our case, but this process should be taken into account when dealing with nanocarriers for drug delivery.

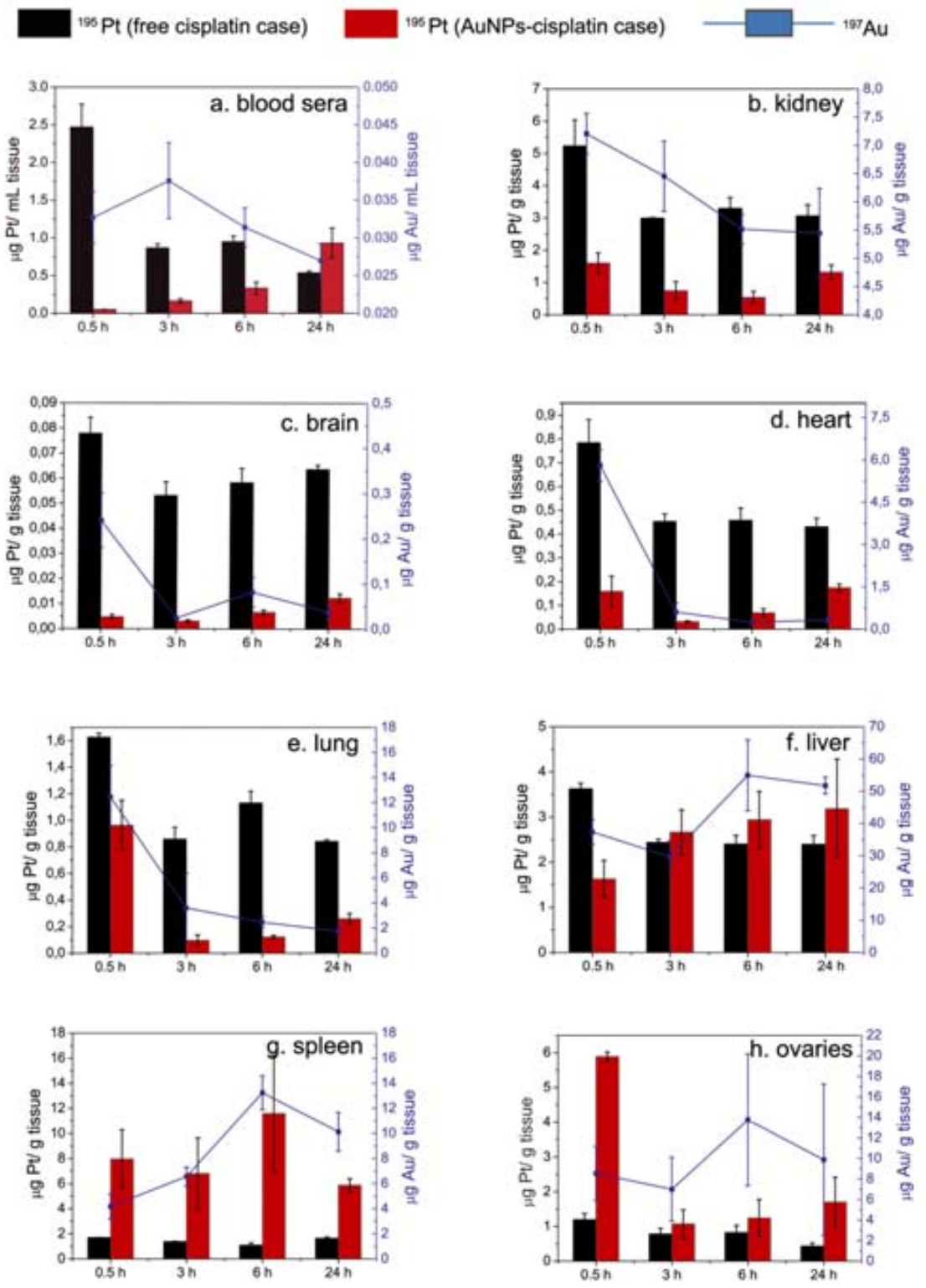

Figure 5.6. Biodistribution of Au and Pt arising from the treatment with free cisplatin (quantification of Pt, black) and AuNP–cisplatin (quantification of Pt and gold, black and blue respectively). The amounts of Pt and Au were analyzed in relevant organs at 0.5, 3, 6, and 24 h after injection by ICP-MS. Errors are standard error of the mean (n=3). See text for extended analysis of this data.

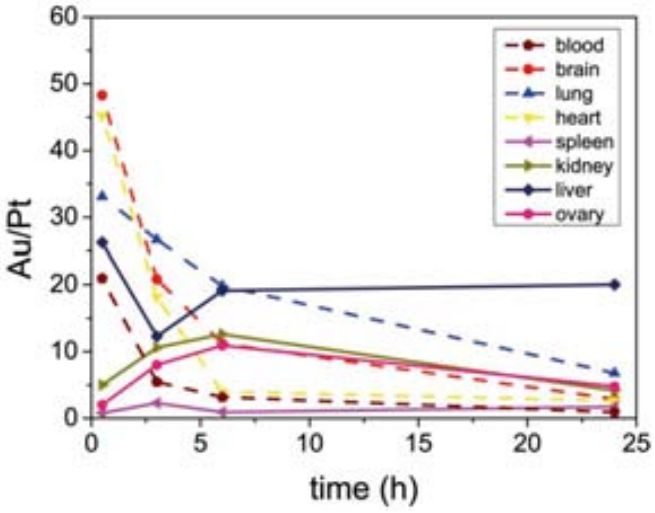

Figure 5.7. Time evolution of the ratio Au/Pt in different organs. Two different behaviors were observed: the one indicated by continuous lines (organs in which tissue macrophages are present) shows an increase of this ratio at the first times which indicates a depletion of Pt, likely due to the secondary release explained in the main text. Consequently, the other organs which are irrigated by continuous capillaries can take this Pt up and therefore the ratio decreases.

A detailed analysis of the biodistribution of the conjugates showed no evidence of accumulation of Au or Pt in the brain, heart, or lung other than that coming from the blood present in these tissues (Figure 5.6 c-e). Of course, 13 nm AuNPs are not expected to cross the blood–brain barrier,[26] hence it is not surprising that the lowest Au content of all the analyzed organs was found in the brain. In all of these organs the amounts of Pt are 5-10-fold lower in the treatment with AuNPs-cisplatin than when treated with free cisplatin. A markedly different behavior was observed in liver and spleen (Figure 5.6 f, g) which are responsible for clearance of nanocarriers[12, 26-29]. In fact, these —together with the ovary (Figure 5.6h) — are the only organs in which the Pt contents were higher in the case of AuNP–cisplatin treatments than for free cisplatin. These organs are highly phagocytic and will take up the AuNP–cisplatin conjugates and process them. Macrophages are found in the organs of the mononuclear phagocytic system (liver and spleen) as well as in the peritoneum (close to the ovary) and in the periphery of the kidneys. Accumulation of AuNP–CisPt conjugates in the ovaries, whose tumor is treated with cisplatin[15], is probably a consequence of the intraperitoneal administration. In fact, this route has been proposed for treatment of ovarian cancer with nanoparticles since they show a slower absorption profile into the lymphatic system than that of the free drug by this administration route[30]. In the general picture, it is also expected that in 24 h a significant amount of the conjugates

is still in the peritoneum or lymph nodes, at the beginning of the journey that they perform during the treatments.

5.3.5 Avoiding cisplatin-induced toxicity

The main limitation of therapies involving the use of cisplatin and other platinum drugs is the high toxicity profile. They are specially toxic for kidneys. Indeed, kidneys are the major route of clearance of cisplatin, thus receiving a high exposure of cisplatin. Renal toxicity induced by cisplatin is primarily tubular dysfunction, which progresses to acute renal failure.[31] To ameliorate patient safety, a number of strategies such as administer the drug together with diuretic agents have been implemented. Second generation drugs based on Pt such as oxaliplatin or carboplatin have been designed to reduce cisplatin-induced toxicity.[32, 33] However, nephrotoxicity is still the cause of stopping treatment before the full benefits of the drug are reached in too many cases. Thus, it is clear that the kidney deserves special consideration if a reduction of cisplatin-induced toxicity is wanted.

Pt levels were reduced considerably in the kidney when AuNP–cisplatin was administered, compared to free cisplatin (Figure 5.6 b), at all times. Moreover, the AuNPs that reached the kidneys were trapped by peripheral macrophages, which thus diminished the potential damage induced by cisplatin as histopathology studies showed (Figure 5.8). Histological analysis of the kidneys after treatment with free cisplatin and AuNP–cisplatin (21 days, 3 doses of 5 mg cisplatin/kg mice in both cases) revealed a lack of damage in the latter case, while in the case of free cisplatin, the kidneys were severely damaged. The morphological changes were consistent with cisplatin-induced acute nephrosis.[31]

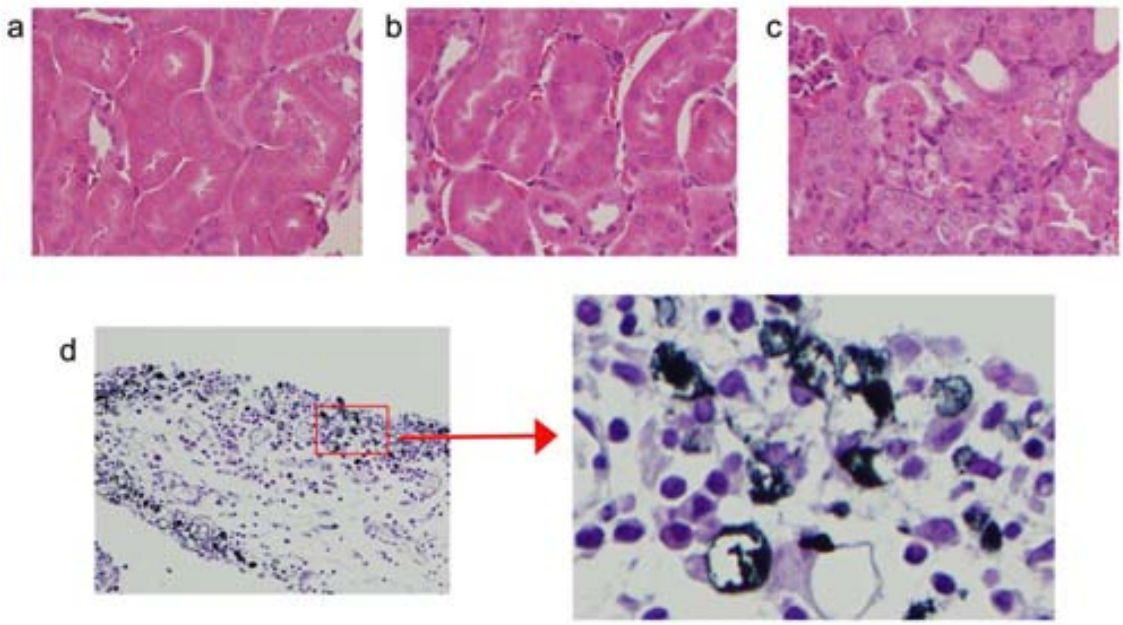

Figure 5.8. Nephrotoxicity induced by cisplatin. The appearance of histopathological changes in the proximal tubuli is evidence of nephrotoxicity. (a) Normal appearance of kidney section of control animals and (b) mice treated with AuNP-cisplatin. (c) Proximal tubular degeneration of animals taking high-dose free cisplatin. (d) AuNPs that reached the kidneys were trapped by peripheral macrophages.

When comparing the weight of the kidney in the different treatments (Figure 5.9), a clear reduction was observed in the case of mice treated with free cisplatin; this is consistent with the observed nephrosis. A significant increase of weight of the spleen treated with NPs was also observed. To exclude any spleen toxicity induced by the nanoparticles, histological analysis of the spleen were also performed. Representative microscopy images of spleen slices of the control, the sample treated with free cisplatin, and a sample from the AuNP-cisplatin treatment do not show any adverse effect of the treatments in this organ; no damage or inflammation is observed(Figure 5.10). No significant differences in morphology between control, free cisplatin, and AuNP-cisplatin treated samples were either observed. In the case of AuNPs-cisplatin, one could observe the NPs accumulated in macrophages in the periphery of the spleen, as was previously observed in the kidneys. When using the conjugates, no morphological changes were observed, but a diffuse hyperplasia was observed, which manifested in the weight increase; the most significant alteration was the increased number of megacariocytes (platelet precursors), which can be also related to the increase in circulating platelets. The diffuse hyperplasia of the red pulp was attributed to extramedullary haematopoiesis, likely after anemia due to the

cisplatin treatment. Both anemia and hyperplasia are temporary and sequential and are expected to remedy themselves as cisplatin is being processed. What we observed was a modest lower leukocytes count in both treatments, slightly enhanced when the cisplatin was conjugated.

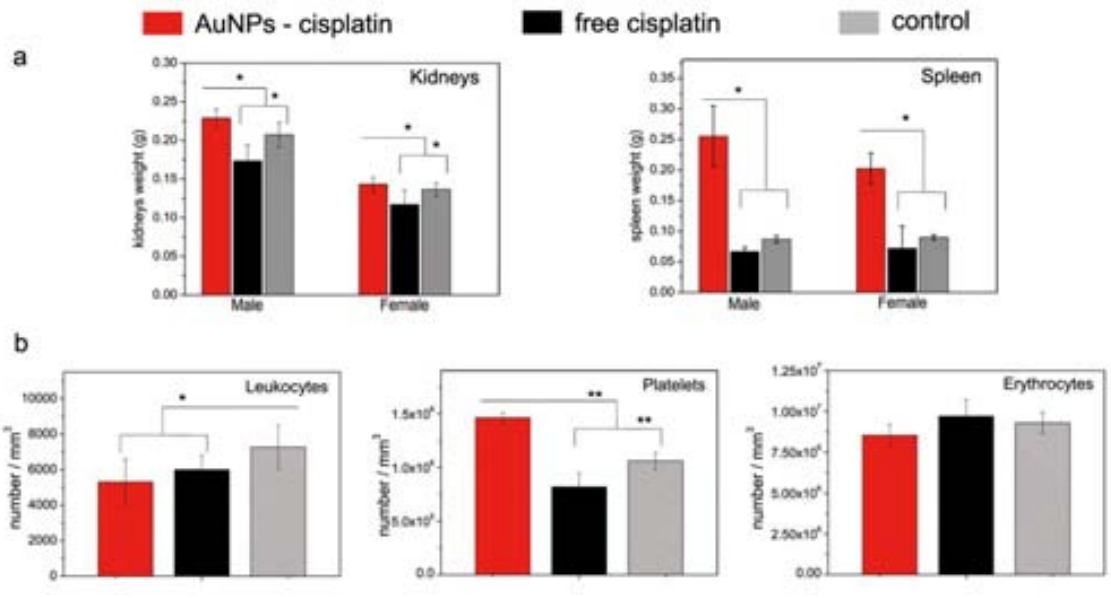

Figure 5.9. Kidney and spleen weights and hematology. (a) Weight of kidneys decreased only in the case of free cisplatin treatment, which agrees the previously observed cisplatin-induced toxicity. On the other hand, spleen weight increased in the case of AuNPs-cisplatin treatment, likely due to a temporal hyperplasia of the red pulp. (b) Leukocytes, platelets, and erythrocytes were also quantified and the organ showed no signs of anemia, but an increased number of platelets in the AuNPs-cisplatin, which is likely related to the hyperplasia of the spleen. * $P < 0.05$, ** $P<0.001$.

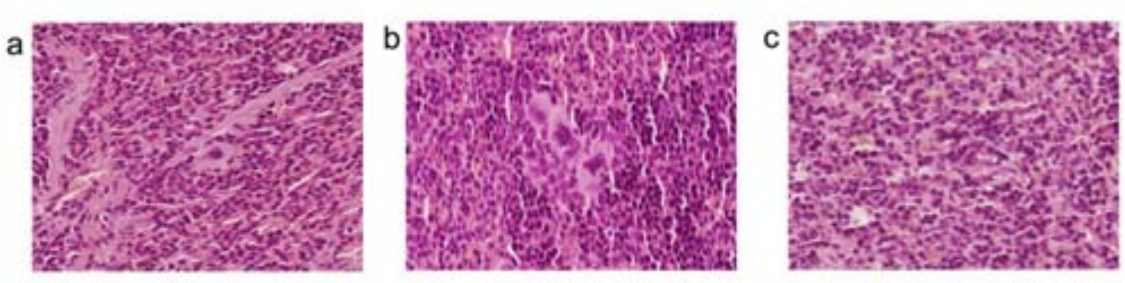

Figure 5.10 Spleen toxicity. Histological slides of spleen showed no signs of pathology in (a) control, (b) AuNPs-cisplatin, and (c) free cisplatin treatment

In addition to the observed absence of histological damage in the mice treated with AuNP-cisplatin, biochemical analysis did not show renal (blood urea nitrogen and creatinine) or liver (transaminases) damage (Table 1). Aspartate transaminase (AST) and Alanine transaminase (ALT) levels indicate that there is no evidence of liver disfunction. Total protein and albumin are also indicators of hepatic function and do not show any alteration. Besides, the renal function is usually determined by the levels of Blood Urea Nitrogen (BUN) and creatinine. Although BUN seems to be higher than levels reported in other works,[34] it should be noted that there is no difference between control and treatment with AuNPs-cisplatin.

	Control		AuNPs-cisplatin	
	Mean	**sd**	**Mean**	**sd**
AST (UI/L)	15.88	4.79	15.46	6.73
ALT (UI/L)	13.64	2.99	13.71	0.41
ALP (UI/L)	109.87	64.68	189.5	99.7
BUN (mg/dl)	55.93	8.3	63.26	11.78
Creatinine (mg/dl)	<0.5		<0.5	
Total protein (g/dl)	13.8	4.28	11.81	3.95
Albumin (g/dl)	7.85	3.64	9.47	3.98

Table 1. Analysis of relevant biochemical markers of renal and hepatic funtion.

Evaluation of systemic toxicity is commonly performed by measuring the body weight loss. We divided 15 mice in three groups of mice that received no treatment (control), free cisplatin, or AuNP–cisplatin (three injections of 5 mg cisplatin /Kg mouse in both cases; in a 13 day experiment) (Figure 5.11). After the initial loss of weight in both treatments, weight recovery was most evident in mice treated with AuNP-cisplatin. More significantly, after the second dose, mice treated with free cisplatin decreased in weight more dramatically and showed no signs of recovery, which can be attributed to the cumulative toxic effects of cisplatin,[35] whilst the mice treated with AuNP-cisplatin experienced a smaller weight decrease, again and a rapid recovery, and no evidence of memory effects.

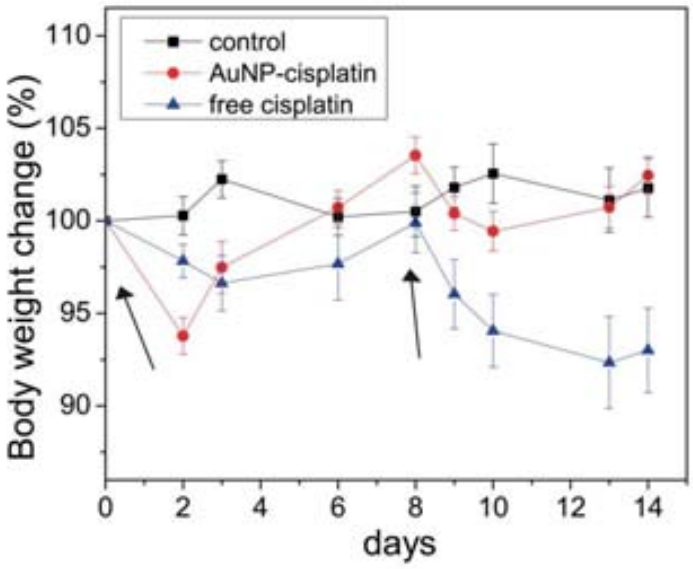

Figure 5.11. Body weight loss after **different treatments.** Body weight change of control mice and mice that received the same amount of free cisplatin or conjugated to AuNPs (4 mg Kg^{-1}, days 0 and 8). The arrows indicate the day of injection. Loss of weight and further recovery capacity is a clinical test to assay systemic toxicity.

From these results it can be concluded that nephrotoxicity is clearly reduced, if not totally avoided, by using cisplatin conjugated to AuNPs. Interestingly, the organs where AuNPs were more accumulated did not show any evidence of toxicity except for a temporal hyperplasia of the spleen. In addition, body weight dropped and animals showed no signs of recovery after the second cycle of free cisplatin treatment. This expected behavior of free cisplatin treatments is indicative of systemic cumulative toxicity. This was not observed in the case of conjugated cisplatin. This absence of toxicity might be beneficial not only in terms of patient safety, but also in efficiency since it is known that nephrotoxicity is dose limiting and moreover the treatment is often stopped before reaching the full benefits of the drug due to toxicity issues.

5.4 Conclusions

Cisplatin is widely used to treat a great variety of tumors. However, its use is seriously limited by the induction of nephrotoxicity and other side effects. Thus, efforts are focused to improve the delivery of the drug to the tumor avoiding organs in which cisplatin is known to produce adverse effects.

We showed that our vehicle, which is stable at physiological conditions, enters the cell via an endocytic pathway. The pH in the endosomes drops, allowing the release of drug which then can continue its journey to the DNA. Although the accumulation in the DNA, and therefore the cytotoxicity, is lower than for free cisplatin in *in vitro* assays, this is largely compensated in *in vivo* assays due to the different pharmacokinetics: Rapid renal clearance and deactivation by plasma proteins are avoided for cisplatin conjugated to AuNPs. Thus, experiments using tumor-bearing mice demonstrated that the anticancer effect of cisplatin was maintained in mice treated with AuNPs-cisplatin.

We showed that the cisplatin-induced toxicity was clearly reduced using AuNPs-cisplatin. It is known that pharmacokinetic properties depend on physicochemical properties of the carrier rather than on the ones of the drug. Thus, instead of the widespread distribution observed for free cisplatin, AuNPs-cisplatin showed the typical accumulation in the organs of the mononuclear phagocytic system (i.e. liver and spleen) largely reported in the literature. Interestingly conjugated cisplatin was diverted from the kidneys, which contributed to the absence of histopathological damage, namely absence of proximal tubular degeneration and nephrosis, as observed in treatment with free cisplatin. Moreover, toxicity in the spleen and liver was also discarded by histology analysis as well as by normal levels of several biomarkers. Also body weight, which is indicative of systemic toxicity, was maintained in normal values along the treatment, except for a temporal decrease after injection. All the data indicates that cumulative toxic effect of cisplatin is avoided, which would allow to continue the treatment for longer times or to change the strategy of administration. Thus, we demonstrated a reduction of toxicity of a very effective drug that is still limited by its side effects without affecting its efficacy. This would help to improve the efficiency of the treatment with cisplatin since classic treatment has to be often stopped before the full benefits of the treatment are reached due to toxicity issues.

Although these encouraging results contributed to move one step forward the drug delivery field, there are still some points that can be improved in future work. For example, the release of drug after pH drop is low due to the high strength of the coordination bond between Pt and MUA-SAM. This ensures that unspecific release is not produced, but on the other side, only a small percentage of the cisplatin that is attached to the AuNPs is released and has the chance to reach the cell nucleus. Thus, improving the triggering of the release would result in a greater efficacy and it would make possible to reduce the dose needed to achieve therapeutic benefits. Thus it would minimize the potential risks of using high concentration of NPs. Another issue that every nanocarrier

has to deal with is the penetration into tumors. It is known that macromolecular carriers (and nanoparticles) fails to penetrate deep into the tumors and are generally accumulated just some micrometers away from the vessels.[8, 36-38] However, the greater accumulation of active drug when attached to AuNPs (the drug is protected against deactivation by plasma proteins) and the possibility of successive treatments (if cisplatin toxicity is clearly reduced) may overcome the lower penetrability of the vehicles,[36] allowing the progressive erosion of the tumor.

Another issue which should be studied is the expulsion of NP from the organism since it might influence long time toxicity. In general terms, it seems clear that small NPs (<6 nm) are rapidly excreted by kidney filtration. For example, more than 80 % of 4 nm quantum dots were found in the urine 4 hours after injection.[39] Glomerular filtration in kidneys is ineffective for larger NPs. Then, the preferred route of excretion is through the fecal matter, via the hepatobiliary clearance route.[40] This route of excretion is slower. Thus, NPs which are larger than 6 nm not only increase their blood-half-life avoiding renal clearance, but also showed a greater accumulation in organs of the RES increasing the likelihood of toxicity in this organs. Therefore, the absence of toxicity at long times in liver and spleen should be ensured for NPs that are not cleared by kidneys.

5.5 References

(1) Michel, C. C.; Curry, F. E., Microvascular Permeability. *Physiological Reviews* **1999,** 79, 703-761.
(2) Takakura, Y.; Hashida, M., Macromolecular Carrier Systems for Targeted Drug Delivery: Pharmacokinetic Considerations on Biodistribution. *Pharmaceutical Research* **1996,** 13, 820-831.
(3) Lipinski, C. A.; Lombardo, F.; Dominy, B. W.; Feeney, P. J., Experimental and computational approaches to estimate solubility and permeability in drug discovery and development settings. *Advanced Drug Delivery Reviews* **1997,** 23, 3-25.
(4) Vistoli, G.; Pedretti, A.; Testa, B., Assessing drug-likeness - what are we missing? *Drug Discovery Today* **2008,** 13, 285-294.
(5) Allen, T. M.; Cullis, P. R., Drug Delivery Systems: Entering the Mainstream. *Science* **2004,** 303, 1818-1822.
(6) Dreher, M. R.; Liu, W.; Michelich, C. R.; Dewhirst, M. W.; Yuan, F.; Chilkoti, A., Tumor Vascular Permeability, Accumulation, and Penetration of Macromolecular Drug Carriers. *Journal of the National Cancer Institute* **2006,** 98, 335-344.
(7) Khlebtsov, N.; Dykman, L., Biodistribution and toxicity of engineered gold nanoparticles: a review of in vitro and in vivo studies. *Chemical Society Reviews* 40, 1647-1671.
(8) Perrault, S. D.; Walkey, C.; Jennings, T.; Fischer, H. C.; Chan, W. C. W., Mediating Tumor Targeting Efficiency of Nanoparticles Through Design. *Nano Letters* **2009,** 9, 1909-1915.

(9) Maeda, H.; Wu, J.; Sawa, T.; Matsumura, Y.; Hori, K., Tumor vascular permeability and the EPR effect in macromolecular therapeutics: a review. *Journal of Controlled Release* **2000,** 65, 271-284.
(10) Farokhzad, O. C.; Langer, R., Impact of Nanotechnology on Drug Delivery. *ACS Nano* **2009,** 3, 16-20.
(11) Ruenraroengsak, P.; Cook, J. M.; Florence, A. T., Nanosystem drug targeting: Facing up to complex realities. *Journal of Controlled Release* **2010,** 141, 265-276.
(12) Zhang, G.; Yang, Z.; Lu, W.; Zhang, R.; Huang, Q.; Tian, M.; Li, L.; Liang, D.; Li, C., Influence of anchoring ligands and particle size on the colloidal stability and in vivo biodistribution of polyethylene glycol-coated gold nanoparticles in tumor-xenografted mice. *Biomaterials* **2009,** 30, 1928-1936.
(13) Klein, A. V.; Hambley, T. W., Platinum Drug Distribution in Cancer Cells and Tumors. *Chemical Reviews* **2009,** 109, 4911-4920.
(14) Jung, Y.; Lippard, S. J., Direct Cellular Responses to Platinum-Induced DNA Damage. *Chemical Reviews* **2007,** 107, 1387-1407.
(15) Wang, D.; Lippard, S. J., Cellular processing of platinum anticancer drugs. *Nat Rev Drug Discov* **2005,** 4, 307-320.
(16) Cho, E. C.; Zhang, Q.; Xia, Y., The effect of sedimentation and diffusion on cellular uptake of gold nanoparticles. *Nat Nano* **2011,** 6, 385-391.
(17) Dobrovolskaia, M. A.; McNeil, S. E., Immunological properties of engineered nanomaterials. *Nat Nano* **2007,** 2, 469-478.
(18) Collins, R. J.; Verschuer, L. A.; Harmon, B. V.; Prentice, R. L.; Pope, J. H.; Kerr, J. F. R., Spontaneous programmed death (apoptosis) of B-chronic lymphocytic leukaemia cells following their culture in vitro. *British Journal of Haematology* **1989,** 71, 343-350.
(19) Kim, B.; Han, G.; Toley, B. J.; Kim, C.-k.; Rotello, V. M.; Forbes, N. S., Tuning payload delivery in tumour cylindroids using gold nanoparticles. *Nat Nano* 5, 465-472.
(20) DeConti, R. C.; Toftness, B. R.; Lange, R. C.; Creasey, W. A., Clinical and Pharmacological Studies with cis-Diamminedichloroplatinum(II). *Cancer Research* **1973,** 33, 1310-1315.
(21) Rehemtulla, A.; Stegman, L. D.; Cardozo, S. J.; Gupta, S.; Hall, D. E.; Contag, C. H.; Ross, B. D., Rapid and quantitative assessment of cancer treatment response using in vivo bioluminescence imaging. *Neoplasia* **2000,** 2, 491-5.
(22) Vasir, J. K.; Reddy, M. K.; Labhasetwar, V. D., Nanosystems in drug targeting: Opportunities and challenges. *Current Nanoscience* **2005,** 1, 47-64.
(23) Arvizo, R. R.; Miranda, O. R.; Moyano, D. F.; Walden, C. A.; Giri, K.; Bhattacharya, R.; Robertson, J. D.; Rotello, V. M.; Reid, J. M.; Mukherjee, P., Modulating Pharmacokinetics, Tumor Uptake and Biodistribution by Engineered Nanoparticles. *PLoS ONE* **2011,** 6, e24374.
(24) Bajaj, G.; Yeo, Y., Drug Delivery Systems for Intraperitoneal Therapy. *Pharmaceutical Research* 27, 735-738.
(25) Peleg-Shulman, T.; Najajreh, Y.; Gibson, D., Interactions of cisplatin and transplatin with proteins: Comparison of binding kinetics, binding sites and reactivity of the Pt-protein adducts of cisplatin and transplatin towards biological nucleophiles. *Journal of Inorganic Biochemistry* **2002,** 91, 306-311.
(26) Cho, W.-S.; Cho, M.; Jeong, J.; Choi, M.; Cho, H.-Y.; Han, B. S.; Kim, S. H.; Kim, H. O.; Lim, Y. T.; Chung, B. H.; Jeong, J., Acute toxicity and pharmacokinetics of 13 nm-sized PEG-coated gold nanoparticles. *Toxicology and Applied Pharmacology* **2009,** 236, 16-24.
(27) Sonavane, G.; Tomoda, K.; Makino, K., Biodistribution of colloidal gold nanoparticles after intravenous administration: Effect of particle size. *Colloids and Surfaces B: Biointerfaces* **2008,** 66, 274-280.
(28) Khlebtsov, N.; Dykman, L., Biodistribution and toxicity of engineered gold nanoparticles: a review of in vitro and in vivo studies. *Chemical Society Reviews* **2011,** 40.
(29) Lipka, J.; Semmler-Behnke, M.; Sperling, R. A.; Wenk, A.; Takenaka, S.; Schleh, C.; Kissel, T.; Parak, W. J.; Kreyling, W. G., Biodistribution of PEG-modified gold nanoparticles

following intratracheal instillation and intravenous injection. *Biomaterials* **2010,** 31, 6574-81.
(30) Lu, H.; Li, B.; Kang, Y.; Jiang, W.; Huang, Q.; Chen, Q.; Li, L.; Xu, C., Paclitaxel nanoparticle inhibits growth of ovarian cancer xenografts and enhances lymphatic targeting. *Cancer Chemotherapy and Pharmacology* **2007,** 59, 175-181.
(31) Vickers, A. E. M.; Rose, K.; Fisher, R.; Saulnier, M.; Sahota, P.; Bentley, P., Kidney Slices of Human and Rat to Characterize Cisplatin-Induced Injury on Cellular Pathways and Morphology. *Toxicologic Pathology* **2004,** 32, 577-590.
(32) Graham, M. A.; Lockwood, G. F.; Greenslade, D.; Brienza, S.; Bayssas, M.; Gamelin, E., Clinical Pharmacokinetics of Oxaliplatin: A Critical Review. *Clinical Cancer Research* **2000,** 6, 1205-1218.
(33) Reedijk, J., Improved understanding in platinium antitumour chemistry. *Chemical Communications* **1996,** 0, 801-806.
(34) Tseng, C.-L.; Su, W.-Y.; Yen, K.-C.; Yang, K.-C.; Lin, F.-H., The use of biotinylated-EGF-modified gelatin nanoparticle carrier to enhance cisplatin accumulation in cancerous lungs via inhalation. *Biomaterials* **2009,** 30, 3476-3485.
(35) Miller, R. P.; Tadagavadi, R. K.; Ramesh, G.; Reeves, W. B., Mechanisms of Cisplatin Nephrotoxicity. *Toxins* 2, 2490-2518.
(36) Dreher, M. R.; Chilkoti, A., Toward a systems engineering approach to cancer drug delivery. *Journal of the National Cancer Institute* **2007,** 99, 983-5.
(37) Ruenraroengsak, P.; Cook, J. M.; Florence, A. T., Nanosystem drug targeting: Facing up to complex realities. *Journal of Controlled Release* 141, 265-276.
(38) Minchinton, A. I.; Tannock, I. F., Drug penetration in solid tumours. *Nat Rev Cancer* **2006,** 6, 583-592.
(39) Soo Choi, H.; Liu, W.; Misra, P.; Tanaka, E.; Zimmer, J. P.; Itty Ipe, B.; Bawendi, M. G.; Frangioni, J. V., Renal clearance of quantum dots. *Nat Biotech* **2007,** 25, 1165-1170.
(40) Kumar, R.; Roy, I.; Ohulchanskky, T. Y.; Vathy, L. A.; Bergey, E. J.; Sajjad, M.; Prasad, P. N., In Vivo Biodistribution and Clearance Studies Using Multimodal Organically Modified Silica Nanoparticles. *ACS Nano* **2010,** 4, 699-708.

Chapter 6

The use of Functionalized Gold Nanoparticles as Radiosensitizers

6.1 Introduction

Radiotherapy is a major modality to treat cancer. Its aim is to deliver a therapeutic radiation dose to the tumor whilst sparing the damage to the surrounding tissue.[1] However, radiotherapy is still limited by tumor cells that are radioresistant, underirradiated or outside the target region.[2] Moreover, tumor and surrounding tissue normally present similar X-ray absorption characteristics. To overcome these limitations, beam delivery methods are in constant improvement. The use of heavy elements that can be accumulated on the tumors has been also proposed due to their higher mass energy absorption coefficients.[3] Among these elements, gold nanoparticles (AuNPs) are of special interest due to their strong photoelectric absorption coefficient. Additionally, AuNPs can be synthesized with control of the size and very narrow size distribution compared to other nanosystems[4], their surface can be easily functionalized[5], and they are biocompatible.[6] It is also well known that nanoparticles (NPs) are passively accumulated into the tumors due to the enhanced permeation and retention effect (EPR).[7] Briefly, the leaky vessels of the tumor allow the NPs to permeate into the tumor tissue where they are accumulated due to the absence of a functional lymphatic system. Therefore, the contrast between tumors and normal tissue would be improved if AuNPs accumulated into the tumor.

The results derived from this chapter will be submitted for intellectual property protection and therefore are not showed in this version of the thesis dissertation.

6.5 References

(1) Butterworth, K. T.; McMahon, S. J.; Currell, F. J.; Prise, K. M., Physical basis and biological mechanisms of gold nanoparticle radiosensitization. *Nanoscale* **2012,** 4, 4830-4838.
(2) Hainfeld, J. F.; Dilmanian, F. A.; Slatkin, D. N.; Smilowitz, H. M., Radiotherapy enhancement with gold nanoparticles. *Journal of Pharmacy and Pharmacology* **2008,** 60, 977-985.
(3) McMahon, S. J.; Hyland, W. B.; Muir, M. F.; Coulter, J. A.; Jain, S.; Butterworth, K. T.; Schettino, G.; Dickson, G. R.; Hounsell, A. R.; O'Sullivan, J. M.; Prise, K. M.; Hirst, D. G.; Currell, F. J., Biological consequences of nanoscale energy deposition near irradiated heavy atom nanoparticles. *Sci. Rep.* **2011,** 1, 18, 9 pp.
(4) Bastús, N. G.; Comenge, J.; Puntes, V. c., Kinetically Controlled Seeded Growth Synthesis of Citrate-Stabilized Gold Nanoparticles of up to 200 nm: Size Focusing versus Ostwald Ripening. *Langmuir* **2011,** 27, 11098-11105.
(5) Eugenii, K.; Itamar, W., Integrated Nanoparticle-Biomolecule Hybrid Systems: Synthesis, Properties, and Applications. *Angewandte Chemie International Edition* **2004,** 43, 6042-6108.
(6) Khlebtsov, N.; Dykman, L., Biodistribution and toxicity of engineered gold nanoparticles: a review of in vitro and in vivo studies. *Chemical Society Reviews* **2011,** 40.
(7) Maeda, H.; Wu, J.; Sawa, T.; Matsumura, Y.; Hori, K., Tumor vascular permeability and the EPR effect in macromolecular therapeutics: a review. *Journal of Controlled Release* **2000,** 65, 271-284.

List of Abbreviations

A549: Adenocarcinomic Human Alveolar Basal Epithelial Cells

ALT: Alanine Transaminase

AST: Aspartate Transaminase

AuNPs: Gold Nanoparticles

BSA: Bovine Serum Albumin

BUN: Blood Urea Nitrogen

CCM: Cell Culture Media

DDS: Drug Delivery System

DLS: Dynamic Light Scattering

DMEM: Dulbecco's Modified Eagle Medium

DSB: Double Strand Break

EGF: Epidermal Growth Factor

EPR: Enhanced Permeation and Retention (effect)

ES-MS: Electrospray Mass Spectroscopy

FBS: Fetal Bovine Serum

FITC: Fluorescein Isothiocyanate

ICP-MS: Inductively Coupled Plasma Mass Spectroscopy

Ip: intraperitoneal (injection)

Iv: intravenous (injection)

IVIS: In Vivo Imaging System

LET: Linear Energy Transfer

MDA-MB-231: Adenocarcinomic Breast Epithelial Cells

MUA: 11-Mercaptoundecanoic acid

NER: Nucleotide Excision Repair (mechanism)

NIR: Near Infra-red

NPs: Nanoparticles

PEG: Polyethylene Glycol

PI: Propidium Iodide

RES: Reticuloendothelial System

ROS: Reactive Oxygen Specie

SAM: Self-Assembled Monolayer

SCID: Severe Combined Immunodeficiency

SPR: Surface Plasmon Ressonance

SSB: Single Strand Break

TEM: Transmission Electronic Microscopy

TNF: Tumor Necrosis Factor

Z-potential: Zeta Potential (ζ-Potential)

List of Publications

1. J. Comenge and V.Puntes. **Tuning Protein Corona Formation in Gold Nanoparticles via PEG conformation.** In preparation

2. J.Comenge and V. Puntes. **Stabilizing AuNP conjugates in Physiological conditions by PEGylation**. Chapter in Methods in Molecular Biology. Vol: Nanomaterials Interfaces in Biology. (accepted)

3. J. Comenge, C. Sotelo, F. Romero, O. Gallego, A. Barnades, F. Domínguez, V. Puntes. **Detoxifying antitumoral drugs via nanoconjugation: the case of gold nanoparticles and cisplatin.** PLoS One (2012), 7(10), e47562.

4. J. Comenge, I. Ardao, M. D. Benaiges, V. Puntes, G. Alvaro. **Rational Nanoconjugation Improves Biocatalytic Performance of Enzymes: Aldol Addition Catalyzed by Immobilized Rhamnulose-1-Phosphate Aldolase.** Langmuir (2012), 28(15), 6461-6467

5. I. Ojea-Jimenez, J. Comenge, L. Garcia-Fernandez, Z.A. Megson, Z. A, E. Casals, V. Puntes. **Engineered inorganic nanoparticles for drug delivery applications.** Current drug metabolism (2012) (in press, PMID:23116108)

6. N.G. Bastús, J.Comenge, V. Puntes. **Kinetically-controlled Seeded Growth Synthesis of Citrate-Stabilized Gold Nanoparticles up to 200 nm: Size Focusing vs. Ostwald Ripening.** Langmuir (2011), 27(17), 11098-1110

7. J. Comenge, F. Romero, C. Sotelo, F. Domínguez, V. Puntes. **Exploring the binding of Pt drugs to gold nanoparticles for controlled passive release of cisplatin.** Journal of Controlled Release, 148, e31-e32 (2010).

8. R. A. Sperling, E. Casals, J. Comenge, N. G. Bastús, V. Puntes. **Inorganic Engineered Nanoparticles and Their Impact on the Immune Response**. Current Drug Metabolism, 10, 895-904 (2009).

9. E. Casals, N. G. Bastus, S. Vazquez-Campos, M. Varon-Izquierdo, J. Comenge and V. Puntes. **Inorganic Nanoparticles and Biology**. Contributions to Science 4(2), 171-177 (2008).